CONTROL STRATEGIES OF DC MICROGRID TO ENABLE A MORE WIDE-

SCALE ADOPTION

A Dissertation

by

SHUNLONG XIAO

Submitted to the Office of Graduate and Professional Studies of
Texas A&M University
in partial fulfillment of the requirements for the degree of

DOCTOR OF PHILOSOPHY

Chair of Committee,   Robert S. Balog
Committee Members, Prasad Enjeti
                                 Shankar P. Bhattacharyya
                                 Natarajan Gautam
Head of Department, Miroslav M. Begovic

May 2018

Major Subject: Electrical Engineering

ABSTRACT

Microgrids are gaining popularity in part for their ability to support increased penetration of distributed renewable energy sources, aiming to meet energy demand and overcome global warming concerns. DC microgrid, though appears promising, introduces many challenges in the design of control systems in order to ensure a reliable, secure and economical operation. To enable a wider adoption of DC microgrid, this dissertation examines to combine the characteristics and advantages of model predictive control (MPC) and distributed droop control into a hierarchy and fully autonomous control of the DC microgrid. In addition, new maximum power point tracking technique (MPPT) for solar power and active power decoupling technique for the inverter are presented to improve the efficiency and reliability of the DC microgrid.

With the purpose of eliminating the oscillation around the maximum power point (MPP), an improved MPPT technique was proposed by adding a steady state MPP determination algorithm after the adaptive perturb and observe method. This control method is proved independent with the environmental conditions and has much smaller oscillations around the MPP compared to existing ones. Therefore, it helps increase the energy harvest efficiency of the DC microgrid with less continuous DC power ripple.

A novel hierarchy strategy consisting of two control loops is proposed to the DC microgrid in study, which is composed of two PV boost converters, two battery bi-directional converters and one multi-level packed-u-cell inverter with grid connected. The primary loop task is the control of each energy unit in the DC microgrid based on model predictive current control. Compared with traditional PI controllers, MPC speeds up the control loop since it predicts error before the switching signal is applied to the converter. It is also free of tuning through the minimization of a

flexible user-defined cost function. Thus, the proposed primary loop enables the system to be expandable by adding additional energy generation units without affecting the existing ones. Moreover, the maximum power point tracking and battery energy management of each energy unit are included in this loop. The proposed MPC also achieves unity power factor, low grid current total harmonics distortion. The secondary loop based on the proposed autonomous droop control identifies the operation modes for each converter: current source converter (CSC) or voltage source converter (VSC). To reduce the dependence on the high bandwidth communication line, the DC bus voltage is utilized as the trigger signal to the change of operation modes. With the sacrifice of small variations of bus voltage, a fully autonomous control can be realized. The proposed distributed droop control of different unit converters also eliminates the potential conflicts when more than two converters compete for the VSC mode.

Single-phase inverter systems in the DC microgrid have low frequency power ripple, which adversely affects the system reliability and performance. A power decoupling circuit based on the proposed dual buck converters are proposed to address the challenges. The topology is free of shoot-through and deadtime concern and the control is independent with that of the main power stage circuit, which makes the design simpler and more reliable. Moreover, the design of both PI and MPC controllers are discussed and compared. While, both methods present satisfied decoupling performances on the system, the proposed MPC is simpler to be implemented.

In conclusion, the DC microgrid may be more widely adopted in the future with the proposed control strategies to address the current challenges that hinder its further development.

DEDICATION

To *My Parents*

Yongmao Xiao and Huaying Li

& My Beloved

Lijuan Shen

ACKNOWLEDGEMENTS

First and foremost, I would like to express my gratitude to my advisor, Dr. Robert S. Balog, for his consistent support, invaluable counselling and creative thinking throughout my research. I value the freedom that he gave to me to explore the new ideas and challenges I am interested in. He is knowledgeable and good at leading men by an orderly method. Without his patient guidance, it would be hard to complete the dissertation. I am also grateful for the support he offered so that I may attend professional conferences to present my research work, interact with other scholars and develop my academic career. I firmly believe the encouragements and lessons received from him during my Ph.D. study here at Texas A&M University will be of great inspiration for my career and future life.

I would also like to thank Dr. Enjeti, Dr. Bhattacharyya, and Dr. Gautam for serving as my committee members and their advice and support throughout the course of this research.

I would like to acknowledge the Office of Graduate and Professional Studies at Texas A&M University for awarding me the Department Scholarship and Teaching Assistants during my Ph.D. research work here.

Thanks also go to my friends and fellow colleagues Dr. Baoming Ge, Dr. Mohammad Shadmand, Dr. Souhib Harb, Dr. Xiao Li, Dr. Haiyu Zhang, Mostafa Mosa, Bo Tian, Hezi Zhu, Stephen McConnell, Morcos Metry, Minjeong Kim, Lance Alpuerto, Haitham Kanakri, Sivasai Praneeth Nanduri and Muhammed Ekin in Renewable Energy & Advanced Power Electronic Research Laboratory, Dr. Harish Sarma Krishnamoorthy, Dr. Somasundaram Essakiappan, Dr. Ahmed Morsy, Dr. Michael T. Daniel, Dr. José Juan Sandoval, Dr. Jorge Ramos, Yong Zhou, Taeyong Kang, Austin Clay, Sinan A. Sabeeh Al-Obaidi and Weiran Dai in Power Quality

CONTRIBUTORS AND FUNDING SOURCES

TABLE OF CONTENTS

LIST OF FIGURES

LIST OF TABLES

1. INTRODUCTION

1.1 Background

1.1.1 The opportunities for a DC microgrid

Facing the fact of limited fossil energy, the threats of environmental pollution and the request for higher stability and quality electricity supply, more and more countries are actively investing and developing the renewable energy such as solar, wind, bioenergy and fuel cell etc.
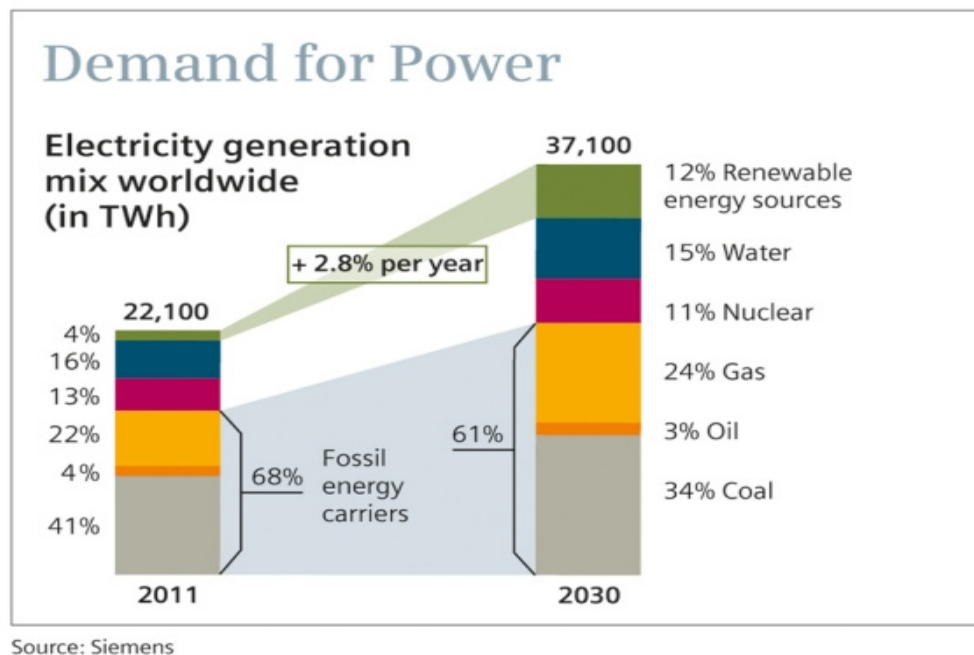
Figure 1 Increasing demand of renewable power generation

From the Figure 1, renewable energy sources (excluding hydro power) will provide 27 percent of global electricity use at the end of 2030, 7 percent increase compared to that in 2015. On the other hand, fossil energy generation shares decrease significantly from 68 percent to 61 percent [1]. The World Energy Outlook 2013 estimates that renewable energy generation share will rise to more than 30 percent worldwide by 2035, and to considerably over 40 percent in the EU [2]. According

to the 'Renewables Global Futures Report' published by the REN21 international policy network,

all of the energy experts agreed that renewable energy deployment will continue to expand in the

future, and that the technical and economic potential of renewables are largely untapped. Actually,
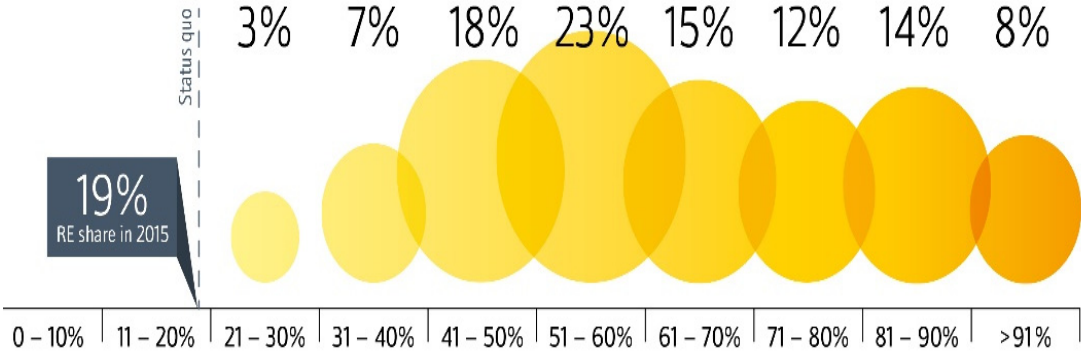
Figure 2 The Prediction of share of renewable energy consumption by 2050

as shown in Figure 2, where the x axis stands for the share percent of renewable energy

consumption by 2050 and the circle size stands for the percent of experts, over 90% of experts

estimated that the share of global renewable energy in total energy consumption will double to

40%, and possibly more, by 2050 [3].

Despite the fact that the future of renewable energy is promising, the high penetration of

renewable power systems introduces new challenges to the operations of traditional utilities and

end-users. It may cause serious reliability and power quality issues in the grid system due to the

uncontrolled fluctuations in renewable power generation and the lack of updated grid codes. The

answer may be to develop a smart grid (SG) to better integrate renewable energy resources (RES).

However, the highly distributed nature of RES makes the direct implementation into the existing

grid too difficult. One alternative is to construct a microgrid first and then connect the microgrid

into the larger smart grid. This approach deals with the distributed RES, intermixed and co-located

with the load and distributed storage, but also interconnected to improve the system reliability and energy availability.
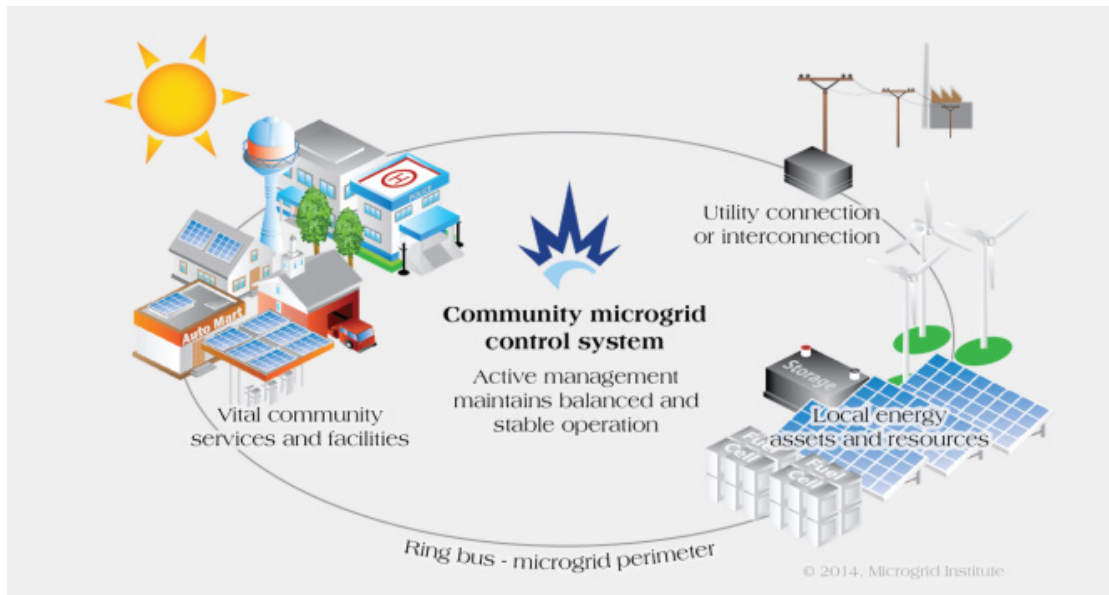
Figure 3 One definition of a microgrid

The microgrid concept, given by the U.S. Department of Energy shown in Figure 3, is a local grid consisting of renewable energy sources, energy storage systems, and dispersed loads, which may operate in both grid-connected and islanded modes. The microgrid may switch to islanded mode when un-expected faults happened on the grid side. The addition of energy storage systems can help offset the power fluctuations and increase the system reliability. In fact, the implementation of the microgrid will provide many benefits to both the end users and the electric utility provider. From the user perspective, the microgrid can provide secure and reliable energy especially to critical loads or rural areas where utility service is not available, and reduce their electricity cost through buying and selling electricity into the energy markets. From the utility perspective, it will decrease the cost spent on the central grid and infrastructures upgrade to smart grid, reduce the power losses in the distribution lines, improve the grid resistibility to extreme

weather, provide more control flexibility to the high energy demand and load unbalances, and most importantly, integrate the renewable energy sources to face the global warming effects and energy crisis. Therefore, the microgrid (MG) is the key solution to implement smart grid for integration of renewable and distributed energy resources.

The microgrid can be classified into two forms by their common power point: direct current (DC) microgrid and alternating current (AC) microgrid. The debate on the advantages of one over another is historical and as old as the competition to the world's first economic power distribution system back in the nineteen century. The ac system stood out at that time because the transformers could be used to step up voltage to lower the transmission losses and then step down for use at the load, the loads were incandescent lamps and induction motors and the sources were synchronous generators [4]. However, the development of power electronics over the past few decades makes a significant difference. High frequency and high power-density converters can replace the bulky transformers as the power-conditioning unit or interconnecting point. Solid state, high-efficiency light emitting diodes (LED) will likely render incandescent lamps obsolete [5]. Where motors are used, line-start induction motors are being replaced by efficient motor-drive pairs that increase the performance while reducing weight and cost [6]. All of these modern loads are inherently DC power. In addition, most of the renewable energy sources and energy storage systems such as solar, fuel cells, and battery banks generate or absorb direct current power directly. Hence, the DC microgrid facilitates the interconnection of these sources, loads, and energy storage to improve the efficiency, reliability, and performance of the system. The advantages of the DC microgrid over the ac are summarizes as follows [7-16]:

(a) Less energy conversion stages makes system efficiency of DC microgrid higher,

(b) Requirements like reactive power compensation and frequency control are not there,

4

(c) The DC microgrid has a fault ride through capability on its own. When a fault or voltage sag occurs in the utility grid, it does not affect the DC bus voltage of the DC microgrid directly due to the stored energy of the battery or DC capacitor,

(d) No need to track the frequency and phase, improves the controllability of the system.

1.1.2 The development of a DC microgrid

Chart 1.1   Annual Total Microgrid Market Capacity and Implementation Revenue by Region, World Markets: 2015-2024

(Source: Navigant Research)
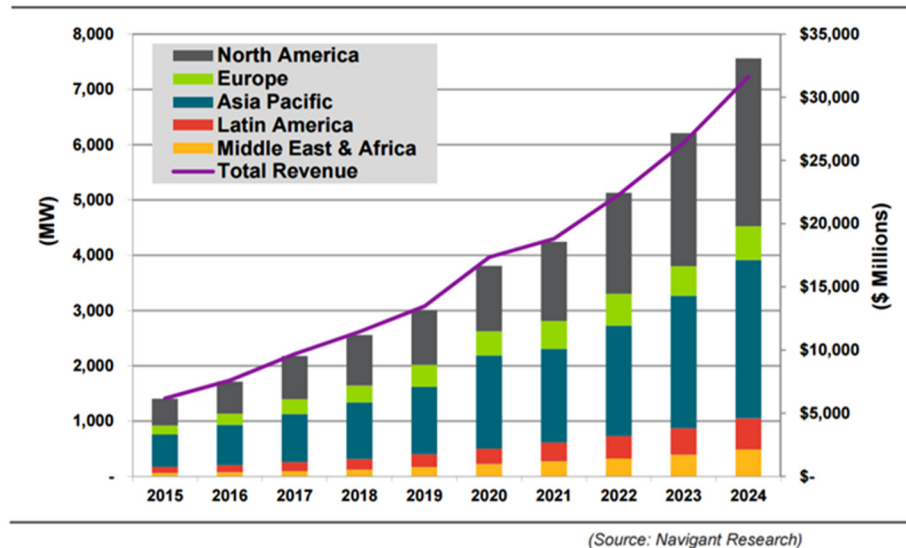
Figure 4 Microgrid capacity market development

With the characteristics and benefits introduced above, DC microgrid are gaining increased popularity in part for their ability to support increased usage of renewable energy sources to meet energy demand and overcome global warming concerns. According to Navigant Research's data in Figure 4, spending on microgrid projects is expected to increase more than five-fold over ten years, from $6 billion in 2015 to $31.5 billion in 2025. Navigant has identified 126 new microgrid projects in its recently released 4Q16 microgrid deployment tracker. In all, Navigant counted 1,681 microgrid projects worldwide, representing 16,552.8 MW. While still nascent, the microgrid

5

industry is slated for steep growth with the global microgrid capacity is expected to increase from 1.4 GW in 2015 to 7.6 GW in 2024. This is more than 400% growth in capacity over 10 years [17].
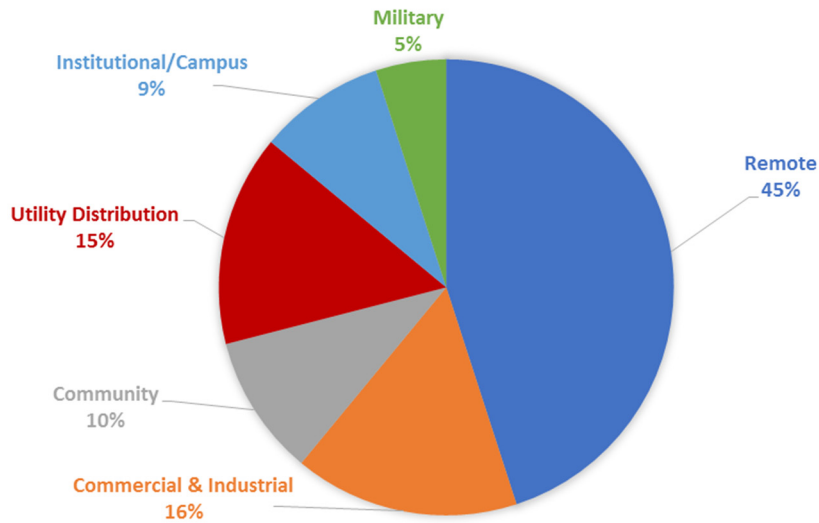
Figure 5 Microgrid applications categorized based on the market segment

Microgrids can be categorized based on the size, connection to the grid and applications. The global capacity of each microgrid market segment in 2017 is shown in Figure 5 [18].

1) Remote microgrid: This type of microgrid is in geographically remote areas with no interconnection to the utility, a common scenario in rural areas. The main objectives are gaining access to electricity and reduction of fuel costs. It is the largest share of the global market.

2) Commercial & industrial (C&I) microgrid: This is a microgrid with single or multiple ownership models. The global C&I microgrid is expected to reach 5,389.1 MW by 2026, up from 448.3 MW in 2017. This growth increases the market share from 16 percent in 2017 to 35 percent by 2026 [19]. Typical customers could be mining companies, oil & gas companies, data centers.

3) Utility distribution microgrid: This technology enables utilities to manage distributed energy resources at the distribution system. The main barrier for this microgrid segment is required

6

regulatory reforms. It is expected that capacity and revenue of utility distribution microgrids will reach 241 MW and $917 million in the US by 2024. This is a significant growth from 29 MW capacity and the annual revenue of $161 million in 2015 [20].

4) Community microgrid: This type of microgrid is mainly to provide uninterrupted power supply to the community. The application includes date centers, telecommunication stations, hospitals and government buildings.

5) Institutional/campus microgrid: This type of microgrid includes buildings with a single ownership such as a university or corporation campus. The objective is to increase the reliability and power quality, reduce the power cost and conduct research on microgrid application. Many research facilities had already built numerous of this kind of microgrid.

6) Military microgrid: This is the smallest segment in terms of global capacity. The main objective is to focus on the cyber security of the reliable power supply at both island and grid-connected modes.

As shown in Figure 4, the largest market in 2015 is Asia Pacific, with the 581.9 MW of the total capacity. North America is the second largest with 490.7 MW capacity. This trend changes by 2024, as the North American microgrid market reaches 3.0 GW, while Asia Pacific is expected to grow to 2.8 GW. Some representative microgrid projects implemented in theses leading market areas will be introduced to give an intuitive understanding of the composition, operation and development of microgrids.

A. North American
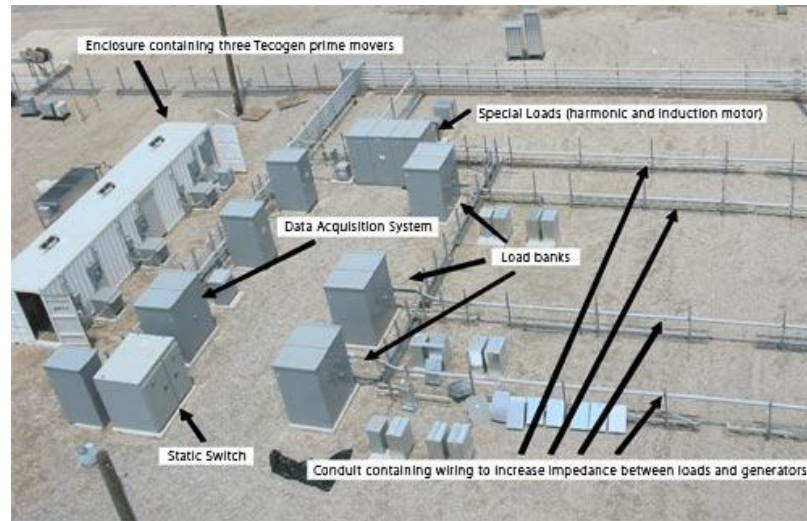
(a) CERTS microgrid test bed

b) Fuel cell as part of Santa Rita Jail microgrid

Figure 6 Real microgrid projects

In the United States, a well-known microgrid test site is the Consortium for Electric Reliability Technology Solutions (CERTS) microgrid near Columbus, Ohio as shown in Figure

6(a). This test bed, powered by three 60 kW generators, was developed by a consortium involving US government national laboratories, universities, and electric utilities (such as American Electric Power) in order to test several microgrid technologies (such as autonomous controllers in ac local area power and energy systems) from November, 2016 [21]. It is reported that the testing fully confirmed earlier research that had been conducted initially through analytical simulations, then through laboratory emulations, and finally through factory acceptance testing of individual microgrid components. The islanding and grid-reconnection method met all Institute of Electrical and Electronics Engineers 1547 and power quality requirements. The electrical protection system was able to distinguish between normal and faulted operation. The controls were found to be robust under all conditions, including difficult motor starts. A few DC microgrid projects were later derived from this initial test site, such as the Santa Rita Jail microgrid in Figure 6(b). Its approximately 1.5 MW of PV, a 1.0 MW molten carbonate fuel cell, back-up diesel generators can function grid connected or islanded using a 4 MWh Lithium-Ion battery as the only balancing resource.

Many college and universities have valuable experience operating and optimizing microgrids, developed over many years of integration and focus on delivering highly reliable energy services to mission critical end-users, such as laboratories, research centers, surgeries and data centers. Table 1 shows the rapid development of campus microgrid in the United States from 2011 to 2017. Actually, these research institutions host more than 80% of campus microgrid capacity in this country according to the States from Navigant Research [22]. The combined heat and power (CHP) based microgrid at UT-Austin is a model for campuses across the country: 99.9998% reliability (only four outages in 35 years), $4.8 million annual savings, and campus CO_2 emissions lower than 1977 levels despite a 40% larger campus, all while providing the campus

Table 1 Campus microgrid in the United States

North America	Capacity (MW)			Revenue ($)		
	2011	2017	CAGR %	2011	2017	CAGR %
Total	**603**	**1572**	**17.3**	**59.73**	**735.65**	**52.0**
By Segment:						
Commercial	71	179	16.6	8.95	80.91	44.3
Education	488	1281	17.5	45.48	603.71	53.9
Government	34	73	13.8	4.28	28.56	37.2
Healthcare	10	31	20.4	0.85	16.73	64.3
Industrial		4		–	3.06	N/A
Research	0	4	64.5	0.18	2.68	56.6

energy independence and versatility [23]. The UCSD microgrid project in Figure 7(a) supplies electricity, heating, and cooling for 450-hectare campus with a daily population of 45,000. It consists of two 13.5 MW gas turbines, one 3 MW steam turbine, and a 1.2 MW solar-cell installation that together supply 85% of campus electricity needs, 95% of its heating, and 95% of its cooling. The turbines produce 75% fewer emissions of criteria pollutants than a conventional gas power plant [24]. Other notable college microgrids are New York University, Princeton University, and Texas A&M University [22].

B. Pacific Asia

China is accelerating its research on the microgrid projects though starting late compared to other countries. Two government-funded microgrid-development-programs motivated the collaborations between universities, national electrical companies, and the companies across the world. Tulufan became the first smart city in China to operate the microgrid with 8.7 MW PV arrays, 1MW energy storage and one electrical-bus charging station in 2017. The Energy

Department of China also announced 28 new microgrid projects with 899 MW newly solar-cell installation. In Japan, the Sendai Microgrid Project in Figure 7(b) was probably the most recognized microgrid demonstration on this planet because of its excellent performance during the 2011 earthquake and tsunami. Following a service loss of a few hours, its engine generators were started and the microgrid supplied the hospital of Tohuku Fukushi University, on whose campus it is located, with both power and heat for the duration of the two-day blackout [24]. A typical island microgrid is Hong Kong's Town Island, which is currently powered by three diesel generators, and where there are plans for adding 180 kW in photovoltaic power and 12 kW in wind power [21].

C. European Union

a) UCSD campus in US   b) Japan Tokyo

Figure 7 Typical microgrid sites

The United Kingdom has a number of microgrid projects such as the Centre for Alternative Technology's microgrid in Wales, and Eigg Island's microgrid, which has a total capacity of 144 kW in renewable energy sources divided into110 kW from small hydroelectric power, 10 kW from solar power, and 24 kW from small wind power [21]. The Universitat Politècnica de Catalunya in

Spain and Aalborg University in Denmark have been working on both joint and individual microgrid projects [21]. In Italy, ERSE has been testing a microgrid with various generating and energy-storage technologies [21]. In the Netherlands, a microgrid that powers 108 homes with 315 kW of photovoltaic energy and is able to operate independently from the grid was built in Bronsbergen [21]. The Kythnos Island in Greece has a generation capacity mix of 665 kW in wind power, 100 kW in photovoltaic power, and 2 MWin diesel engine–driven power in order to meet a demand that in the year 2000 peaked at 2 MW during the summer. The island also has enough lead-acid batteries to power a 500 kW load for 10 minutes [21].

1.2 The challenges and state-of-art-research of DC microgrid

1.2.1 Challenges

Microgrid, though appears promising, introduces several challenges in the design of control systems in order to ensure a reliable, secure and economical operation.

Without the need for frequency control and phase synchronization, the DC microgrid may simplified the design of both filter and the controller compensation for devices. However, lack of phase information in DC power architectures may make implementation of autonomous controls more difficult than in ac systems [25]. Although DC microgrid is free from the stability issues related to reactive power and frequency control, stability issues are inherently associated to the need for energy conversion through point-of-load converters, which act as instantaneous constant-power loads that introduce the well-known destabilizing effect into the system [26, 27]. Dc microgrid may also complicate addressing arguably the most important present disadvantage of DC systems versus ac systems: the difficulty in clearing fault currents. As is well known, DC currents are difficult to interrupt because, unlike ac currents, DC currents do not have zero crossings that facilitate arc extinction, particularly in systems with voltages over 300V [28, 29].

12

This makes the DC microgrid hard to clear fault current and the implementation of protection circuits. Some other challenges are summarized as below [30, 31]:

● Reengineering of the protection schemes at the distribution level to account for bidirectional power flows.

● Schedule and dispatch of units under supply and demand uncertainty, and DC bus voltage regulation.

● Reliable and economical operation of microgrid with high penetration levels of intermittent renewable energy generation in stand-alone mode of operation.

● Resynchronization with the power grid in a reliable and secure seamless transfer

● Energy management control complexity.

● Lack of standard codes to guide the design, testing and operation of microgrid.

1.2.2   State-of-art-research of DC microgrid

To address the challenges of furthering the development of DC microgrid, the majority of the researcher focus is on the control strategies of the DC microgrid. In the microgrid environment, characterized by having many different time-scale variations in power generation, load demand and by different requirements from electronic-interfaced distributed units, hierarchical control structure is usually adopted to ensure a reliable operation of the whole DC microgrid [13, 15, 16, 32]. The hierarchical control scheme is consisted of two or three layers differentiated by their response time to the system [33], as shown in Figure 8. The primary control in local controller is responsible for power distribution between distributed energy resources (DERs) to avoid circulating current, and control of distributed energy resources (DERs) according to their specific features, such as the maximum power tracking of renewable power generation and the power management of energy storage system. The secondary control is to restore the DC bus voltage

13
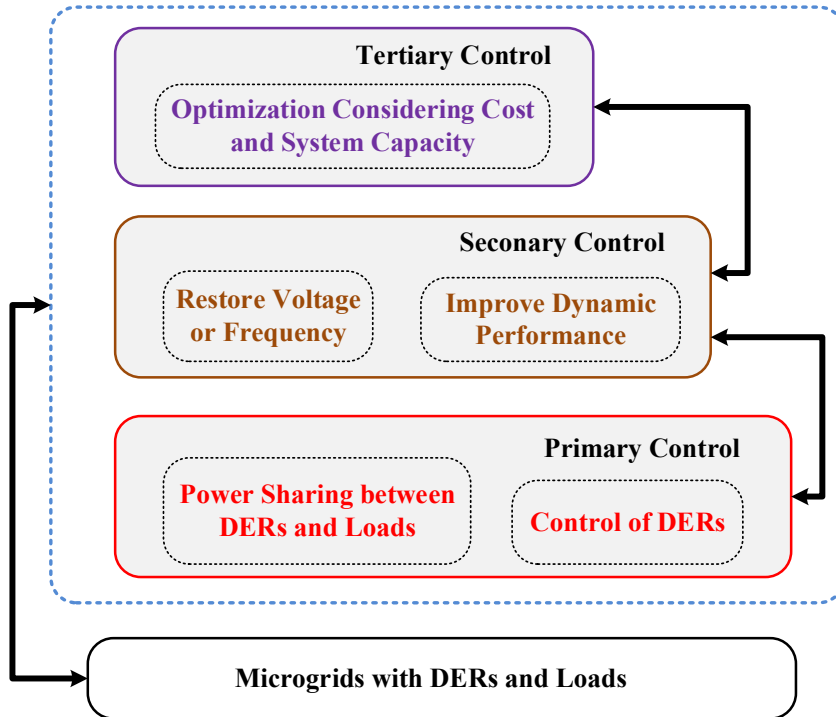
Figure 8 Hierarchy control scheme of microgrids

produced by the action of the primary controller during load change or power variation of renewable resources, while the tertiary control in the top of the hierarchical scheme is to optimize the microgrid operation from the economic and environmental point of views.

1.2.2.1 Primary control loop

Primary control directly dictates the action of the switches in the local power electronics coupled converters, thus this loop has the most important instantaneous influences on the operation of the DC microgrid. However, the primary control applied to the converter itself may not need consider the operation of the microgrid system on the above layer since that is the responsibility of the secondary control loop. Furthermore, the control methods in the primary control loop can be roughly divided into two categories: traditional control methods commonly found in literature

on power electronics converters and the control methods proposed in particularly to address the distinguished features of renewable energy sources (RES) and energy storage system (ESS).

A. Traditional power electronics control methods

The inverter plays a critical role in the DC microgrid by connecting it to the ac grid. The inverter control should not only ensure the seamless transfer of the DC microgrid from the islanded mode to the grid-connected mode and vice versa, but also the reliable and safe operation in the grid-connected mode. The inverter control typically consists of an outer voltage control loop, and an inner current regulation loop. The common design to the control loops is the implementation of proportional–integral (PI) controllers, with additional feed-forward compensation to reject the disturbances from the input voltage or load current [34-36]. Model predictive control with multiple control objectives have been proposed in [37-40] to improve the dynamic performances such as the seamless-transfer and fault ride-through ability of system in study. A general overview of grid-side converter controllers is given in [14], [24], in which controllers are categorized based on their reference frame: synchronous (dq), stationary ($\alpha\beta$), and natural (abc). Upon the safety requirement and the voltage ratings, the inverter can be either transformer-less or transformer-based. High frequency transformer is proposed in [41]. Freedom center proposed the solid-state transformer (SST) to interact with the grid [16]. Compared with the conventional transformer plus rectifier architecture, the SST-enabled [42], but can also potentially supply reactive power, compensate harmonic currents, etc. [43]. Furthermore, it provides an interface for both ac and dc residential grids to the distribution system. Similar control methods such as PI, fuzzy logic, MPC and sliding mode control can also be applied to the DC-DC converters in the DC microgrid.

B. Custom control methods to the converters interfaced with the RES and ESS

While the power electronic-interfaced units dominated in the DC microgrid can enhance the system dynamic performance, they also introduce low inertia side effect that may lead to severe system instability [12]. Energy storage enables large-scale integration of intermittent renewable energy sources with higher efficiency and system reliability [44]. It can also provide a functionality similar to that of the inertia of a synchronous enervator by absorbing surplus power and providing deficit power instantaneously to stabilize the system operation under dynamic changing operating condition. The power management of the energy storage system remains as large as the benefits it may provide. The control challenges include the state of charge (SoC) estimation and discharging and charging balancing algorithms. In some papers, the power managements of the energy storage system is classified into the secondary control loop [12].

1.2.2.2   Secondary control loop

Based on the communication structure of the controllers inside the DC microgrid, the secondary control strategies can be defined as either centralized or decentralized. In centralized control strategies, the central controllers collect all necessary information from the local primary controllers and send back the corresponding control references simultaneously to decide the behavior of each local controller. On the contrary, in the decentralized control strategies, the local controllers determine their own actions by local available measurements. Although heavily dependent on the high bandwidth communication line and thus more vulnerable to single point of failure, the former method enjoys more accurate power sharing, higher efficiency, and thus lower cost because of the easier implementation of optimization algorithms to the cost function with multi-constraints [45-47]. To integrate a mixture of renewable energy sources with different kinds of loads, the decentralized control strategies are the natural choices [31]. Furthermore, with the

16

implementation of modular power converters, the distributed architecture can expand the system capacity gradually as the load increases over time [31, 48].

A. Centralized control strategies

A high-band and reliable communication is usually required for the centralized control to exchange sensed information and control references with every DER and load unit within the dc microgrid. Power or current reference can be determined by many approaches such as master-slave, average load sharing and additional central controller [49]. For the master-slave control, one of the DER converters behaves as the voltage regulator to maintain the output voltage within a permissible range, while others operate as current sources tracking the current/power references given by the master converter controller [50]. Automatic master and rotating master are proposed in [45] to decrease the control dependence on the specified module and to improve the system reliability. For the average load sharing control, the current reference of each distributed converter is determined by the weighted average current of all converters sharing a communication line [51]. This methods can achieve accurate current sharing among distributed converter units, but the communication is crucial and its fault may result in system failure. An additional central controller is proposed in [52] to regulate the voltage in a whole, where each DER converter current are measured and transmitted to the central controller. Then, based on the characteristic of each DER unit, the current/power set points are sent back to determine the contribution of each unit in regulation of the dc bus voltage. This method can increase the system dynamic performance speed, while it is critical rely on the robustness of communication lines.

B. Decentralized control strategies

The decentralized control is dominated by droop control, which originates from the concept of power balance of distributed synchronous generator in large scale power systems. An imbalance

17

between the input mechanical power of the generator and its output electric active power causes a change in the rotor speed which is translated into a deviation in frequency [12]. On the other hand, the mismatch between the output real and command reactive power leads to the deviation in voltage magnitude. These relationship can be expressed as below:

$$\begin{cases} \omega_0 = \omega^* - K_P(P_0 - P^*) \\ V_0 = V^* - K_Q(Q_0 - Q^*) \end{cases} \quad (1)$$

When the droop method being applied to the power electronics interfaced microgrid, the basic principle becomes that, the voltage amplitude decreases with increase of reactive power, and the frequency decreases with the increases of output active power. While, in dc microgrid, there is no ac frequency droop control requirement. As a result, the droop control has been frequently referred to as the autonomous method due to its communication-less characteristics between the power converters and the control is merely based on local measurements. [9, 10, 13, 15, 16, 32, 53-56]. However, in the hierarchical structure a secondary controller is commonly adopted to restore voltage/frequency deviation with a communication line with primary controller [33].

To enhance the current sharing performances in the decentralized droop controlled dc microgrid, a low bandwidth communication based on local area network is required in many papers [9, 10, 53-56]; therefore, these methods are not fully autonomous control. Hierarchy power management of the dc MG system is proposed in [13-16, 32, 57-59] to realize fully autonomous control; however, the parameters of PI controller in different control loops are coupled and thus are hard to tune in this complicated system, which limits the system expandability. Model predictive control of the DC microgrid is found in literature using averaged model [60], which lacks accuracy in guiding practical implementation.

In the literature, the methods applied on the improvement of droop control can be summarized in Table 2.

Table 2 Different improvement droop methods in the literature

References	Methods	Problem to solve
[61, 62]	Virtual powers	P & Q coupling
[63]	Modified voltage method	Line impedance
[64]	Active power injection	Line impedance
[65]	Virtual output impedance	Harmonics and oscillations
[66-68]	Additional control loop	Stability
[14, 69, 70]	Small signal analysis	Stability
[36, 71]	Adaptive droop function	Transient performance
[72, 73]	Virtual inductive impedance	Power sharing inaccuracy

1.2.2.3   Tertiary control loop

The tertiary controller is usually employed in grid-connect mode, since there is not enough response time for the optimization calculation in primary controller and the priority is to react to
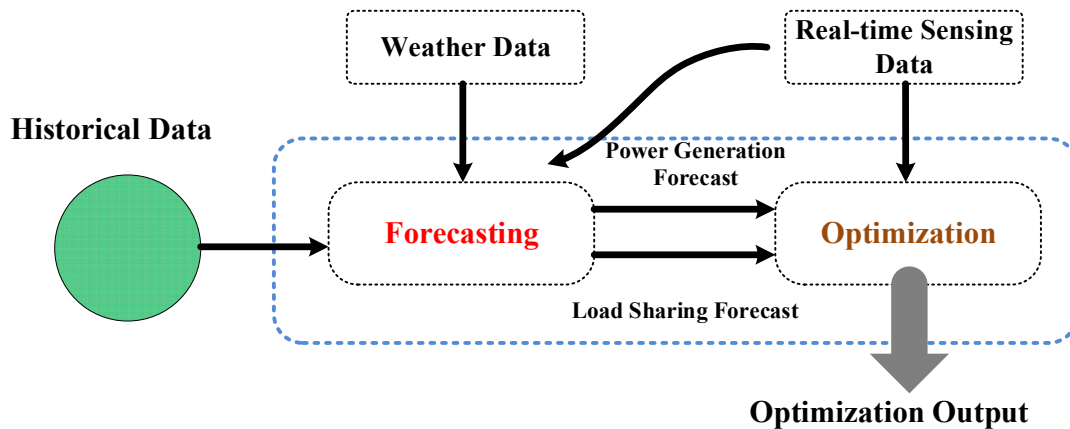
Figure 9 Tertiary control loop with optimization and forecasting

the secondary controller to ensure the stable operation of DC microgrid in islanded mode. In [74], optimal operation is achieved through the emulation of a market environment using a Multi-agent System (MAS), where the local agents (local controllers) first exchange information with a central controller to determine their buying and selling bids then control the individual distributed energy units. The tertiary loop consists of two modules: The Forecasting Module is to forecast the power generation of renewable energy resources and demand of load; the Optimization Module is to run the optimal algorithm to find the optimal system operation parameters. As shown in Figure 9, the Forecasting Module uses weather information and historical data to construct the forecast model [11]. In [41, 75], a neural network model is applied to forecast the renewable resources power productions, with the real-time sensing data. In addition, the neural network can be trained by historical data of weather and power generation. The Optimization Module solves the multi-objective problem to makes optimal decisions to every generation, storage, and sometimes load units, according to estimated generation, demand and market power price. The optimization method in literature includes: the linear programing [76], Genetic Algorithm [77], and Partial Swarm Optimization [78].

According to [12], the tertiary control is responsible for coordinating the operation of multiple microgrids interacting with one another in the system, and communicating needs or requirements from the host grid. Since tertiary control is beyond the control of the DC microgrid itself, this control loop will not be discussed further in this dissertation.

1.3 Research motivation and objectives

Based on the previous research efforts and in light of the development of DC microgrid is still limited to some advanced developed areas, the focus of this dissertation is to explore the unsolved technical problems associated with the DC microgrid by proposing new control strategies

to enable a more wide scale adoption of DC microgrid all over the world. The main objectives of this research project can be summarized in the Figure 10.

1. Control of the power electronics interfaces at the distribution level to account for bidirectional power flows.
2. DC bus voltage regulation with energy storage management
3. Improved Maximum Power Tracking technique
4. Schedule and dispatch of loads under supply and demand uncertainty
5. Supervisory control of Microgrid with high penetration levels of intermittent generation to achieve reliable and wide-scale adoption
6. Control of DC Microgrid in grid-connected mode, such as seamless-transfer ability and double-line ripple minimization

Figure 10 Research objectives of this dissertation

1.4 Dissertation outline

This section gives the structure and main contributions of each sections in this dissertation.

To begin with, **Section 1** presents the background of the DC microgrid including its opportunities and development. Then, the state-of-art research on the control challenges of the DC microgrid is briefly reviewed. As a result, the motivation, objectives and the outline of this dissertation are given.

Subsequently, **Section 2** proposes an improved adaptive perturb and observe maximum power point tracking (MPPT) technique to mitigate the renewable power oscillation around the maximum power point to increase the efficiency and reliability of the DC microgrid system. The purpose of MPPT is to adjust the effective load resistance presented to the PV modules so that the

system operates at the maximum power point (MPP). As such, two requirements must be met by an effective MPPT controller: first, converge to the MPP quickly especially during dynamic weather conditions; second, exhibit small oscillation around the MPP under steady state. Knowing that oscillation will adversely affect the system stability with continuous power ripple, many MPPT propose to adaptive change the variation step according to the power variation. These methods still do not suppress the steady sate oscillations around MPP effectively. As such, this paper proposed an improved adaptive MPPT technique by adding a steady state MPP determination algorithm after the adaptive perturb & observe method, which helps harness more renewable energy with reliable and high-efficiency tracking capability in a DC microgrid. The method is also independent with the environmental conditions and has smaller oscillation around the MPP compared to other adaptive P&O ones. The proposed method is verified by both simulation and experimental results under different irradiance levels and dynamic weather conditions.

While section 2 is limited to the control of single PV systems, **section 3** investigates the control strategies of a DC microgrid consisting of two PV system, one battery storage system and the grid-connected inverter, which operates in islanded mode. Energy storage systems (ESS) are commonly required in microgrids to compensate the fluctuating net power flow from renewable power generators to loads. In this system, the energy generation units are the photovoltaic (PV) and battery power systems. However, the ESS may not function well at all times; each energy generation unit converter should be able to switch between two different modes: current source converter to generate/consume power or voltage source converter to regulate the bus voltage. In order to address these two main challenges, a new autonomous algorithm consisting of two control loops is proposed. The main characteristics of the proposed system are fast dynamic responses to

changes in the ambient condition of PV modules and demand in the system, seamless transfer between modes of operation, and independent control. The primary loop task is the control of each energy unit based on model predictive current control (MPCC), realizing simple controller design and play & plug feature. Thus, the proposed distributed controller enables the system to be expandable by adding additional energy generation units without affecting the existing ones in the system. Moreover, the maximum power point tracking and battery energy management of each energy unit are included in this loop. The secondary loop based on a distributed droop control identifies the operation modes for each converter: current source converter or voltage source converter. The feasibility and effectiveness of the proposed control algorithm are verified under various case studies on dSPACE real-time simulation platform.

Continue from section 3, **the section 4** first introduces the control strategies of a DC microgrid consisting of one PV system, one battery storage system and the grid-connected multilevel packed-u-cell (PUC) inverter, which operates in grid-connected mode. Then, the model predictive control for the grid-connected battery systems with PUC inverter is proposed. Direct-current (DC) microgrids (MG), consisting of distributed renewable energy units and energy storage units, is expected to be the key enabling of future smart grid. The intermittent nature of renewable-energy units, coupled with the unpredictable changes in the load, requires the energy storage units compensate the fluctuating generated power and to regulate the DC-bus voltage. The grid can be considered to be infinite energy storage, so the interfacing inverter is always working under voltage source converter mode and the remaining ones work as current source converter. The novel autonomous algorithm consisting of two layers of control proposed in last section is also applied to this system, achieving good system dynamic, reliable seamless transfer between grid-connected and islanded modes and satisfying decoupling performances. Grid-connected battery charger

systems have been widely implemented in uninterruptible power supplies (UPS) for residential scale systems, where energy storage and bi-directional power flow is required when operating in off-grid condition. In this section, a packed U cells (PUC) seven-level inverter has been selected as the interface between the battery charger and the grid for its low cost and fewer numbers of components. Additionally, PUC has higher energy conversion quality when compared to traditional H-bridge. Compared to traditional PI controller, Model Predictive Control (MPC) is attracting more interest due to its good dynamic response and high accuracy of reference tracking, through the minimization of a flexible user-defined cost function. The proposed MPC technique expects to realize unity power factor, low grid current total harmonics distortion at grid side, and reliable control of bi-directional power flow in the batteries-PUC system, while balancing/tracking the two PUC capacitors' voltages at desired values. The feasibility and effectiveness of the proposed control algorithm was verified under various case studies on dSPACE 1007 real-time simulation platform.

Finally, in **Section 5**, a power decoupling circuit with dual buck converters and two different control strategies are proposed. Single phase inverter and rectifier systems have double line frequency ripple power which is inherent to the ac-side of the circuit but adversely affects the DC-side performance. Typically, an aluminum electrolytic capacitors is placed at the DC side to absorb this power ripple, but reduces the power density and reliability of the converter. Therefore, active decoupling methods have been proposed in the literature to transfer the ripple power to smaller storage components by extra switches to the converter. However, the existing active power circuits are mostly composed of half bridge circuit, which has inherent shoot-through potential problem and could degrade the system reliability. Moreover, the existing active power decoupling methods are normally implemented through

predetermined voltage of storage component using conventional PI control method, which limits the decoupling dynamic performance of the system. In this paper, a novel active power decoupling method based on dual buck circuit and model predictive control is proposed. The dual buck circuit is composed of two separate buck converters operating in each half cycle and two split small DC-link capacitors to eliminate the DC-link voltage ripple. The topology is free of shoot-through and deadtime concern and the control is independent with that of the main power stage circuit, which makes the design simpler and more reliable. By applying model predictive control, the proposed control strategy is proved to have good dynamic performance by both simulation and experimental results.

Section 6 draws the conclusion of the dissertation work and future research directions.

2. MAXIMUM POWER POINT TRACKING TECHNIQUE OF PHOTOVOLTAIC ARRAYS[1]

2.1 Introduction
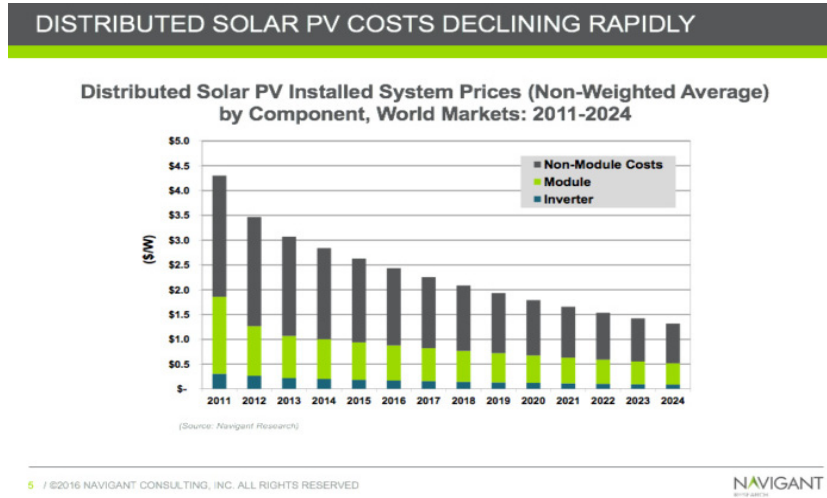
Figure 11 Solar PV costs declining rapidly
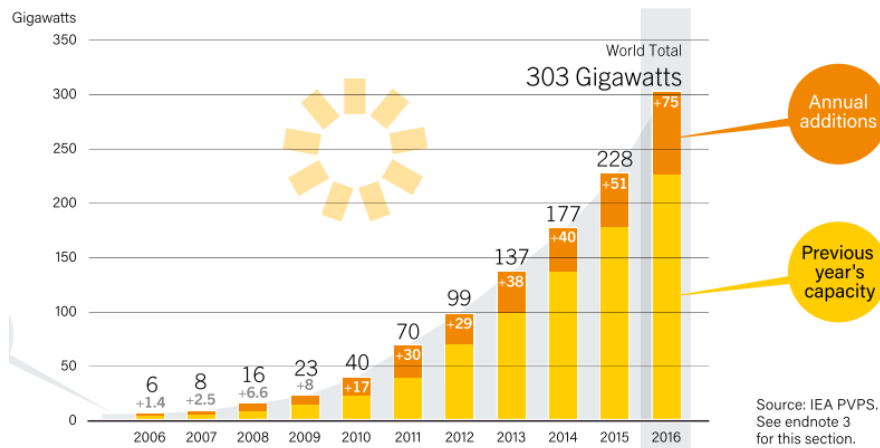
Figure 12 Solar PV installation increasing rapidly

Solar energy, as a prime important component of any renewable energy portfolio, has experienced phenomenal growth in recent years due to technological improvement and cost reduction shown in Figure 11, as well as government policies supportive of renewable energy development and utilization [79]. Solar energy is now an economically viable energy source. Actually, 75 GW of solar PV capacity was added worldwide during 2016 in Figure 12, which is equivalent to the installation of 31,000 solar panels every hour.

To increase the solar energy harvest efficiency of a photovoltaic (PV) panel, a converter/inverter with maximum power point tracking (MPPT) technique is inserted between the
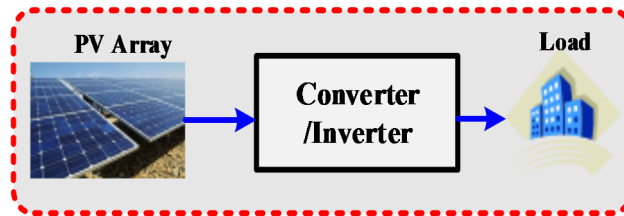
Figure 13 Converter with MPPT interfaces the load to the PV source
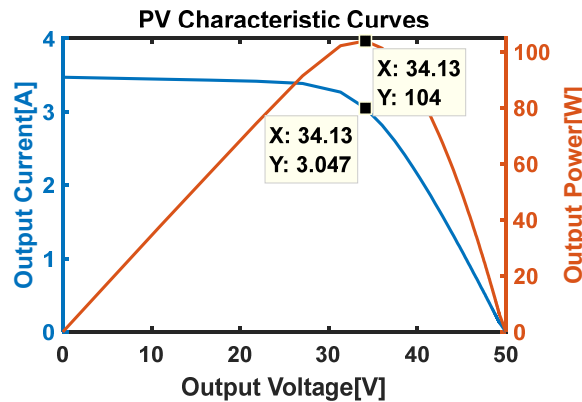
Figure 14 PV *v-i* and *p-v* curves with maximum power point for an example PV module

PV array and the load as shown in Figure 13. The purpose of MPPT is to adjust the effective load resistance so that the Thevenin equivalent circuit transfers maximum power from the PV source

to the load – the so-called maximum power point (MPP). Figure 14 shows the MPP on both the v-i and p-v curves for the PV. The inherent nature of intermittence of PV solar arrays, which is highly dependent on solar irradiation levels and environmental temperature, requires an effective MPPT controller to meet the following two criteria: first, converge to the MPP quickly especially during dynamic weather conditions, second, small oscillation around the MPP under steady state working operations [80].

2.2 Brief survey of typical P&O methods

In the literature, more than 30 different MPPT techniques have been proposed since the early 1980s [81]. Table 3 below lists some representative MPPT methods with their characteristics.

Table 3 Characteristics of representative MPPT methods

MPPT	PV Array Dependent	Complexity	Convergence Speed	Oscillation
Analog PI	No	Low	Low	Med
P&O	No	Low	Fast	High
IncCon	No	Med	Fast	Med
Fractional V_{OC}	Yes	Low	Fast	High
Fractional I_{SC}	Yes	Med	Fast	High
Fuzzy Logic	Yes	High	Fast	Med
Neural Network	Yes	High	Fast	Med

Limited methods are implemented by analog control [82], which suffers slower convergences time compared to those dominated by digital control methods based on Micro-Controller-Units (MCUs). Thanks to the powerful computation capability of MCUs, there are minimal tracking speed differences among these digital control characteristic MPPT methods [83].

Many MPPT techniques have evolved from the perturb and observe (P&O) method due to the ease of implementation and reliable performances [84]. The flowchart of the P&O algorithm is shown in Figure 15. It can be seen that the perturbation step is fixed, thus the steady state oscillation will be proportional to the step size. Larger perturb size achieves faster convergence to the MPP, but smaller size is preferred to limit steady state oscillation, often called ripple [81, 85].

One solution to the tradeoff between convergence speed and the steady state oscillation is to use variable perturbation step size [86-90]. References [87-90] adaptively change the
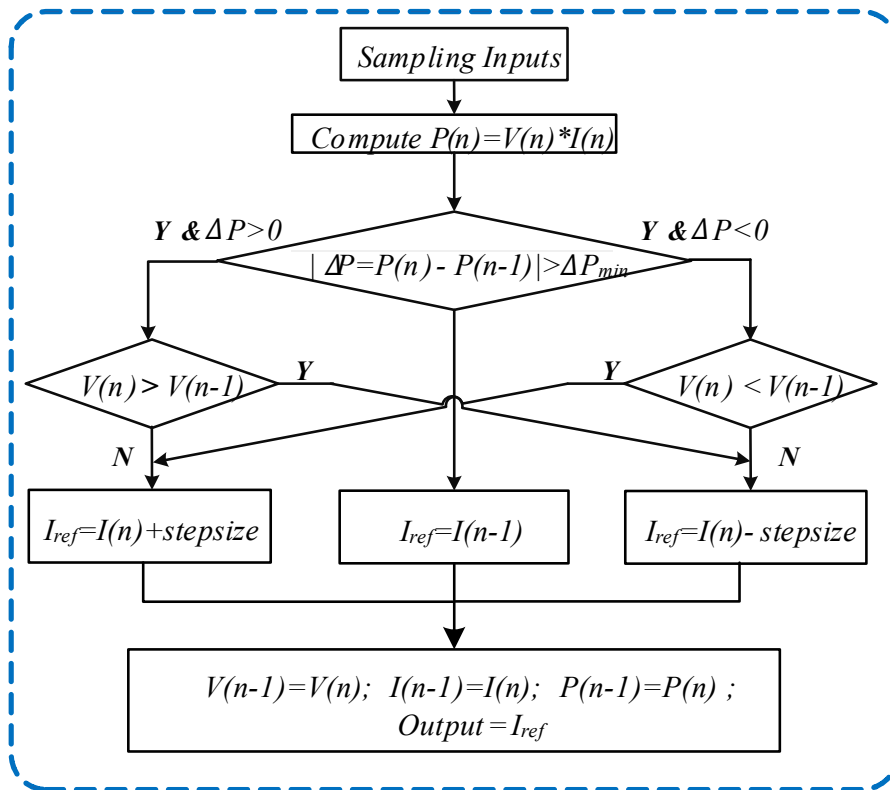
Figure 15 The flowchart of traditional P&O algorithm

perturbation step through a predefined scaling factor S multiplied with a fixed perturbation size, while, reference [86] tune the step size by a PI controller in real-time. Other novel and aggressive methods turn to nonlinear equations, fuzzy logic or neural genetic methods to

address this issue [91-94]. These methods effectively improve the tracking performances compared to the traditional P&O counterparts, while, they need initial environmental or system dependent constant for the scaling factor and PI controller tuning and thus not generic to different PV systems and vulnerable to varying weather conditions. Moreover, some add large computational load on the MCUs which may impair the other paralleling tasks or increase the cost if upgrade needed.

In light of the challenges discussed above, this section proposed an improved adaptive P&O method that has the following advantages:

1. Independent operation regardless of the initial system parameters and the weather conditions;

2. No tracking oscillation under steady-state maximum power point;

3. Simple to implement and low computational load on low-cost controllers.

According to the literature review above in the introduction section, the typical P&O methods can be categorized into the following five groups.

2.2.1 Traditional P&O with fixed perturbation stepsize
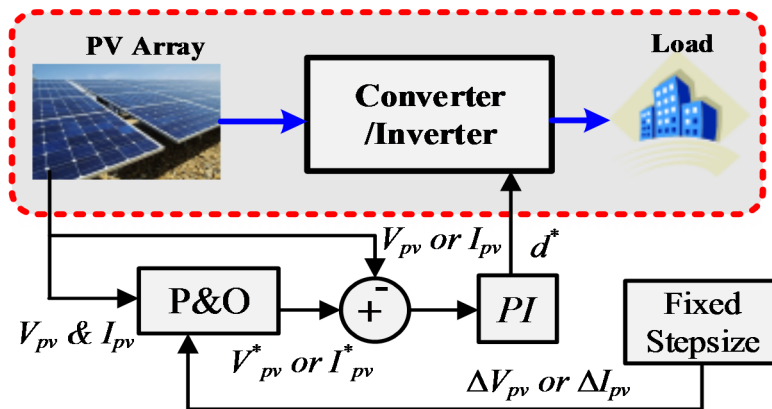
Figure 16 Control blocks of traditional P&O

Since the P-I and P-V curves shown in Figure 14 have both one to one corresponding relationships, either the PV voltage or current can be perturbed by a fixed step-size. The direction of perturbation depends on the power differences between the current P&O calculation cycle and the previous cycle as shown in the flowchart of Figure 15. The fixed step-size is predefined by the user based on previous experiences and thus not generic to other systems and environment parameters. Moreover, the PI controller here need tuning and add extra computational load. Last, this method is well known to have the aforementioned tradeoff between the steady state oscillation and the dynamic convergences time [95]. In Figure 16, the feedback loop ensures that the reference v or i for the PV is being tracked. Equation (1) shows the voltage perturbation (step-size) scheme.

$$v_{ref}(n) = v_{ref}(n-1) \pm stepsize$$

(1)

Table 4 DC-DC Converters Characteristics

DC-DC Converter	Output Voltage	Effective Input Impedance
Buck	$V_{in}*D$	R_o/D^2
Boost	$V_{in}/(1-D)$	$R_o*(1-D)^2$
Buck Boost	$-V_{in}*D/(1-D)$	$R_o*(1-D)^2/D^2$

2.2.2 Modified P&O with fixed perturbation stepsize

If a DC-DC converter is used between the PV array and the load, then, the effective input impedance is only dependent on the real load and the duty cycle as seen in Table 4. Therefore, the duty ratio can be used directly as the perturbation variable instead of the PV output voltage or current carried out in the algorithm of part A. Comparing Figure 17 to Figure 16, this method eliminates the PI block and thus greatly simplifies the controller design [96]. However, the perturbation step-size is still fixed, thus the tradeoff issue remains.

31
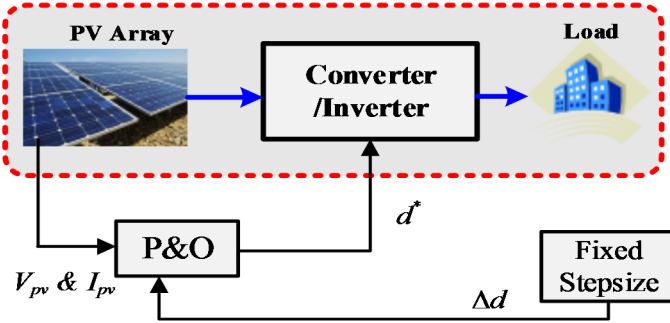
Figure 17 Control blocks of modified P&O

2.2.3 Modified P&O with direct adaptive perturbation stepsize

The tradeoff between the convergence speed and the steady state oscillation can be controlled by a variable perturbation step size [85-89]. Reference [97] initially uses a 10% open-circuit voltage perturbation voltage, then gradually decrease the step-size by half of previous until the MPP is reached. This method is not truly adaptive since the step-size is open-circuit voltage dependent. References [86-89] adaptively change the perturbation step through a predefined scaling factor S multiplied with a fixed perturbation size as shown in Figure 18. These methods though improves the tracking performances greatly under both steady state and dynamics conditions, still need initial system knowledge to predefine the scaling factor S, which can be
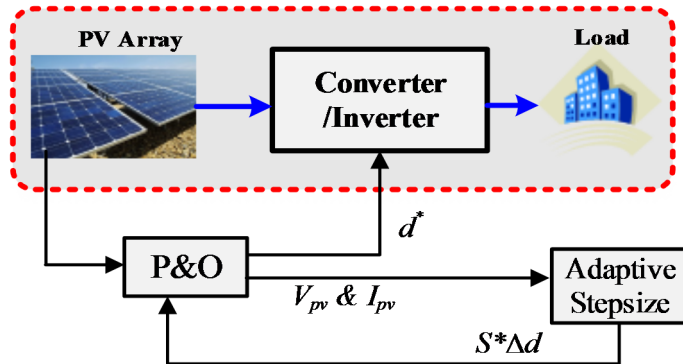
Figure 18 Control blocks of direct adaptive P&O

calculated in (2).

$$d(n) - d(n-1) = S \left| \frac{\Delta P_{max}}{\Delta V_{max}} \right|$$ (2)

2.2.4 Modified P&O with complicated adaptive perturbation

Some novel yet complicated methods using additional PI, fuzzy logic, or neural controllers emerged recently trying to eliminate the shorting comings of system dependent associated with the algorithms aforementioned as shown in Figure 19. Reference [86] tunes the step-size by a PI controller in real-time claiming to be system independent. However, the current PI parameters may
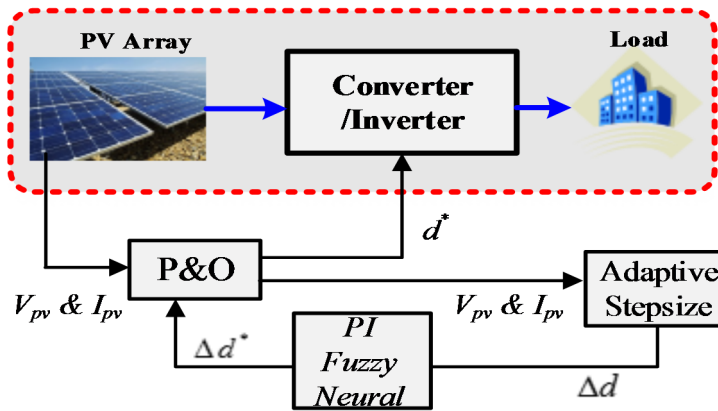
Figure 19 Control blocks of complicated adaptive P&O

not necessarily work well when the environmental conditions vary dramatically. The fuzzy logic and neural logic may help decrease the sensitivity of algorithm to the environmental changes [91-93], the complexity of implementation and heavy computational burden increases cost and hinders its use in a widely range.

2.3 Proposed improved P&O with adaptive perturbation stepsize

In review of the methods introduced above, they achieve acceptable performance regarding the tradeoff of MPPT steady state and dynamic conditions at the cost of heavy computational load or at the penalty of system/environmental parameters dependent. This motivates the author to

propose a system independent P&O MPPT with simple adaptive perturbation, which will be discussed below.

2.3.1 Adaptive Perturbation Stepsize Generation

A study of experimental P–D and P–V curves and their derivatives indicate that the derivatives are uniquely suitable for step size after proper scaling. They meet the requirement for the step size, which should ideally be large when the operating point is away from the MPP, and monotonically decrease as the MPP is approached. Reference [88] indicates that the derivative of power to voltage varies more smoothly as compared to the derivative of power to duty cycle. Thus, in the present system, $\Delta P/\Delta V$ is used as the scaling parameter for the step change in the duty cycle [88]. The adaptive perturbation of duty cycle is the same as the equation proposed in [88]:

$$d(n) = d(n-1) \pm S \left| \frac{p(n) - p(n-1)}{v(n) - v(n-1)} \right|$$

(3)

where scaling parameter S is calculated according to (4) in [88].

$$S = \frac{\left| \Delta V_{max} \right| \left| \Delta D_{max} \right|}{\left| \Delta P_{max} \right|}$$

(4)

2.3.2 Steady State MPP Determination Algorithm

Though the P&O method with adaptive duty cycle perturbation speeds up the dynamic tracking performances, there is still steady state oscillation around the MPP which may cause continuous DC ripple and affect the reliability of the system. Thus, a steady state MPP determination algorithm is proposed to eliminate the oscillation. The core idea is to compare the difference of two calculated consecutive duty cycle with a small constant ε_1 to determine the current working operation. The following procedures describes the algorithm:

34

1) Sense the PV arrays V(n) and I(n) and then through a low pass filter to eliminate the high frequency switching noise, where n refers to the present sampling instant;

2) Calculate both the previous and the current instant PV power:

$$\begin{cases} p_{pv}(n-1) = v_{pv}(n-1) * i_{pv}(n-1) \\ p_{pv}(n) = v_{pv}(n) * i_{pv}(n) \end{cases} \tag{5}$$

3) Perturb the duty cycle according to the (3-4) to generate the initial reference duty cycle

$$d(n) = d(n-1) \pm S \left| \frac{p(n) - p(n-1)}{d(n) - d(n-1)} \right| \tag{6}$$

4) Compare *d(n)* with *d(n-1)* to determine whether the system tracks the MPP and begins oscillation. If the errors between two consecutive duty lies within the ε_1, the system will realize that the PV has already work around the MPP region. Then, the current d(n) will become the fixed duty reference sent to the controller.

$$if \quad |d(n) - d(n-1)| < \varepsilon_1 \tag{7}$$

Where ε_1 is a small enough value predefined

5) If MPP reaches, then set *flag =1* and lock the current duty and voltage

$$\begin{cases} v_{lock} = v_{pv}(n) \\ d_{lock} = d_{ref}(n) = d(n) \end{cases} \tag{8}$$

6) Compare V_{lock} with *V(n)* to determine whether the MPP moves due to environmental changes

$$if \quad |v_{lock} - v(n)| > \varepsilon_2 \tag{9}$$

where ε_2 is a small enough value predefined

7) If MPP moves, then set *flag =0* and output the initial reference duty cycle *d**.

35
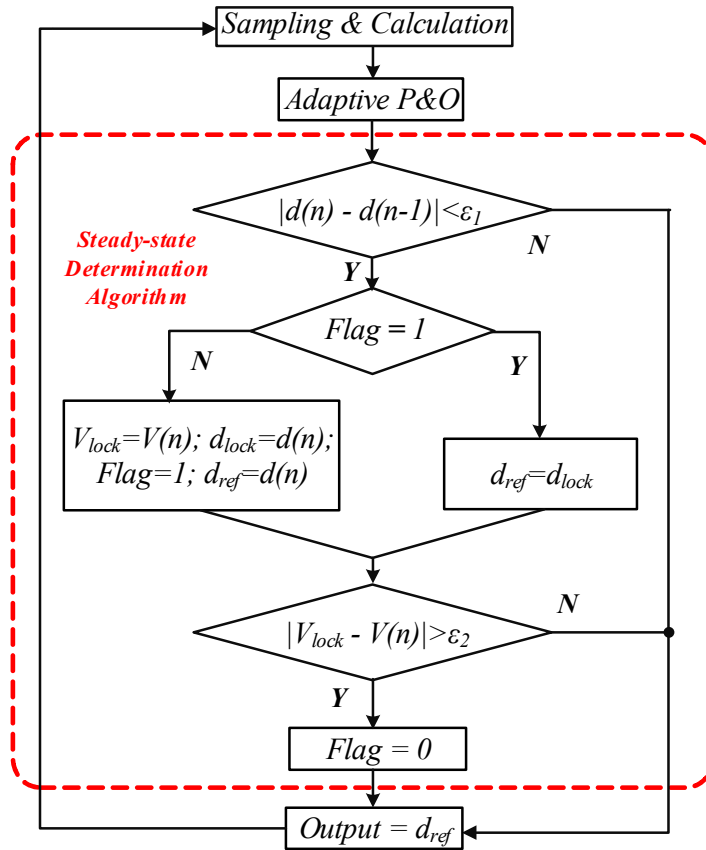
Figure 20 Flowchart of steady state determination algorithm

Figure 20 summarizes the above steps in a flowchart.

2.4   Simulation and experimental results

The system is simulated in Matlab-Simulink. The P&O algorithm is implemented in a 500Hz window with a switching frequency of 50 kHz. Three case studies are analyzed to evaluate the system performance from the proposed algorithm under both steady state and dynamics weather conditions. The comparison of the traditional adaptive P&O technique and the proposed adaptive P&O one are performed through simulation under two different solar irradiance.

2.4.1 Case Study I — simulation results of steady-state operation under 1000W/m² solar irradiance

From the Figure 21and Figure 22, it can be easily seen that the proposed adaptive MPPT technique with MPP determination algorithm can track the desired maximum power point effectively with comparably smaller ripple than the traditional adaptive P&O method.
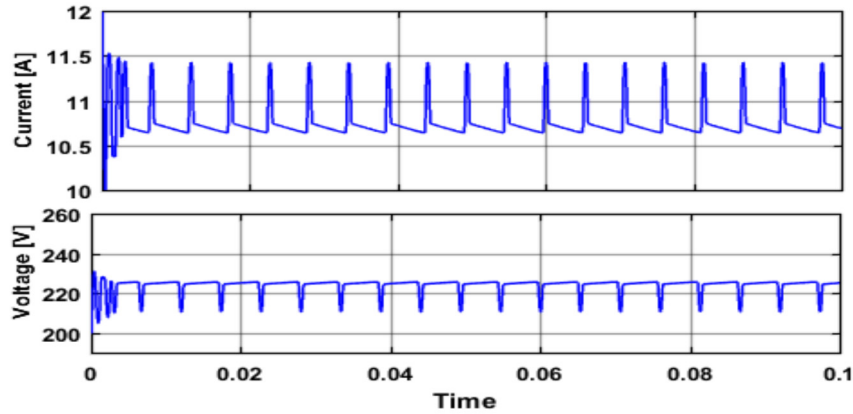
Figure 21 PV voltage and current under steady state by traditional adaptive P&O method at 1000W/m² solar irradiance
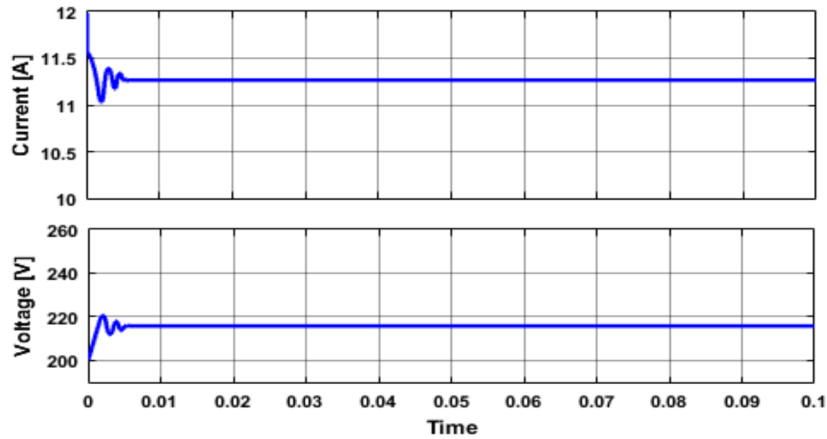
Figure 22 PV voltage and current under steady state by proposed adaptive P&O method at 1000W/m² solar irradiance

2.4.2 Case Study I — simulation results of steady-state operation under 400W/m² solar irradiance

Compare the Figure 23and Figure 24, it can be easily seen that the proposed adaptive MPPT technique with MPP determination algorithm can track the desired maximum power point effectively with comparably smaller ripple than the traditional adaptive P&O method.
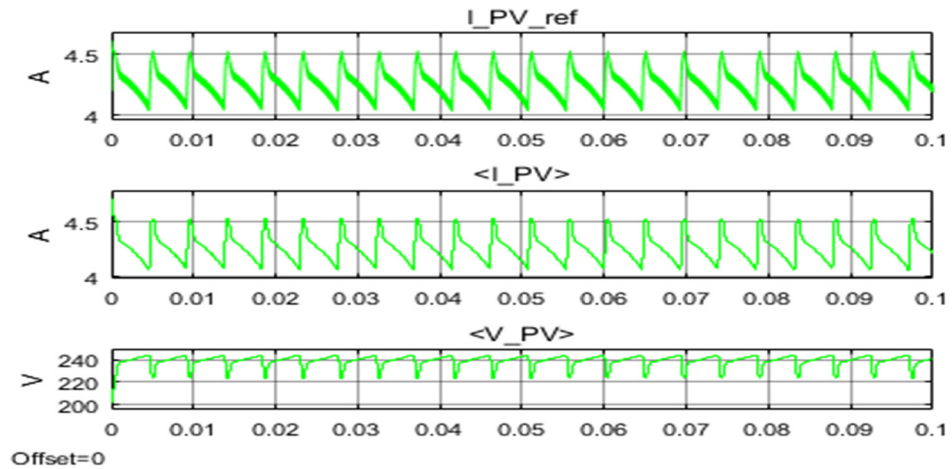
Figure 23 PV voltage and current under steady state by traditional adaptive P&O method at 400W/m² solar irradiance
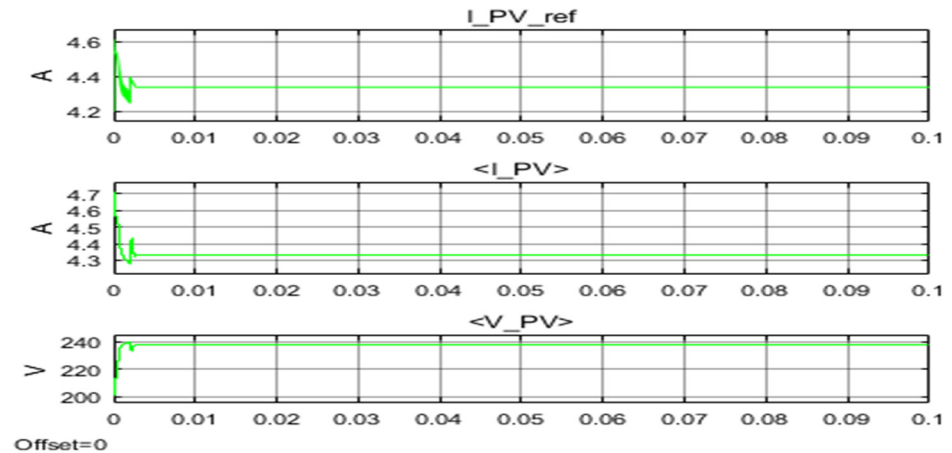
Figure 24 PV voltage and current under steady state by proposed adaptive P&O method at 400W/m² solar irradiance

2.4.3 Case Study II — simulation results of dynamic operation under changing solar irradiance

To verify the dynamic performance of the proposed method, considering that the PV industry test standard for the change rate of solar irradiances is 10 seconds, this paper examines this solar changing effect on the proposed algorithm according to the profile in Figure 25 and
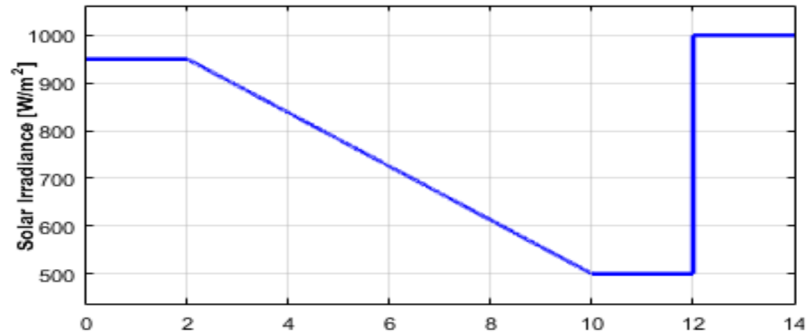
Figure 25 Solar Irradiance changing profile
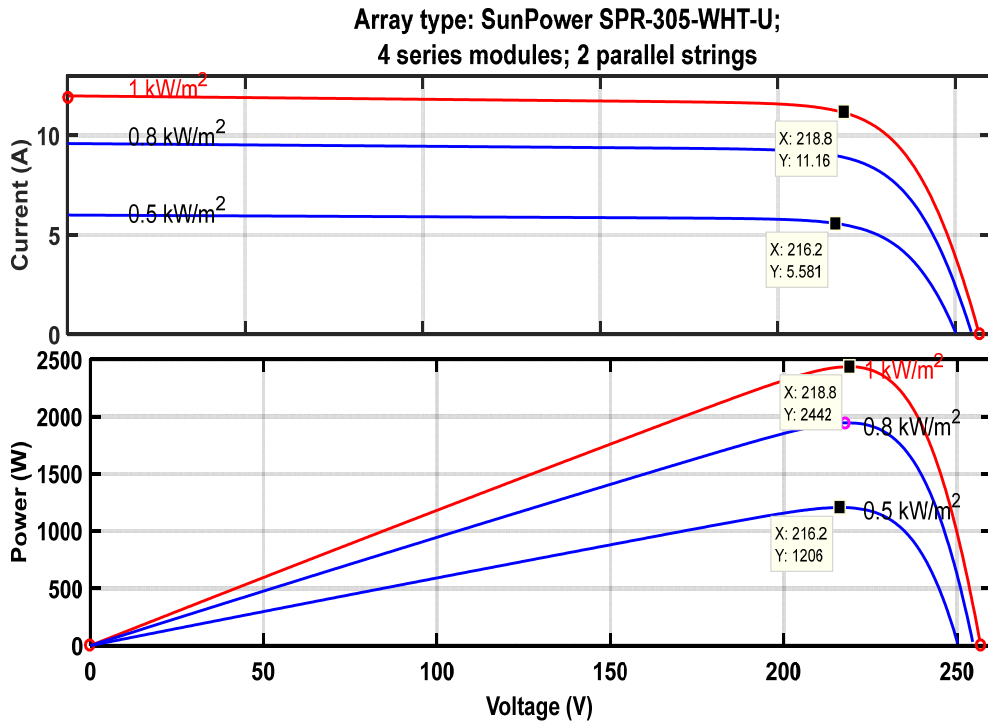
Figure 26 Maximum power point at different solar irradiance

Figure 26. The simulation results with traditional perturb and the proposed adaptive one are shown in Figure 27and Figure 28.
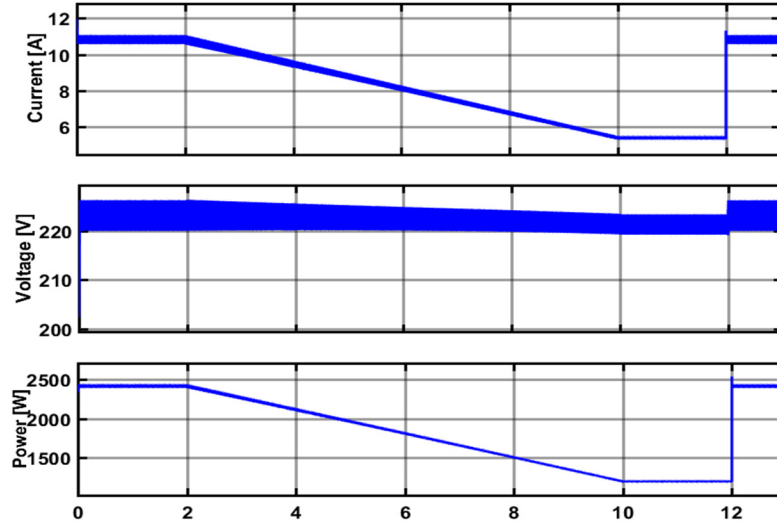
Figure 27 PV voltage, current and power under dynamic changing solar irradiance using traditional adaptive P&O method
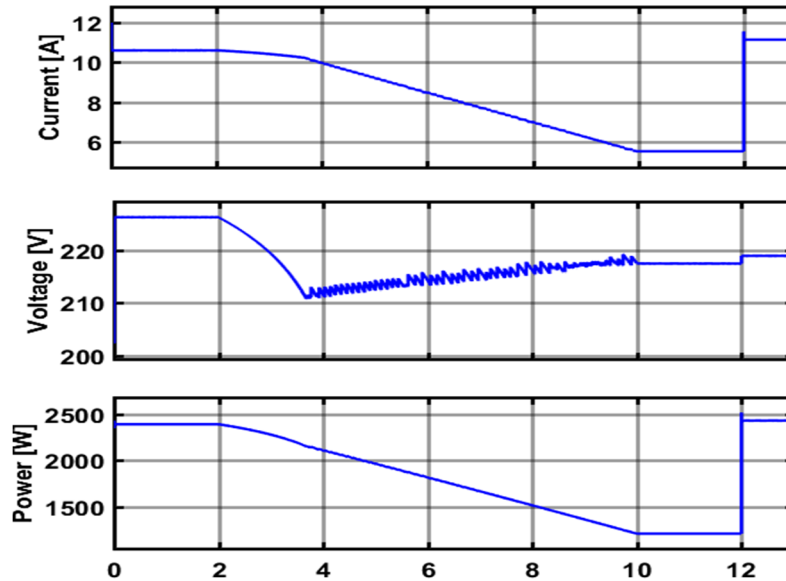
Figure 28 PV voltage, current and power under dynamic changing solar irradiance using proposed adaptive P&O method

In the Figure 25, the solar irradiance begins declining from 950 W/m^2 at 0.2s to 500 W/m^2 at 10s. And then steps up to 1000 W/m^2 at 12s. Though both technique track the maximum power point accurately within 5% error, the current and power ripples of the PV module controlled by the proposed method are comparably smaller, since the steady state tracking points are locked by the proposed adaptive perturb technique.
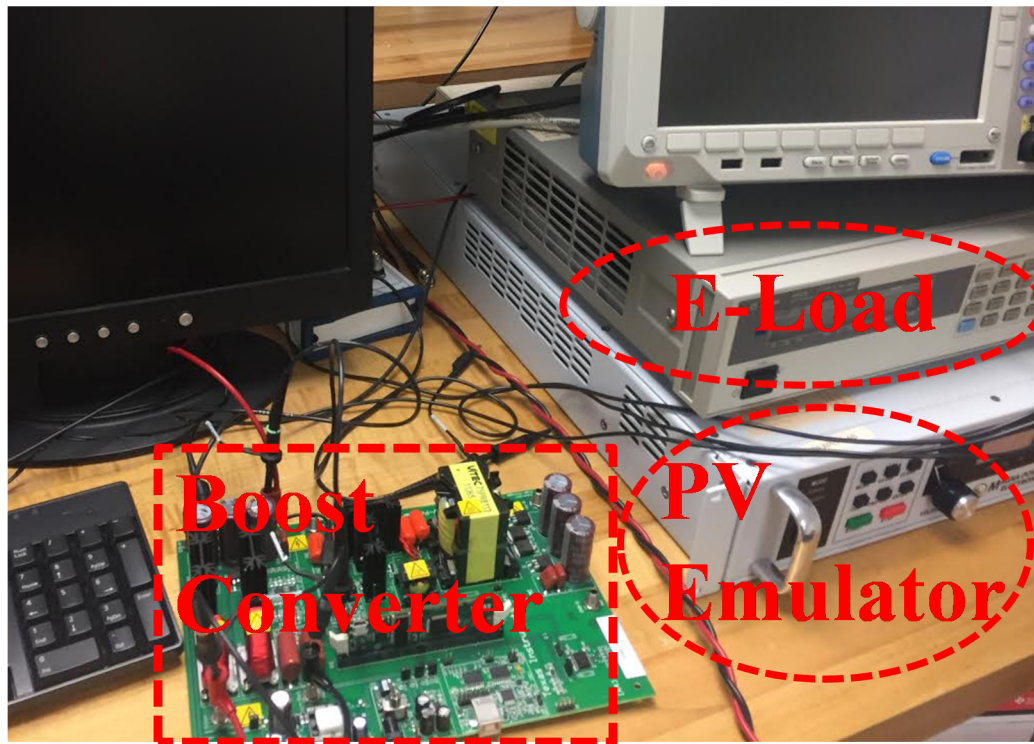
Figure 29 Setup of the experimental verification

2.4.4 Case Study III — experimental results of steady-state operation under constant solar irradiance

The experimental setup is shown in Figure 29 and parameters provided in Table 5. Figure 30 shows the effectiveness of maximum power point tracking of the proposed P&O method in experiment. Moreover, the smaller oscillation around the maximum power point is verified by the experimental result of Figure 31, which shows the PV current and voltage ripples before are only

one fourth and one-third of the respective one after the activation of the proposed technique at half time

2.5 Summary

Demonstrated by the comparisons above, it can be concluded that the proposed technique can help harness more renewable energy with reliable and high-efficiency tracking capability. The method is verified to be independent with the environmental conditions and also has smaller oscillation around the MPP compared to other adaptive P&O methods proposed in previous papers.

Table 5 System parameters of PV converter

Parameter	Value
PV Voc	200 V
PV Isc	1.0 A
PV Vmp	144 V
PV Imp	0.8 A
PV maximum power point	115 W
Switching Frequency	50 kHz
MPPT implementation window cycle	500 Hz
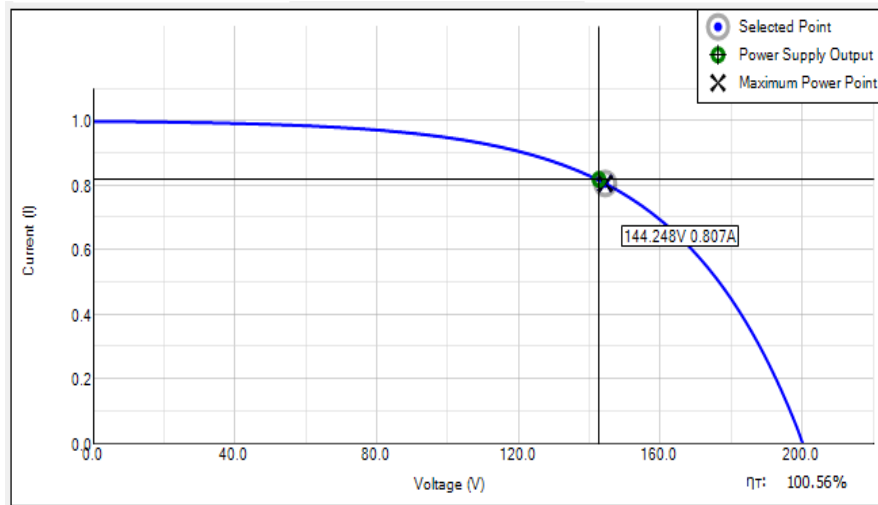
Figure 30 PV emulator V-I curve working on the maximum power point

The core idea of the approach can also be applied to many other applications where system time constant are large.
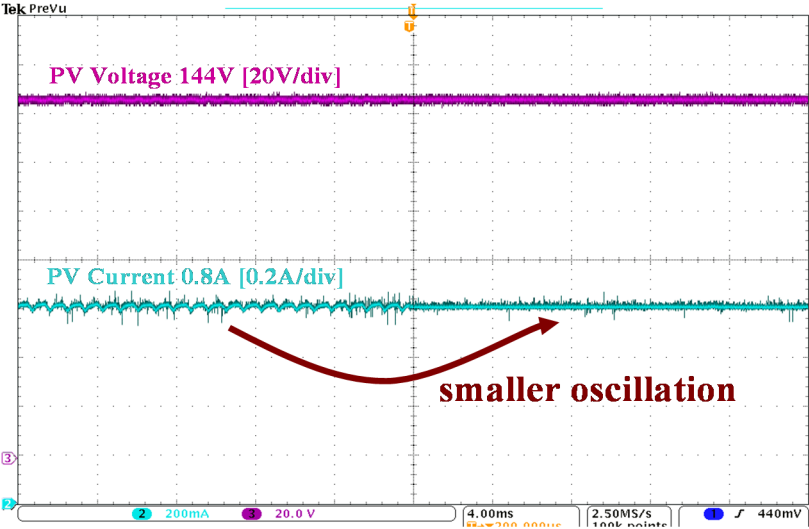
(a) Dc coupled waveform
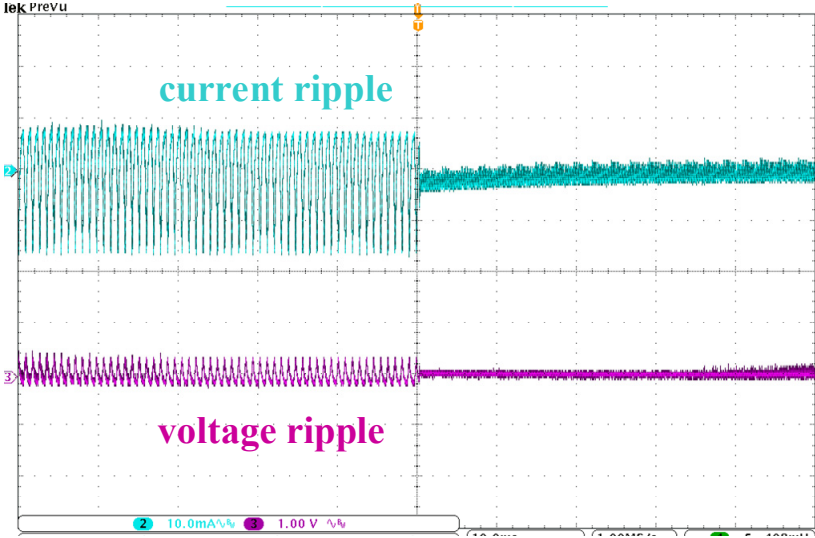
(b) Ac coupled waveform

Figure 31 Smaller oscillation around the MPP when controller changes from traditional adaptive P&O to the proposed one

3. CONTROL STRATEGIES OF DC MICROGRID IN ISLAND MODE[2]

3.1 Introduction
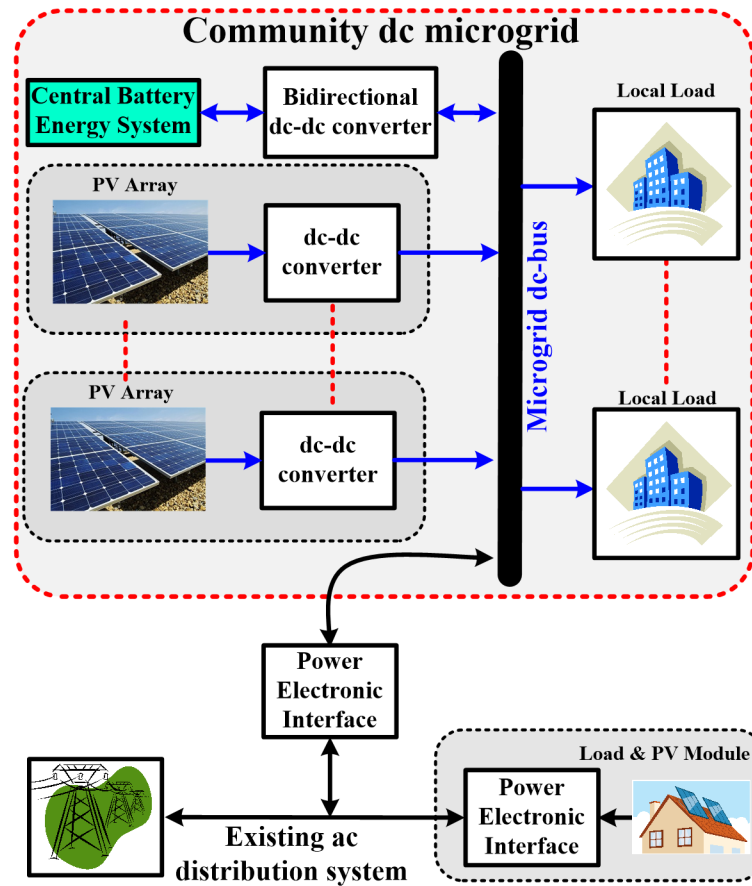
Figure 32 One-line diagram of the REAPER LAPES.

The DC microgrid system with PV arrays and centralized energy storage system, as illustrated in Figure 32, proposed as a Local Area Power and Energy System (LAPES) [4] by the

---

2 © 2017 IEEE. Reprinted, with permission, from S. Xiao, M B. Shadmand, R S. Balog, Haitham Abu-Rub, "Model Predictive Control of Multistring PV Systems with Battery Backup in a Community DC Microgrid" Applied Power Electronics Conference and Exposition (APEC), Tampa, FL, USA, 2017 IEEE.
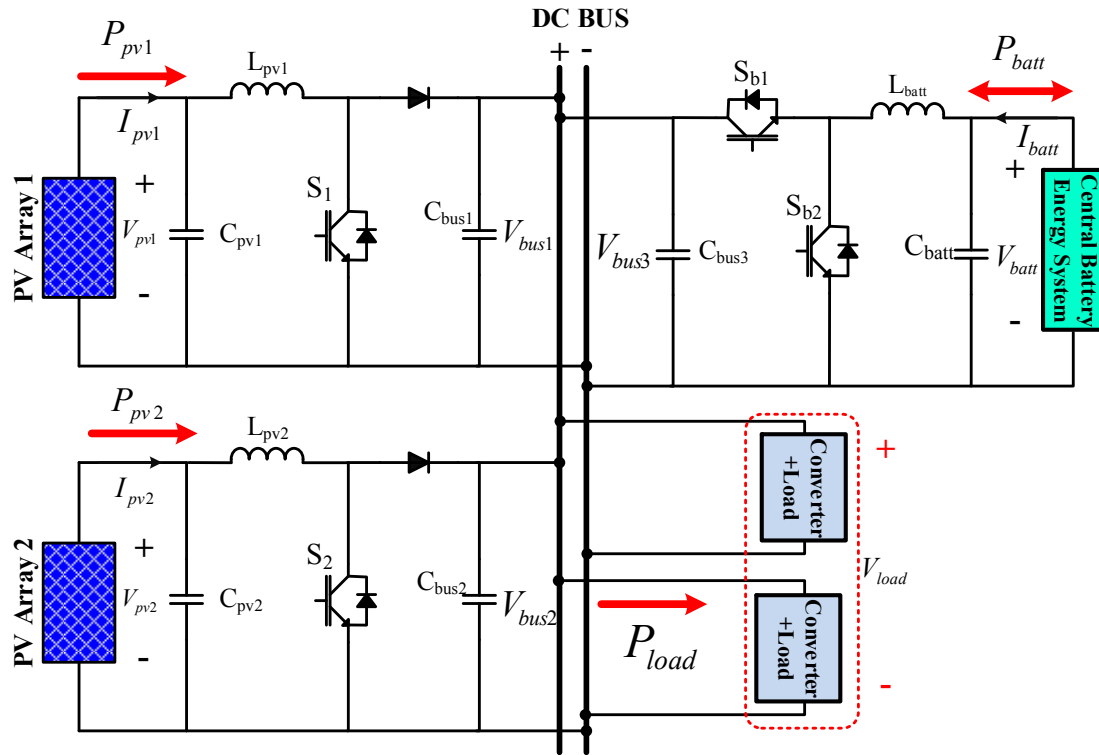
Figure 33 System schematic in islanded mode

Renewable Energy and Advanced Power Electronics Research (REAPER) lab, is an attractive technology solution for residential communities to "go green" while simultaneously ensure reliable electricity. The power electronic interface between utility-power grid and the community DC microgrid could also be the solid-state transformer [5] being developed by the FREEDM Center at the NC State. The power conversion stage of the DC microgrid system includes DC-DC converters to extract the maximum available power from the PV arrays and a bidirectional DC-DC converter for charging and discharging the battery system. A certain amount of power fluctuation can be mitigated using battery-based energy storage [6] to absorb surplus power and provide deficit power instantaneously to stabilize system operation under dynamic changing operating conditions. Previous studies demonstrate that additional mitigation of fluctuation in

power generated from PV arrays can be achieved by distributing the PV arrays in a community DC microgrid [7]. The control, management, optimal power flow between the distributed PV and storage systems illustrated in Figure 33 is critical to achieve efficient systems with high energy availability for local loads.

The control strategies for such a DC microgrid can be classified into two categories in the literature: centralized control and decentralized control [8-22]. Since the centralized control relies on the critical communication line between the central controller and the corresponding converter primary controllers, the system is limited by the high cost of communication setup and vulnerability to communication failure. On the contrary, decentralized or autonomous control employs the droop control to help regulate the bus voltage at the cost of some DC bus voltage variations. This method removes the critical communication lines, fits the distributed nature of DC MG, and thus is given more attention than the previous one in the research. To enhance the current sharing performances in the decentralized droop controlled DC MG, a low bandwidth communication based on local area network is required in many papers [8, 9, 11, 14, 19, 21]; therefore, these methods are not fully autonomous control. Hierarchy power management of the DC MG system is proposed in [10, 12, 13, 15, 16, 18, 20, 22] to realize fully autonomous control; however, the parameters of PI controller in different control loops are coupled and thus are hard to tune in this complicated system, which limits the system expandability. Model predictive control of the DC microgrid is found in literature using averaged model [17], which lacks accuracy in guiding practical implementation.

To achieve a highly efficient and reliable DC microgrid with distributed PV and battery systems, this section proposes to combine the features and advantages of model predictive control and distributed droop control into a hierarchy and fully autonomous control of the DC microgrid

while considering practical implementation [98]. The proposed control on the DC microgrid is implemented by using detailed switch model and is verified by real-time simulation under various cases in islanded mode. The primary controller is based on the model predictive control of input source current. Direct current control combined with the characteristics of model predictive control ensures fast dynamic responses to load and input power disturbances. With the converter parameters already known in the controller, no further tuning is needed when compared with the traditional PI controller, which not only simplifies the system design procedure but also enables the play & plug feature of each distributed energy converter unit. Furthermore, the characteristics of different distributed energy sources are also considered in this loop of control. Specifically, the PV converter can track the maximum power point current under varying environmental conditions, and the battery converter takes consideration of the battery energy management in various working scenarios. The secondary controller is based on the proposed distributed droop control to coordinate the power generation within the DC MG. Each converter can either work as current source mode or voltage source mode, depending on the power availability from the source and the power demand from the load. The proposed distributed droop control determines the working mode for each converter depending on the DC bus voltage level, which eliminates the high-bandwidth communication requirement in many existing literature to achieve a robust autonomous control of the DC MG.

3.1.1 System configuration

The DC MG should work normally with grid-connected mode and shift to islanded mode when the grid fault happens. To examine the proposed control on this two operation modes of DC MG, their schematic diagrams working under each mode are shown in Figure 33, respectively. The design parameters are also summarized in the Table 6 and Table 7. The power ratings for each

converter is scaled down to show the concept of proof. The elements in the system can be categorized into four main groups: renewable energy sources, battery storage sources, utility grid and local loads. To simplify the discussion, only two PV array converters are present to show the

Table 6 PV Converter Parameters.

Parameter	Value
inductor	4mH
inductor DC resistance	0.2Ω
input capacitance	470uF
output capacitance	1130uF
capacitance ESR	0.1Ω
mosfet ratings	650V/20A
diode ratings	650V/20A
converter power rating	3kW
DC bus range	320-460V
sampling time	20us

Table 7 Battery Converter Parameters

Parameter	Value
inductor	1.5mH
inductor DC resistance	0.1Ω
input capacitance	470uF
output capacitance	1130uF
capacitance ESR	0.1Ω
mosfet ratings	650V/20A
converter power rating	3kW
battery rated capacity	6.5A/h
DC bus range	320-460V

effectiveness of the proposed distributed control and the idea of play & plug feature. This configuration allows the DC MG to be expandable with those modular designed converters.

In the islanded mode shown in Figure 33, two DC-DC boost converters are used for extracting the maximum power from each PV arrays and transferring to the DC-bus; a DC-DC converter is used for interfacing the battery bank to the DC-bus with bidirectional power flow. To regulate the DC bus voltage as well as decrease the voltage variation, one of the three converters will be chosen as the voltage source converter. Thus, the remaining ones may work as current source converters to either harvest the maximum power from the PV arrays or charging/discharging the battery units in constant currents.

The novel autonomous control strategy proposed for this system, which helps optimize the system performance and minimize the communication bandwidth requirement, will be introduced.

The rest of the section is organized as follows. Section 3.2 briefly introduces Model Predictive Control (MPC) technique. Section 3.3 describes the proposed primary loop based on the MPC and its application to the PV and battery bi-directional converters while taking into consideration the maximum power point tracking and battery energy management. Section 3.4 discusses the proposed secondary loop based on the distributed droop control and the control diagrams for the PV and battery converters. Section 3.5 shows the simulation and real-time experiment results of different case studies carefully considering all possible working scenarios. Section 3.6 concludes the whole section.

3.2 Model predictive control techniques for power electronics

The power electronics applications which are controlled by model predictive control (MPC) dates back to the 1980s considering high-power systems with low switching frequency [99, 100]. Since high switching frequencies for the MPC algorithm required long calculation time,

widespread adoption was not feasible at that time. With the development of fast and powerful microprocessors, interest in the application of MPC in power electronics has increased considerably over the last decade [101-106].

The main characteristic of MPC is predicting the future behavior of the desired control variables [100, 101] until a specific time in the horizon. The predicted control variables are used to obtain the optimal switching state by minimizing a cost function.

One of the major advantages of predictive controllers is that the concept is simple and straight forward to implement as an example finite control set MPC for two-level converters.

3.2.1 Basic principle

The MPC for power electronics converters can be designed using the following steps [101]:

1. Modeling of the power converter identifying all possible switching states and its relation to the input or output voltages or currents.

2. Determine the discrete-time model of the control variables for predicting their future behavior.

3. Design the cost function, subject to minimization, which demonstrates the preferred behavior of the power converter.

The model used for prediction is a discrete-time model which can be presented as state space model as follow [100]:

$$x(k+1) = Ax(k) + Bu(k) \tag{1}$$

$$y(k) = Cx(k) + Du(k) \tag{2}$$

A cost function that takes into consideration the future states, references, and future actuations can then be defined as:

$$g \;=\; f\left(x\left(k\right), u\left(k\right), \cdots, u\left(k + N - 1\right)\right) \tag{3}$$

The defined cost function g should be minimized for a predefined horizon in time N; the result is a sequence of N optimal actuations:

$$u(k) = \begin{bmatrix} 1 & 0 & \cdots & 0 \end{bmatrix} \arg \min_{u} g \tag{4}$$

At each sampling time the optimization problem is solved again by using new set of measured data to obtain a new sequence of optimal actuation. The MPC principle of working is illustrated graphically in Figure 34.

3.2.2 Controller design
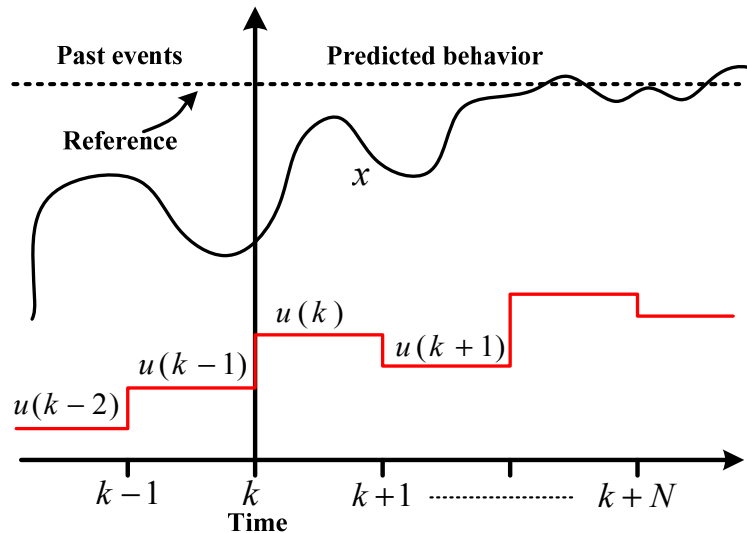
Figure 34 Principle of Model Predictive Control (MPC)

In designing the MPC for a power converter, the basic element is the power switch. Considering ideal operation of common power switches such as MOSFET, they have two states, i.e. "ON" and "OFF". The number of combinations of switching states minus the practical-impossible states is the total number of switching states. These practical-impossible switching

states are the ones that may cause fault conditions, say, short-circuit. Generally, the number of switching states *NSS* is determined as following

$$NSS = \chi^{NP} \tag{5}$$

Where χ is the number of possible states of each phase or leg of the power converter and the number of phases or legs is presented by *NP*. As an example, a three phase, three level converter has 3^3=27 switching states.

Discrete-time model of the control variables should be considered in order to determine their predicted values in future sample time. Several discretization methods exist to determine the discrete-time model of the system. Euler forward method can be used to approximate the derivatives:

$$\frac{dx}{dt} = \frac{x(k+1) - x(k)}{T_s} \tag{6}$$

Where T_s is the sampling time. For higher order system, Euler forward method does not have accurate approximation and the error is higher for these systems. Thus an exact discretization should be used.

The control requirement such as torque, current and power can be included in a single cost function, *g*, subject to minimization. One of the main advantages of MPC is that characteristics where several control variables with different nature and units can be included into single cost function. Each term in the cost function is multiplied by a weight factor to deal with units and magnitudes of the control variables.

Weight factors in the cost function in addition to accommodation of different units and scales, enable prioritization of specific control variables. However, selection of these weight

factors is not straight forward [100]. Several empirical approaches to determine a fix weight factor using trial and error have been investigated in the literature [107].

The general scheme of MPC for power electronics converters is illustrated Figure 35 [101]. In this scheme measured variables, $X(K)$, are used in the model to calculate predictions, $\widetilde{X}(K+1)$, of the controlled variables for each one of the N possible actuations, that is, switching states, voltages, or currents. Then these predictions are evaluated using a cost function which considers the reference values, $X^*(K+1)$, design constraints, and the optimal actuation, S, is selected and applied to the converter. The general form of the cost function, g, subject to minimization can be formulated as

$$
\begin{aligned}
\min g = \lambda_1 \left| \widetilde{X}_1^{\sigma \in \{1:m\}}(k+1) - X_1^*(k+1) \right| + \\
\lambda_2 \left| \widetilde{X}_2^{\sigma \in \{1:m\}}(k+1) - X_2^*(k+1) \right| + \\
\cdots + \lambda_n \left| \widetilde{X}_n^{\sigma \in \{1:m\}}(k+1) - X_n^*(k+1) \right|
\end{aligned}
\tag{7}
$$

Where λ is the weighting factor for each objective. To select the switching state which minimizes the cost function g, all possible states are evaluated and the optimal value is stored to be applied next. The power converter can be from any topology and number of phases, while the generic load
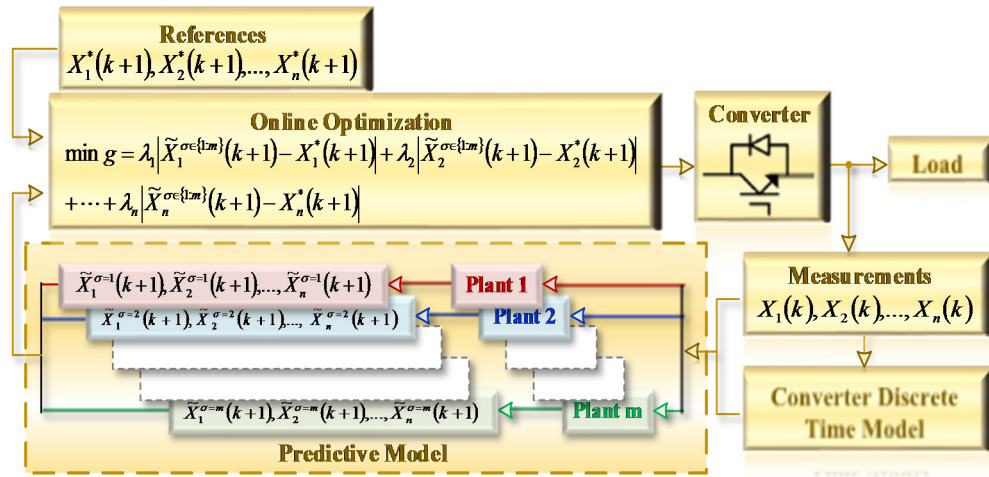
Figure 35 MPC general schematic for power electronics converters

53

shown in Figure 35 can represent an electrical machine, the grid, or any other active or passive load.

3.3 Primary controller based on model predictive control

The primary loop directly indicates the action of the power MOESFETs in the DC-DC converters, so the control method employed on this loop determines the DC MG performance
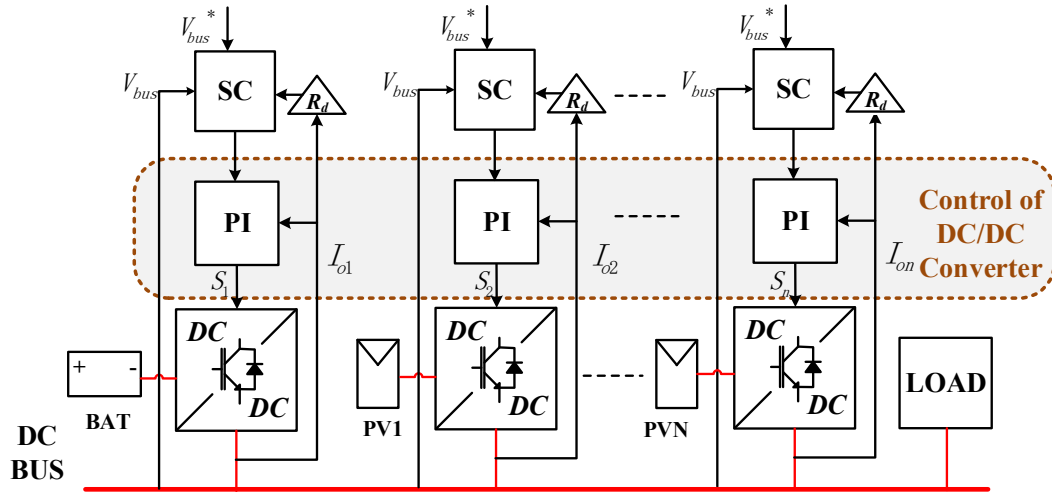
Figure 36 Traditional primary control
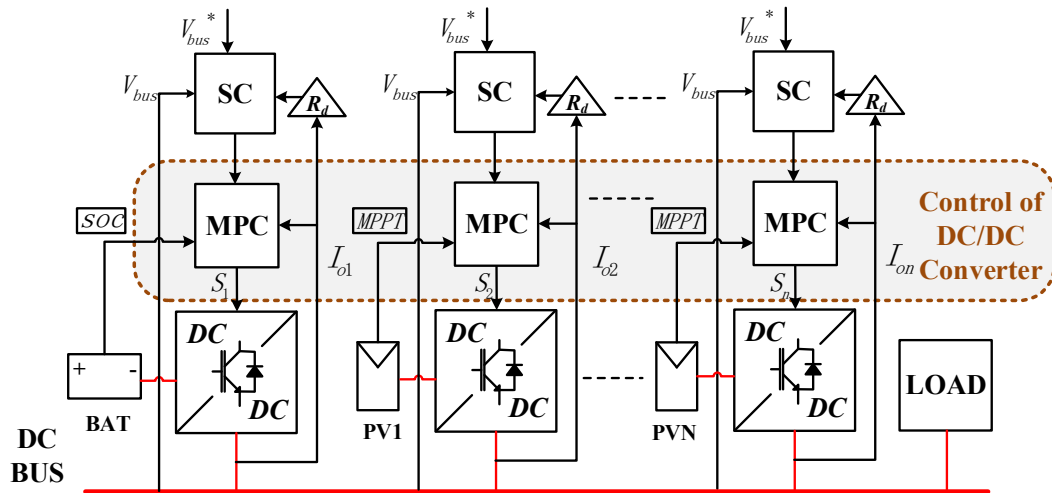
Figure 37 Proposed primary control

largely. To meet the expandability requirement of future DC MG, the converter should have the

play & plug feature. It is observed that the DC-DC converter module used only has one freedom of control. The traditional PI controller needs time-consuming tuning and is used extensively in the primary controller proposed in previous research [10, 13, 15, 16, 32] as Figure 36 shows. However, the proposed MPC approach has the benefits of free tuning and fast dynamic response. This loop of control also considers the characteristics of different distributed energy sources to optimize the energy harvest and minimize the system cost as shown in Figure 37. For example, the PV converter may track the maximum power point under varying solar irradiance conditions, the battery converter may be constrained by the state of charge (SoC) with the battery energy management.

3.3.1 Predictive Model of PV Boost Converter
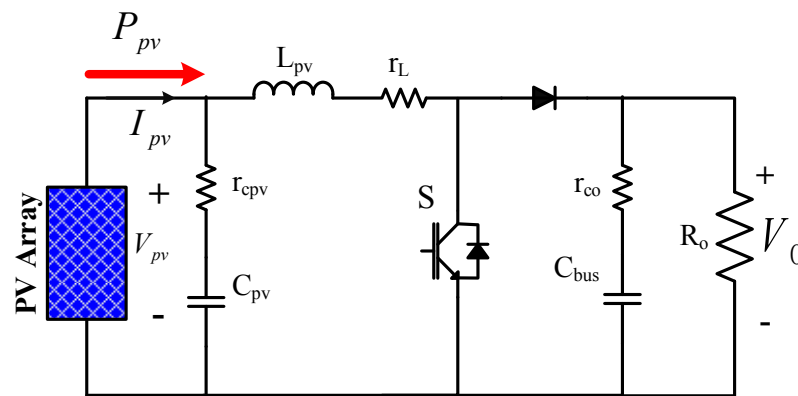
Figure 38 Practical circuit of boost converter

Figure 38 shows the practical circuit of the boost converter interfacing the PV arrays. The PV module voltage is lower than the DC bus, thus a boost converter is chosen as the DC-DC interface to ensure the maximum power point tacking. The incremental conductance (INC) method is used as the ground technique to determine the reference current for the MPC cost function. The proposed methodology is based on the fact that the slope of the PV array power curve is zero at

the predicted MPP, positive on the left and negative on the right of the predicted MPP [81, 108, 109]. The proposed technique predicts the tracking error of the next sampling for both possible switching states per converter (switch ON and OFF) by calculating the cost functions (g_1 and g_2). The switching states that minimize these cost functions will be applied to their corresponding converters. By using its discrete time model and Euler forward method, the behavior of system can be predicted at next sampling time (K+1). Thus, the predicted model of the converter control variable i.e. PV current and output DC voltage when switch is ON and OFF is given in (2-3):

$$
\begin{aligned}
\frac{i_{pv}(k+1)-i_{pv}(k)}{T_s} &= -\frac{sr_L+(1-s)(R_o r_c+r_L(R_o+r_c))}{L(R_o+r_c)}i_{pv}(k)-\frac{(1-s)r_o}{L(R_o+r_c)}v_0(k)+\frac{v_{pv}(k)}{L}\\
&\cong \frac{sr_c-(r_c+r_L)}{L}i_{pv}(k)-\frac{(1-s)}{L}v_0(k)+\frac{1}{L}v_{pv}(k)
\end{aligned}
\tag{8}
$$

$$
\begin{aligned}
\frac{v_o(k+1)-v_o(k)}{T_s} &= \frac{(1-s)R_o}{C(R_o+r_c)}i_{pv}(k)-\frac{1}{C(R_o+r_c)}v_0(k)\\
&\cong \frac{(1-s)}{C}i_{pv}(k)-\frac{1}{C(R_o+r_c)}v_0(k)
\end{aligned}
\tag{9}
$$

where T_s is the sampling time, s represents the switching state and is "1" when the switch is ON and is "0" when the switch is OFF; the other variables are shown in Fig. 4. Since only one freedom of control is available for the boost converter, the PV current is chosen as the subject of the objective cost function in (11) to be minimized. The following two reasons for that choice are given after careful examination of (8)-(9):

1) $V_{pv}(k)$ is readily available, while $R_o(k)$ is complicated to estimate;

2) Direct current control ensures fast dynamic responses and easy implementation of current protection

$$\min g_{\delta \in \{1,2\}} = \| \widetilde{I}_{PV\delta}(k+1) - I^*_{PV\delta}(k+1) \|$$
$$s.b. \qquad s \in \{0,1\} \tag{10}$$

Where δ corresponds to the PV array in the system, $I^*_{PV\delta}(k+1)$ is the next step PV reference given by MPPT.

3.3.2 Predictive Model of Battery Bi-directional Synchronous Buck Converter
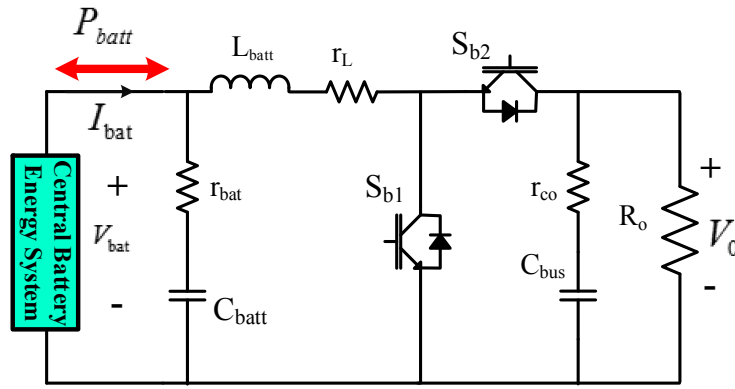
Figure 39 Practical battery bi-directional converter

Figure 39 shows the practical circuit of the buck-boost converter interfacing the battery system. Similar to the previous section, by using the discrete time model of the bidirectional converter and Euler forward approximation, the predicted model of the converter interfacing the battery bank are given by (7-9) below:

$$\widetilde{I}_{batt}(K+1) = \frac{T_S}{L_{Batt}}(V_{bus3}(K) \times S_{b1} - V_{batt}(K)) + I_{batt}(K) \tag{11}$$

$$\widetilde{V}_{bus3}(K+1) = \frac{T_S}{C_{bus3}}(I_{Lbatt}(K) \times S_{b1} - \frac{V_{bus3}(K)}{R_1(K)}) + V_{bus3}(K) \tag{12}$$

$$R_o(K) = \frac{V^2_{bus\sigma}(K)}{V_{PV\sigma}(K)I_{PV\sigma}(K)} \tag{13}$$

Where S_{b1} represents the switching state and is "1" when switch is ON and it is "0" when switch is OFF. Similar to (4), the (9) is used to estimate the terminal impedance of the converter for the predicted battery converter model. The cost function subject to minimization is given by

$$\min g = \| \tilde{I}_{bat}(k+1) - I^*_{bat}(k+1) \|$$
$$s.b.\ s \in \{0,1\}$$

$$(14)$$

Where $I^*_{bat}(k+1)$ is the next step battery reference given by battery secondary controller.

As stated before, battery storage system ensures power balance of the DC microgrid, therefore its energy management based on sate of charge is critical. In addition to the information of the remaining battery capacity to the user, knowledge of SoC exerts extra control over the charging/discharging process, which can potentially increase the battery life [110]. Considering the characteristic of the lead-acid battery chosen in this system, the state of charge (SoC) is estimated online by the most cost effective Coulombs Counting method, as (11) shows:

$$SoC = SoC_0 + \frac{1}{C_N} \int_{t_0}^{t} (I_{batt} - I_{loss}) d\tau$$

$$(15)$$

Where C_N is the rated capacity, SoC_o is the initial state of charge, I_{loss} is the current loss.

Normally, the battery storage system will be used to regulate the DC bus voltage as shown in Fig. 6, in which, the PI voltage loop will generate the $I_{batt\text{-}ref}$ for the inner current model predictive controller, and $I_{batt\text{-}ref} < 0$ means battery is charging, vice versa. Whenever the SoC is out of the range, the battery management will cut off the voltage loop and force the $I_{batt\text{-}ref}$ to zero to avoid either overcharging or discharging. This simple and straightforward battery energy management enabled by the MPC algorithm ensures the optimal and autonomous operation of the DC microgrid, and is verified in the case studies later.

The bi-directional synchronous buck converter is basically the same as the boost converter only with the diode replaced by the switch as in Figure 39. The benefits of choosing this converter when combined with the model predictive of current (5) are as follows:

1)   High efficiency of zero voltage switching available;

2)   Direct current control ensures fast dynamic responses and easy implementation of current protection

3)   Unified control of current

3.4 Secondary controller based on droop control

3.4.1   Secondary Control based on DC Bus Voltage Signal and Droop Control

The secondary controller is based on the proposed distributed droop control to coordinate the power generation within the DC MG. Each converter can either work as current source mode or voltage source mode, depending on the power availability from the source and the power

Table 8 Dc bus range under different modes

	V_{min}	V^*	V_{max}
Mode I	350	360	370
Mode II	370	380	390

Table 9 Functions of converters under different modes

	Mode I	Mode II
Bus Regulation	Battery	PV1 || PV2
Bus Feeding	PV1 & PV2	PV2 || PV1
Bus Loading	Local Load	Battery & Local Load

demand from the load. This information will be reflected on the DC bus voltage value. As a result, the DC bus power line can be used as the communication signal to determine the operation modes of the energy converters.

Normally, the system will work with grid-connected defined as mode III in Table 9, where the grid utility with PUC will regulate the bus voltage within its range limit. When grid disconnected, depending on the power balance between the load demand and the source supply
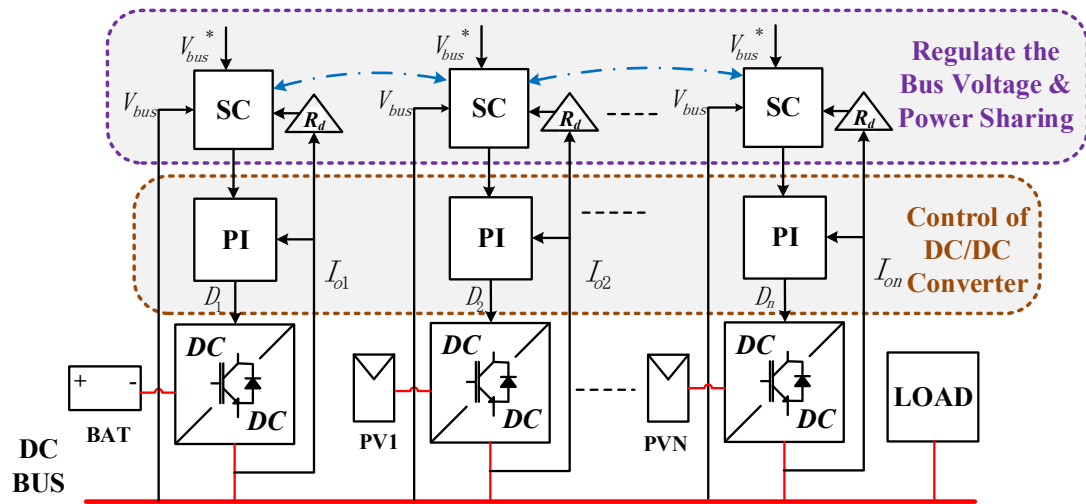
Figure 40 Traditional secondary control
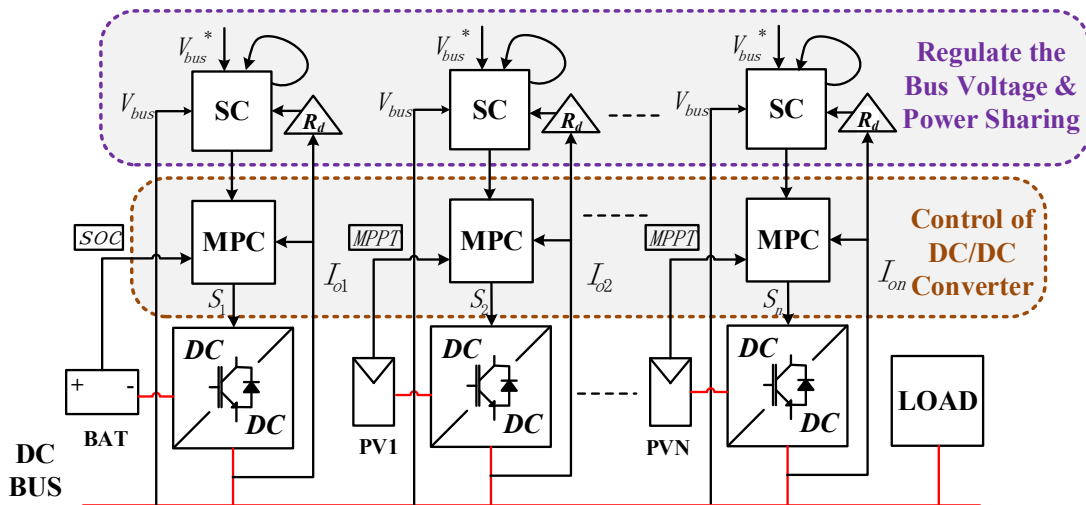
Figure 41 Proposed secondary control

availability, either the battery bank or the PV array will work as voltage source converter to regulate the bus according to the bus voltage range predefined in Table 8.

Traditional droop control shown in Figure 40 originated from power system control is employed in the power electronics converter control to increases the headroom for load transients.
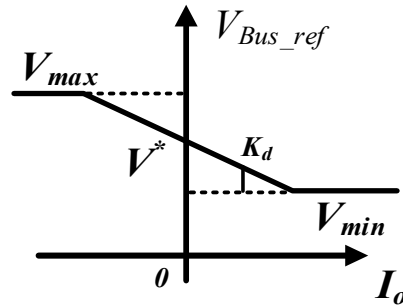
(a) Traditional droop curve
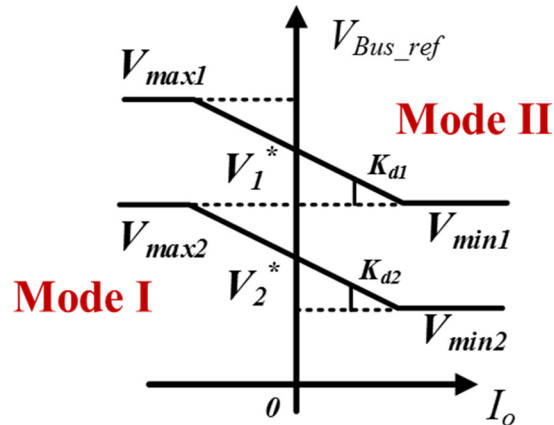
(b) Proposed distributed droop curves for distributed units working on different modes

Figure 42 Droop Control Curves

The bus voltage variations can be predefined into different ranges corresponding to specific energy units working as voltage source mode. This so-called distributed droop control in Figure 41 combined with the mode change logic in the secondary controller may then realize the fully

autonomous control of the DC MG without the need for traditional low-bandwidth communication lines. Here, the droop gain serves as the load sensitivity signal as in Figure 42. When the load current is maximum, the DC bus is minimum, and vice versa, as in equation (7).

$$\begin{cases} V_{min} = V^* + R_d I_{max} \\ V_{max} = V^* + R_d I_{min} \end{cases} \tag{17}$$
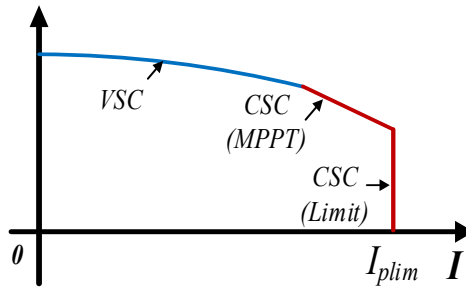
(a) PV operating range
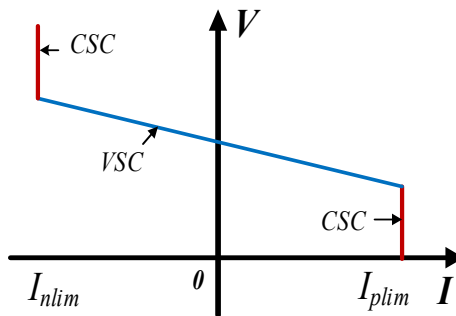
(b) battery operating range

Figure 43 Operating characteristic curves

The operating curves of PV source and battery are shown in Figure 43, where the blue line stands for the region of voltage source converter (VSC) mode and the red for current source converter (CSC) mode.

62

3.4.2 Control Strategies for PV Arrays

Based on the proposed primary and secondary control methods, the control strategies for the PV arrays are heightened in Figure 44. The mode change logic determines the PV array converter working mode by its local PI saturation signal. If it is saturated, which means the bus energy demand is out of the power availability of the PV arrays, then the PV arrays will work as
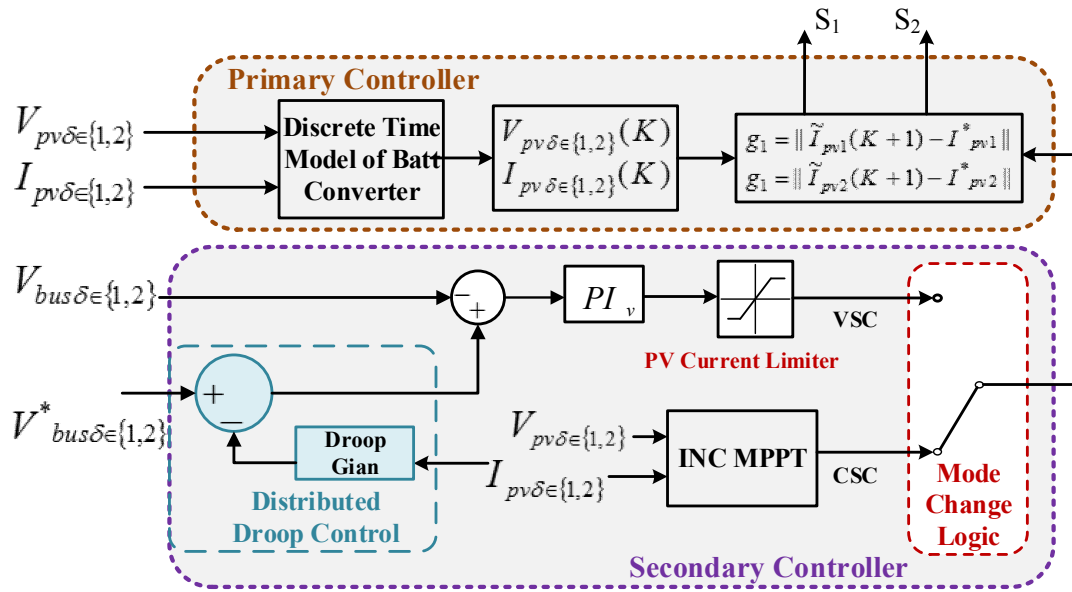
Figure 44 Control strategies for the PV arrays
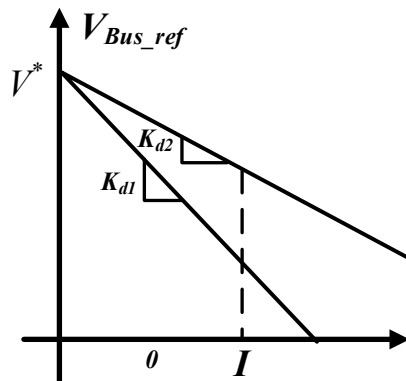
Figure 45 Droop curves for different PV arrays

MPPT mode dictated by the mode change logic. If not, the PV arrays will help to regulate the bus

voltage by changing its power generation. In reality, many PV arrays with converters share the
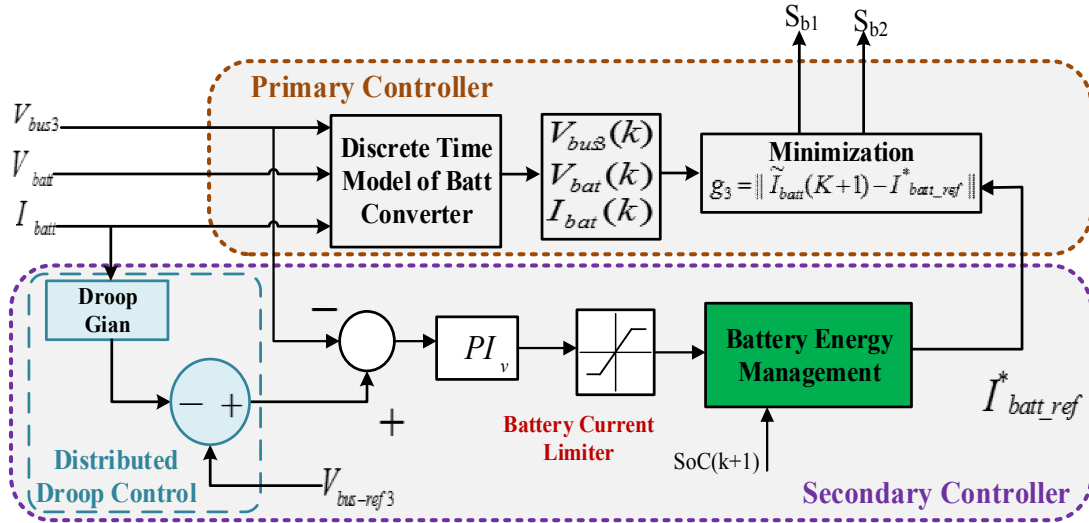
Figure 46 Control strategies for the battery storage system
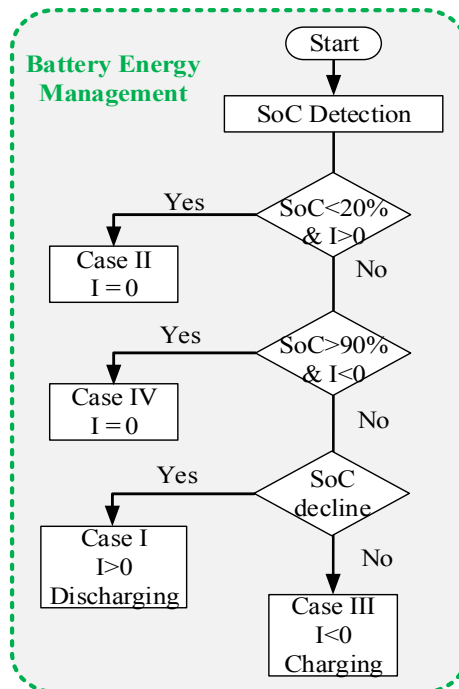
Figure 47 Battery management flowchart

same bus. To minimize the potential conflict of which PV array work as VSC, the droop curves for different PV arrays are configured as different droop gains as in Figure 45. For example, for the same load current, they have different target regulation voltages. Once the bus voltage exceeds the specific value because of surplus energy, the corresponding PV array will decrease its energy generation by switching to VSC. Thus, one or more PV arrays will switch to VSC step by step according to the bus voltage level.

3.4.3 Control Strategies for Battery Storage System

Based on the proposed primary and secondary control method, the control strategies for the battery storage system are heightened in Figure 46. State of charge (SoC) is considered to
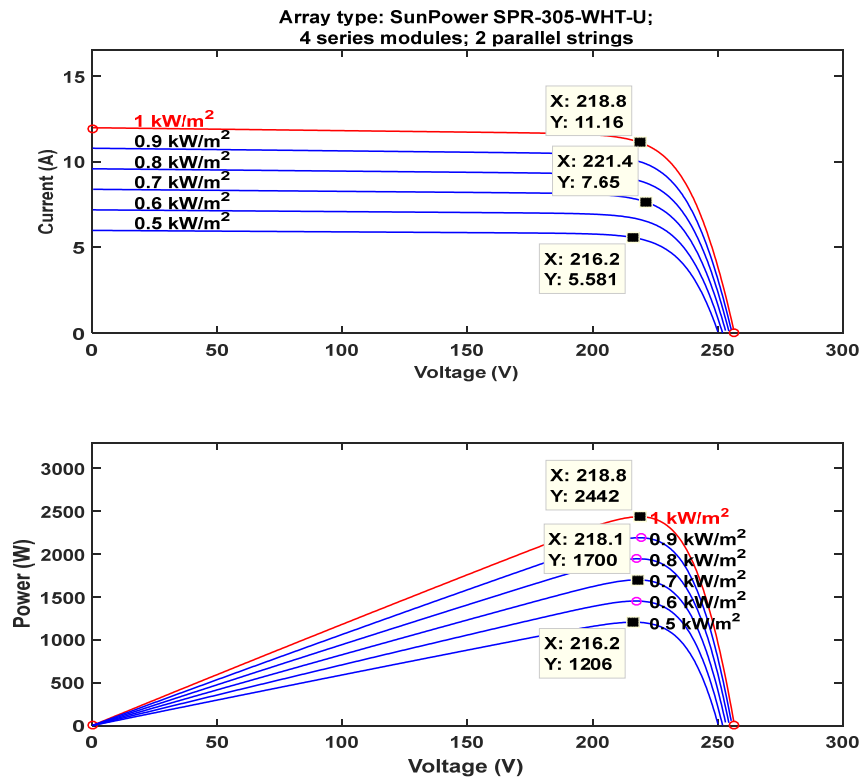
Figure 48 PV modules used ant its characteristics I-V and P-V curves under different solar irradiances

determine when charging/discharging and how much the rate of charge or discharge current is. Equation (8) shows a simple but reliable way to predict the next step state of charge suitable for the model predictive control used in the primary control layer. Battery energy management in Figure 47 is incorporated in consideration of SoC. For example, when the SoC is out of scope of 20%-90% set according to the National Renewable Energy Lab, the battery current will be disabled. The battery current limiter servers as the mode change logic for the battery converter working operations. If the charge or discharge current set by the secondary PI controller is out of the predefined battery current rating, it will disable the function of distributed droop control and then the converter will switch smoothly from VSC to CSC.

$$SoC(K+1) = \begin{cases} SoC(K) - \dfrac{T_S}{E_{batt\_max}} P_{batt}(K) \times \eta_{discharging} & \text{for} \quad P_{batt}(K) \geq 0 \\ SoC(K) - \dfrac{T_S}{E_{batt\_max}} P_{batt}(K) \times \eta_{charging} & \text{for} \quad P_{batt}(K) < 0 \end{cases}$$

(18)

3.5 Results and discussion

The system is mathematically modeled and simulated in Matlab-Simulink. The MPC algorithm is implemented by a sampling time T_S of 20 µs, the expected PV arrays power at MPP are tabulated in Figure 48. In DC islanded condition, eight case studies are analyzed to evaluate the system performance for the common two modes of operation.

66

3.5.1 Case Study I — mode I establishing
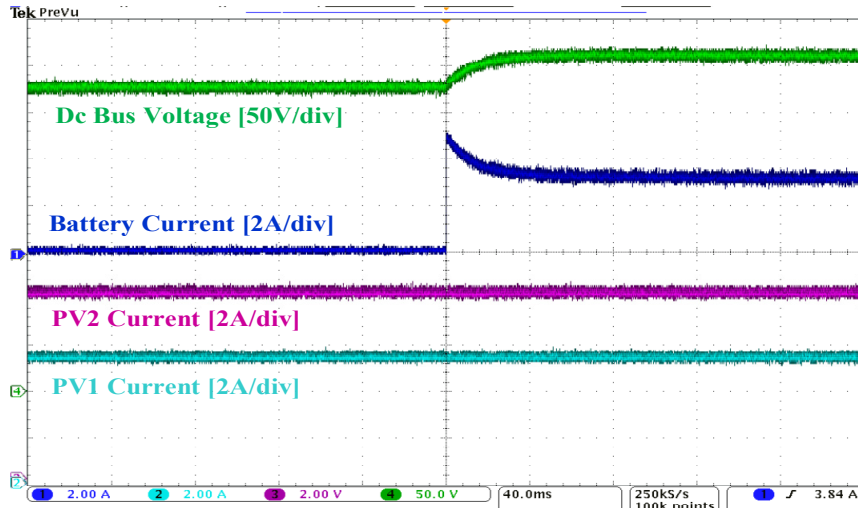
Figure 49 Case 1: Battery system activated at 1s and started regulating bus voltage in less than 0.5s.
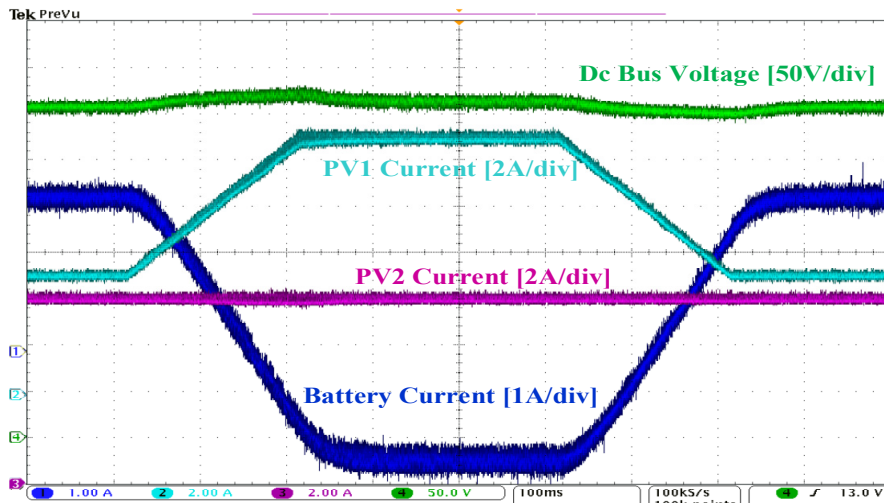
Figure 50 Case 2: DC-bus voltage, PV arrays, load, and battery power waveforms.

As Figure 49shown above, the battery system was activated at 1s and started discharging. Both PV currents remain the same while the battery current increases to regulate the bus voltage to around 360V.

3.5.2 Case Study II — mode I operation under PV power dynamics
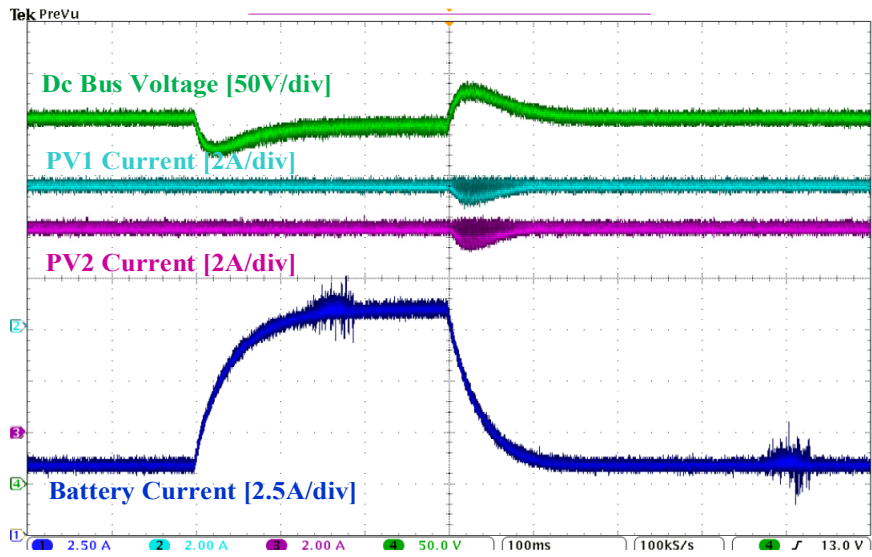
Figure 51 Case 3: DC-bus voltage, PV arrays, load, and battery power waveforms.
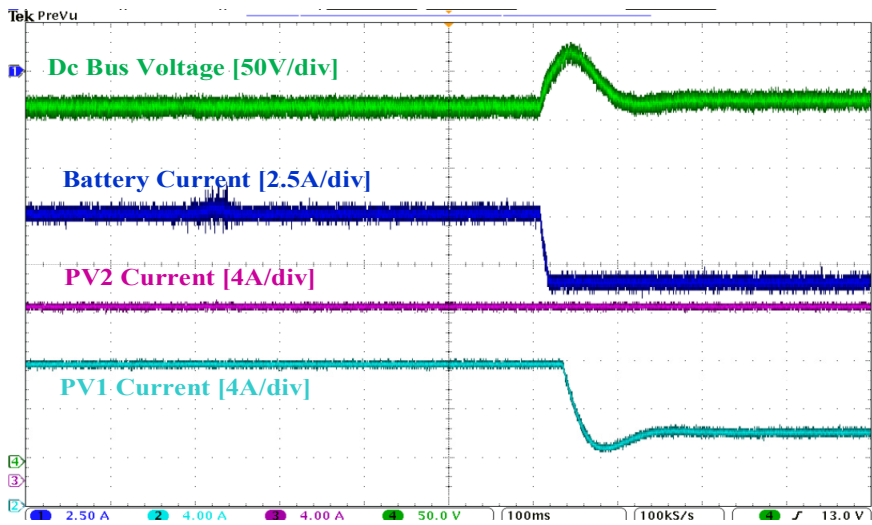
Figure 52 Case 4: DC-bus voltage, PV arrays

As shown in Figure 50, the system performance under PV power dynamic is controlled well with small DC bus voltage variation. The battery power is changing according to the change of PV power to regulate the bus voltage.
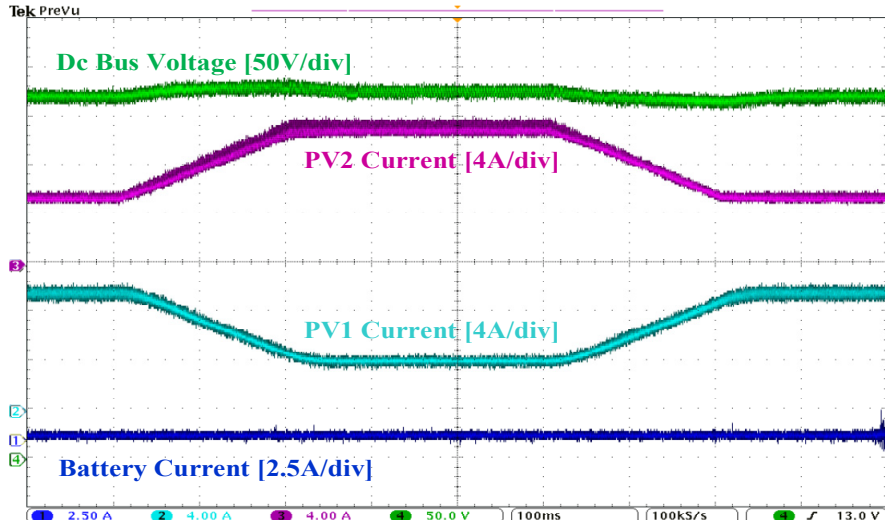
Figure 53 Case 5: DC-bus voltage, PV arrays, load, and battery power waveforms.
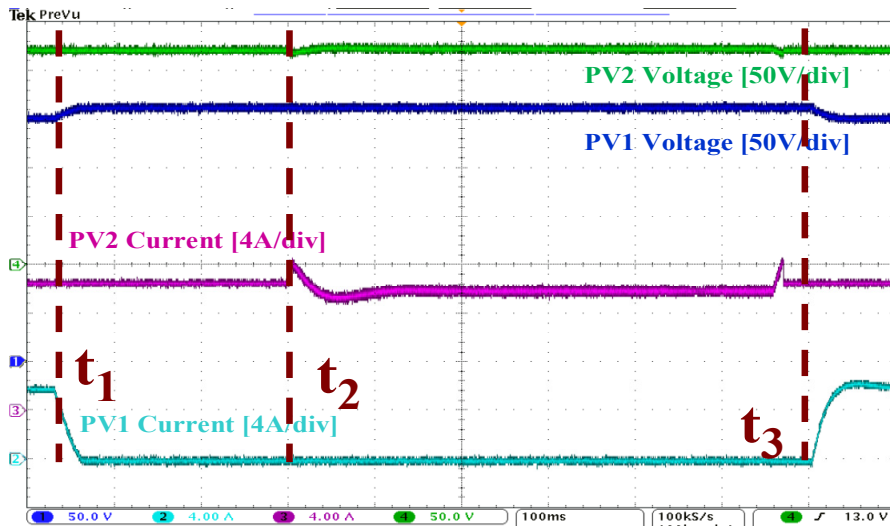
Figure 54 Case 6: DC-bus voltage, PV arrays, load, and battery power waveforms

3.5.3 Case Study III — mode I operation under load dynamics

As shown in Figure 51, the system performance under load power dynamic is controlled well with small DC bus voltage variation. The battery power is changing according to the change of load power to regulate the bus voltage.

3.5.4 Case Study IV — transition from Mode I to Mode II

As shown in Figure 52, when the load suddenly decreases, the battery power goes to maximum current charging mode. The bus voltage still increases because of the surplus power from PV arrays. Therefore, PV1 decreases its power generation automatically to restore the bus voltage to around 380V. In the meantime, the PV2 power remains the same.

3.5.5 Case Study V — mode II operation under PV power dynamics

As shown in Figure 53, the system performance under PV power dynamic is controlled well with small DC bus voltage variation. The PV_2 power is changing power to regulate the bus voltage according to the power change of PV_1.

3.5.6 Case Study VI — mode II operation under load dynamics

As shown in Figure 54, the system performance under load power dynamic is controlled well with small DC bus voltage variation PV_1 first goes to standby mode at t_1 and then PV_2 changes from MPPT mode to VSC mode at t_2. Finally, both PVs come back to MPPT mode at t_3

3.5.7 Case Study VII — battery overcharging protection

As shown in Figure 55, the battery is being charging because of the PV power is larger than the load demand. When the SoC of the battery is over 90%, the battery management automatically cut the battery out of the system and PV$_1$ switch from MPPT to VSC mode to maintain the bus voltage by decreasing its power generation.
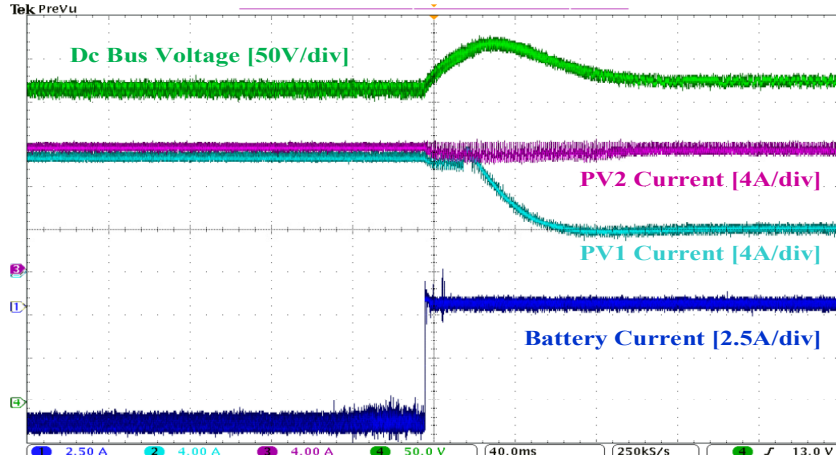
Figure 55 Case 7: DC-bus voltage, PV arrays, load, and battery power waveforms.
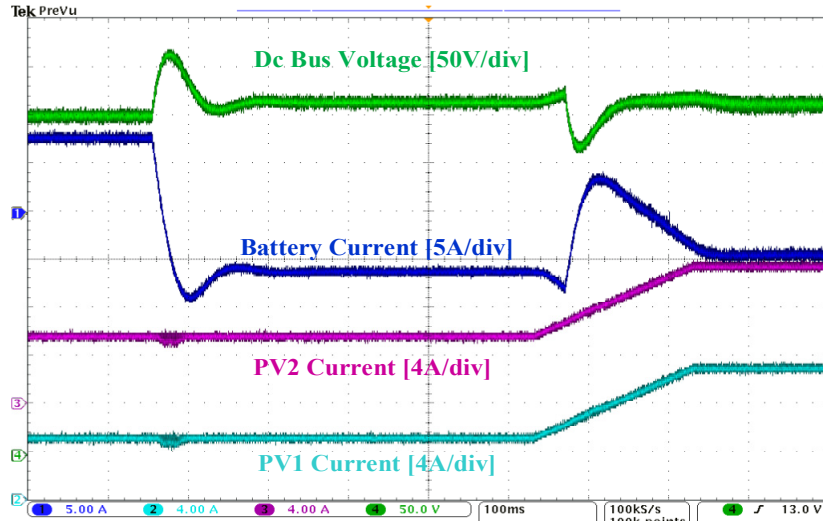
Figure 56 Case 8: DC-bus voltage, PV arrays, load, and battery power waveforms

3.5.8 Case Study VIII — battery overdischarging protection

As shown in Figure 56, the battery was protected by changing from discharging to charging mode when SoC drops below 20%. The non-critical load is shedding because the PV power is not enough to support the bus voltage without the battery system. When the PV's power increases to the point where bus voltage tends to increase, the load is restored and the bus voltage is regulated within range.

The complete overview of the control blocks of DC microgrid with grid-connected is shown in Figure 57.

3.6 Summary

A novel autonomous and distributed control strategies are proposed for the DC microgrid with distributed renewable energy units and storage system in detailed modeling, achieving

	V_{min}	V^*	V_{max}
Mode I	350	360	370
Mode II	370	380	390
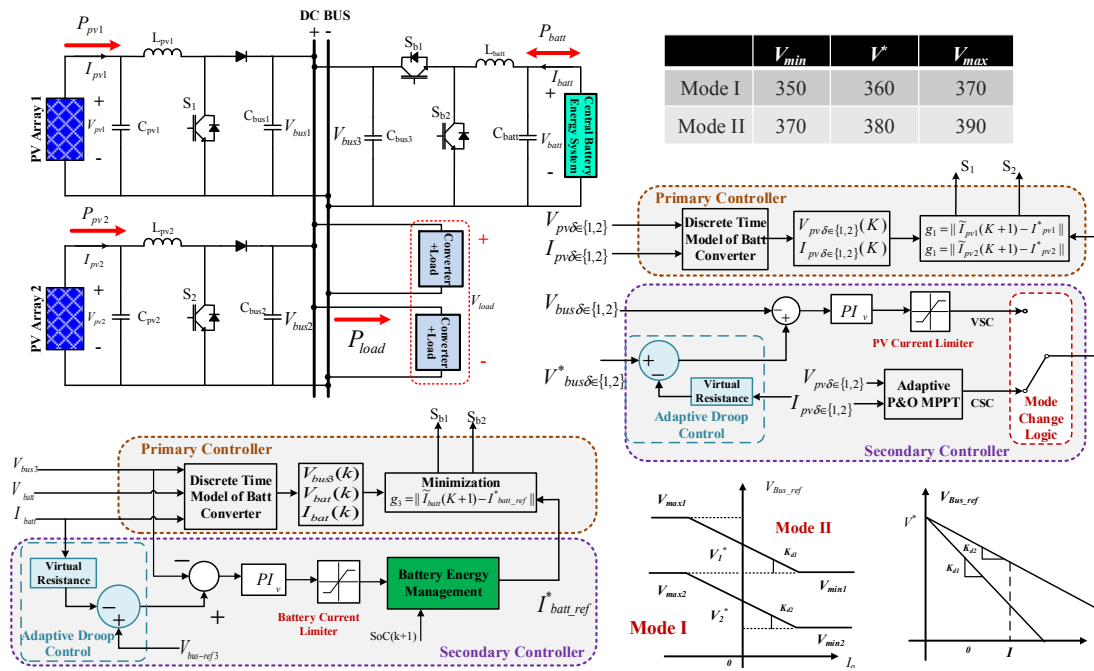
Figure 57 The complete overview of the control blocks of DC microgrid in islanded-mode

regulated DC bus and accurate power sharing under several conditions. The Model predictive control as the primary aims to improve the system dynamic responses and enable the play and plug feature of distributed renewable energy sources and battery storage systems. An improved droop control based on DC bus signaling is able to realize the autonomous operation of the Dc-microgrid in islanded mode with the effective seamless transfer between modes of change of the whole system.

4. CONTROL STRATEGIES OF DC MICROGRID IN GRID-CONNECTED MODE[3]

4.1 Introduction
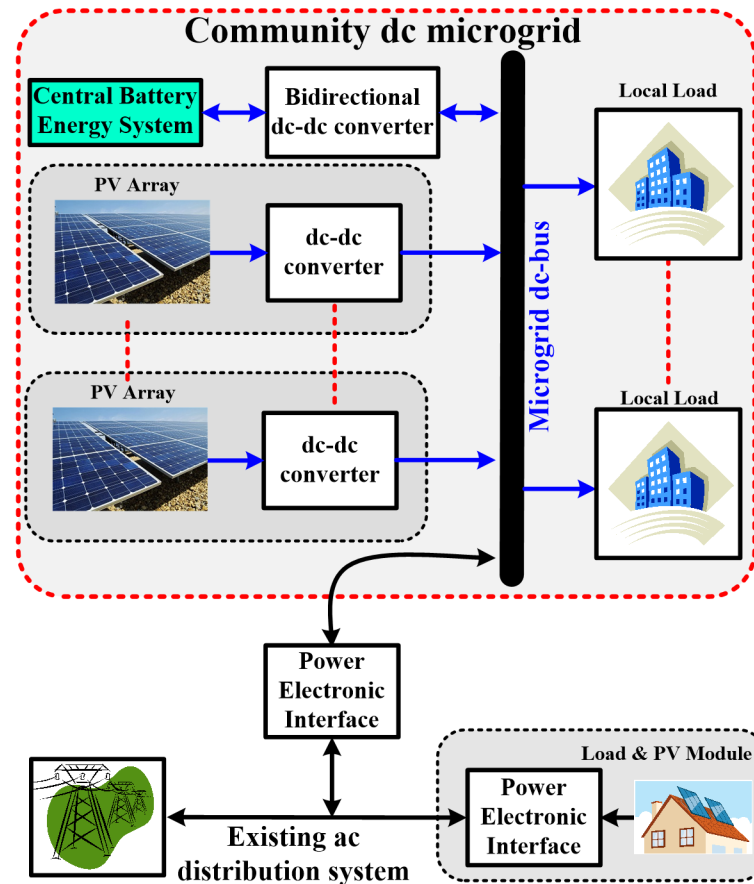
Figure 58 One-line diagram of the REAPER LAPES.

---

3 © 2018 IEEE. Reprinted, with permission, from S. Xiao, R S. Balog, "An Improved Hierarchy and Autonomous Control for DC Microgrid Based on Model Predictive Control and Distributed Droop Control", Applied Power Electronics Conference and Exposition (APEC), San Antonio, TX, USA, 2018 IEEE. © 2016 IEEE. Reprinted, with permission, from S. Xiao, M. Metry, M. Trabelsi, R. S. Balog, and H. Abu-Rub, "A Model Predictive Control Technique for Utility-scale Grid Connected Battery Systems Using Packed U Cells Multilevel Inverter", IEEE Annual Conference of Industrial Electronics Society (IECON), Florence, Italy, 2016.
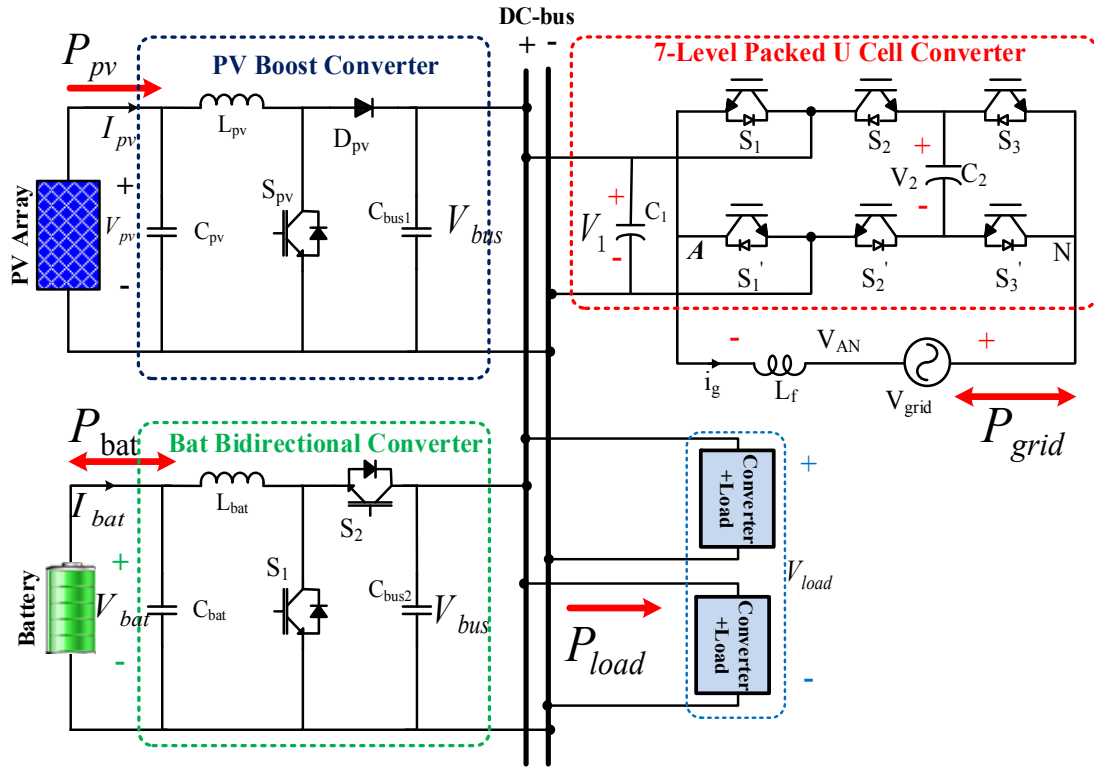
Figure 59 System schematic in grid-connected mode

Microgrids are gaining increased popularity for their ability to integrate increasing penetration of renewable energy sources to meet energy demand and overcome global warming concerns. In particular, direct current (DC) microgrid systems are beneficial due to their higher efficiency, reliability, and easier interconnection of the renewable energy sources compared to alternating current (ac) microgrid systems [2]. Dc microgrid have been proposed to enhance point of load energy availability and for purpose of integration with energy storage systems [3]. Renewable energy sources such as photovoltaic (PV) systems also have natural DC coupling; thus more efficient system can be achieved by directly connecting to a DC microgrid through DC-DC converter modules without the need of ac-DC or DC-ac converter modules in ac microgrid.

The DC microgrid system with PV arrays and centralized energy storage system, as illustrated in Figure 58, proposed as a Local Area Power and Energy System (LAPES) [4] by the Renewable Energy and Advanced Power Electronics Research (REAPER) lab, is an attractive technology solution for residential communities to "go green" while simultaneously ensure reliable electricity.

4.1.1   System configuration

Table I. PUC Converter Parameters

Parameter	Value
grid side filter inductor	15mH
PUC capacitor C1/C2	1130uF
DC bus/C1 voltage	390V
DC bus range	320-460V
C2 voltage	130V
grid voltage(rms)	220V
PUC mosfet ratings	650V/60A
PUC power rating	6kW
grid frequency	50Hz
sampling time	20us

In the grid-connected mode (Figure 59), the DC microgrid is connected to the main grid via a 7-level packed u cell inverter (PUC). Here, to further simplify the discussion, only one PV array converter represents the renewable energy unit. The grid can be considered to be infinite energy storage, so the interfacing inverter is always working under voltage source converter mode and the remaining ones work as current source converter.

The novel autonomous control strategy proposed for this system, which helps optimizes the system performance, and minimize the communication bandwidth requirement, will be introduced [111].

4.2 Primary controller of PUC based on model predictive control
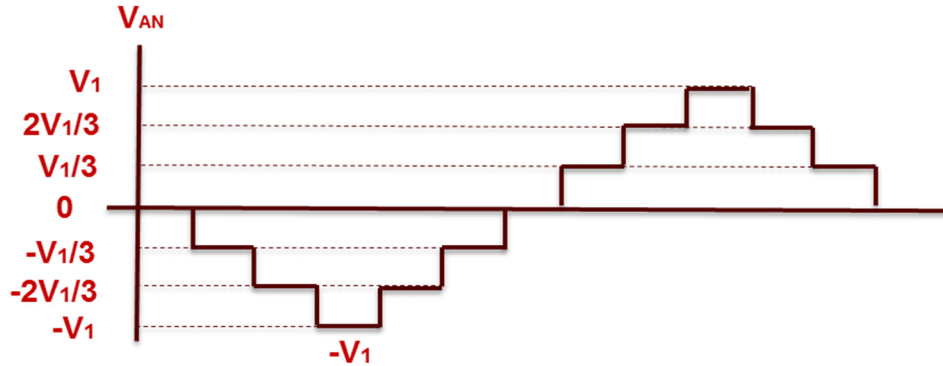
Figure 60 Waveforms of the 7-level PUC output voltage

The primary loop directly indicates the action of the power MOSFETs in the DC-DC converters, so the control method employed on this loop determines the DC MG performance largely. To meet the expandability requirement of future DC MG, the converter should have the play & plug feature. It is observed that the DC-DC converter module used only has one freedom of control. The traditional PI controller needs time-consuming tuning and is used extensively in the primary controller proposed in previous research [10, 13, 15, 16, 32]. However, the proposed MPC approach has the benefits of free tuning and fast dynamic response.

4.2.1   Packed U Cell 3-level Inverter Topology

The presented single-phase 3-cell PUC inverter is illustrated. The system under study consists of three cells separated by two capacitors [112, 113]. Voltage V_1 is the terminal connected to the DC bus, while voltage V_2 is a voltage regulated by the control algorithm around the voltage reference. In this work, the reference voltage for V_2 is set to $V_1/3$ in order to generate the 7-level

output voltage. The switches (S_1, S_1'), (S_2, S_2'), and (S_3, S_3') are controlled in a complementary manner. Let $s_i \in (1, 0)$ $(i=1, 2, 3)$ be the switching function of S_i defined by:

$$s_i = \begin{cases} 1, & \text{if } S_i \text{ is ON} \\ 0, & \text{if } S_i \text{ is OFF} \end{cases}$$

(1)

Table 10 Switching table of the 3-Cell PUC Inverter

State	V_{AN}	s_1	s_2	s_3
1	0	0	0	0
2	$-V_2$	0	0	1
3	V_2-V_1	0	1	0
4	$-V_1$	0	1	1
5	V_1	1	0	0
6	V_1-V_2	1	0	1
7	V_2	1	1	0
8	0	1	1	1

The level of the output voltage is determined by controlling the capacitor voltages V_1 and V_2 using the optimal control actions s_i. Eight possible switching patterns are identified in Table 10. As noted from this table, two states are redundant representing the zero voltage vector and six states are active applying the appropriate voltage level across the load.

Using Kirchhoff laws and Table 10, relations between the capacitor voltages $V_1(t)$ and $V_2(t)$, the grid current $i_g(t)$, and the switching states s_i are expressed by

$$C_2 \frac{dV_2(t)}{dt} = (s_3 - s_2)i_g(t)$$

(1)

$$L_f \frac{di_g(t)}{dt} = (s_1 - s_2)V_1(t) + (s_2 - s_3)V_2(t) - V_{grid}$$

(2)

For the proposed system, the grid current and the capacitor voltages must be jointly controlled to ensure proper operation of the PUC inverter. Thus, the MPC control strategy is used to balance the capacitor voltage $V_2(t)$ and control the output current $i_g(t)$ with unity power factor and low harmonic distortion, given that the input voltage $V_1(t)$ of the DC bus is regulated by the battery MPC algorithm described later.

4.2.2 Predictive Model of 7-level packed u cell inverter
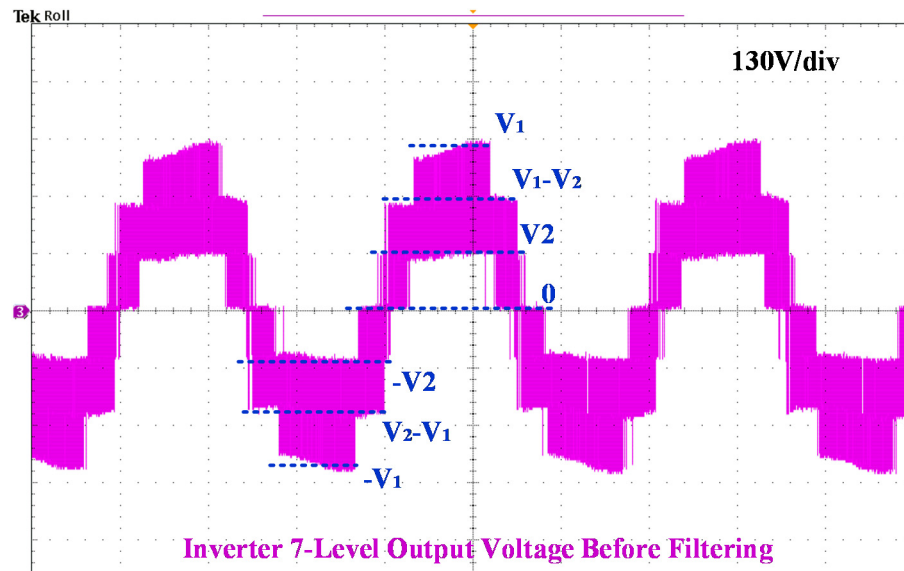
Figure 61 dSPACE Implementation of 7-Level PUC voltage before filtering

As more and more point-of-renewable energy sources integrated, the future requirements of DC-microgrid inverter includes:

1) Higher voltage/current levels, thus higher power ratings

2) Improved inverter processing efficacy

3) More strict on quality of the current injected into grid

Therefore, multilevel inverter is a promising candidate. More specifically, the 7-level packed u cell (PUC) inverter is chosen here as the interface between the DC microgrid and the

mains grid as in Figure 59, considering the facts that it uses reduced number of passive and active components for the same number of output levels and it only needs one DC source which can be the DC bus. By controlling the action combinations of the six switches, it will generate 7 level output voltage levels as in Figure 60. The detailed working principle of it can refer to [8]. It is noted that the control objectives for the PUC is:
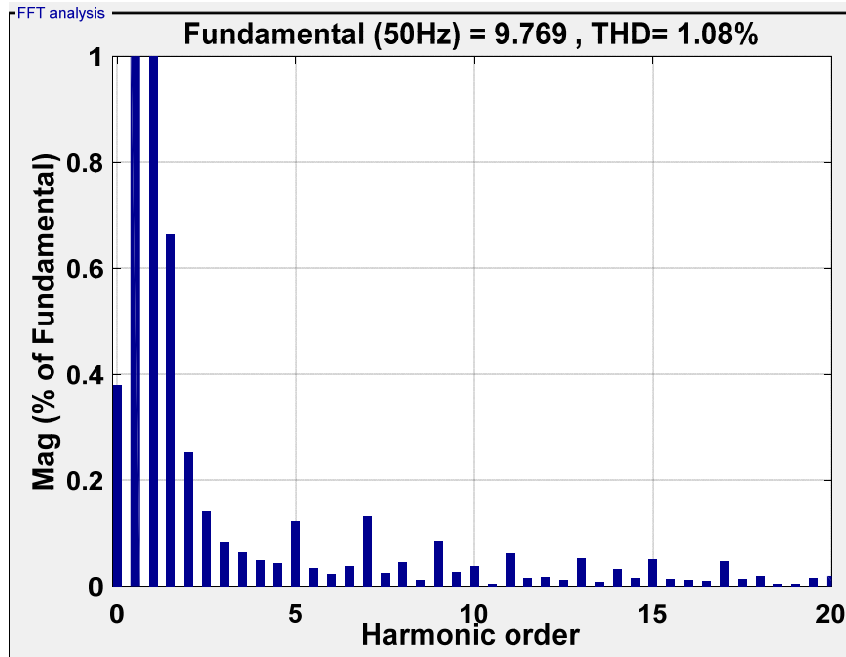
Figure 62 Grid current total harmonic distortion (THD)

1) Output grid-side current Ig, which determines the amount of power either absorbed or generated by the grid;

2) Capacitor C2 voltage to be one-third of that of C1, so that the output voltage levels are equal.

A multi-objective MPC is an idea control method to ensure the tracking of the grid current, capacitor voltages and generation of unity power factor with low THD current simultaneously.

80

By using the discrete time model of the PUC, the predicted model of the converter are given by:

$$\min g = \left\| \frac{V_2^* - \widetilde{V}_2(k+1)}{V_2^*} - \lambda \frac{I_g^* - \widetilde{I}_g(k+1)}{I_g^*} \right\|$$

$$s.b.\, s \in \{0,1\}$$

(3)

Where unit normalization method is proposed to simplify the tuning of weighting factor λ, $I_g^*(k+1)$ is the next step grid current reference given by secondary controller as shown in Figure 63. Comparing the Figure 60 and Figure 61, the control of model prediction output expected waveforms with good performance. The Grid current total harmonic distortion is about 1% which is below the IEEE 519 standard.

4.3 Secondary controller of PUC based on droop control

4.3.1   Secondary Control based on DC Bus Voltage Signal and Droop Control

The secondary controller is based on the proposed distributed droop control to coordinate the power generation within the DC microgrid. Each converter can either work as current source mode or voltage source mode, depending on the power availability from the source and the power demand from the load. These information will be reflected on the DC bus voltage value, as a result, the DC bus power line can be used as the communication line to determine the operation modes of energy converter.

Normally, the system will work with grid-connected defined as mode III in Table 9, where the grid utility with PUC will regulate the bus voltage within its range limit. Either when grid disconnected, depending on the power balance between the load demand and the source supply availability, the battery bank or the PV array will work as voltage source converter to regulate the bus according to the bus voltage range predefined in Table 8.
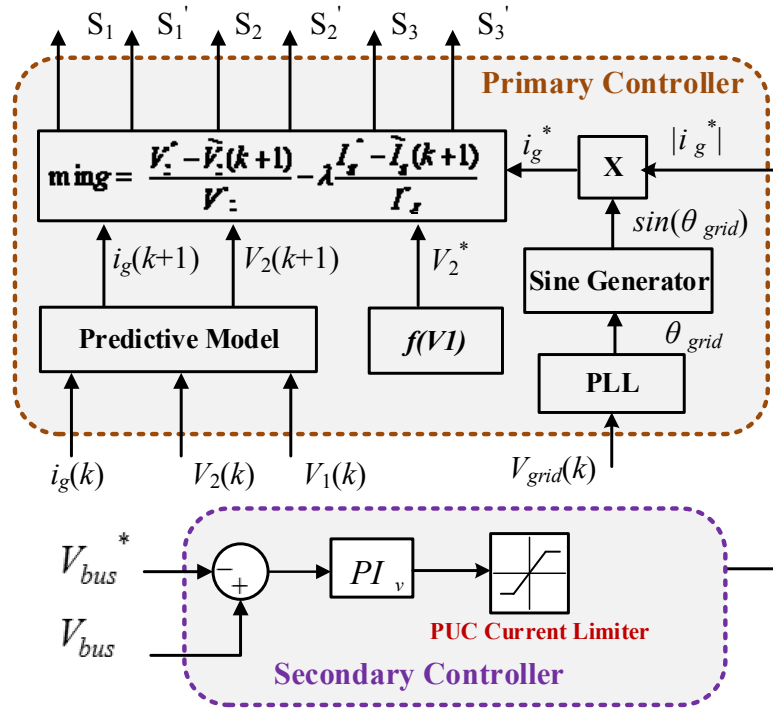
Figure 63 Control block of PUC system

Traditional droop control shown in Figure 40 originated from power system control is employed in the power electronics converter control to increases the headroom for load transients. The bus voltage variations can be predefined into different ranges corresponding to specific energy units working as voltage source mode. This so-called distributed droop control in Figure 41 combined with the mode change logic in the secondary controller may then realize the fully autonomous control of the DC microgrid without the need for traditional low-bandwidth communication lines. Here, the droop gain serves as the load sensitivity signal. When the load current is maximum, the DC bus is minimum, and vice versa, as in equation (4).

$$\begin{cases} V_{min} = V^* + R_d I_{max} \\ V_{max} = V^* + R_d I_{min} \end{cases} \tag{4}$$

4.3.2   Control Strategies for Packed U Cell Inverter
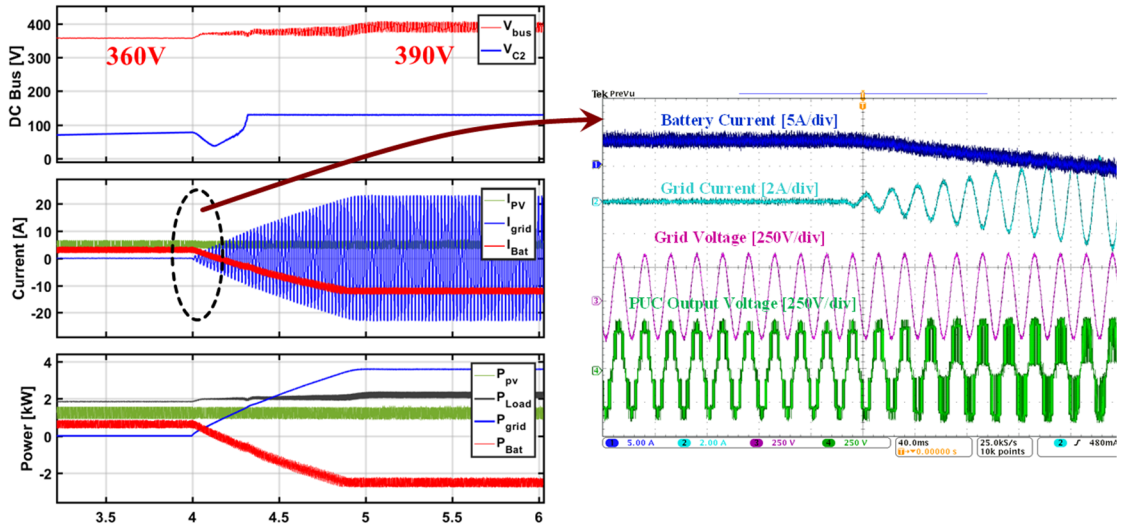
Figure 64 Case Study 1: Transition from islanding mode to grid-connected mode
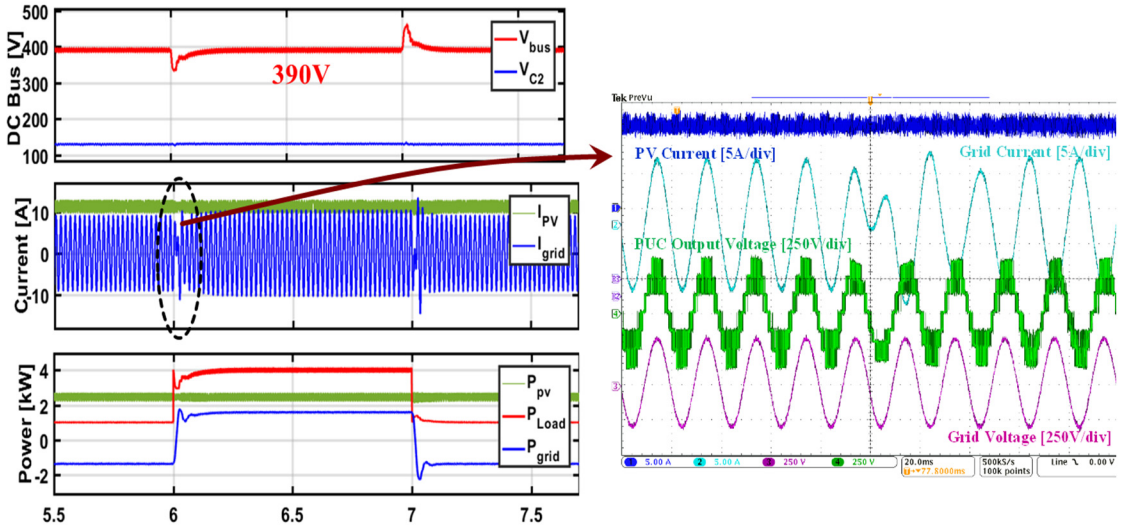
Figure 65 Case Study 2: Dynamic responses at load power changes in grid-connected mode

Based on the proposed primary and secondary control method, the control strategies for the 7-level Paced-U-Cell (PUC) inverter system are heightened in Figure 63. It is noted that the current limit here servers to protect the inverter from overcurrent instead of the mode change logic in the battery system control. As long as the grid works under normal operation, the PUC will work

as voltage source converter to regulate the bus voltage according to the loading demand since the utility grid is regarded to be infinite energy source.

4.4 Results and discussion for DC microgrid in grid-connected mode

The system is mathematically modeled and simulated in Matlab-Simulink. The MPC algorithm is implemented by a sampling time TS of 20 µs, the expected PV arrays power at MPP and other system key parameters are tabulated in Figure 48 and Table 6- Table 7. When the DC microgrid is in islanded mode, eight case studies are analyzed to evaluate the system performance for the common two modes of operation in last chapter. In this chapter, four case studies are shown to validate the proposed method in grid-connected condition and modes change.

4.4.1   Case Study I — transition from islanding mode to grid-connected mode

As shown in Figure 64, when grid connection signal is detected, battery switches from discharging mode to maximum current charging mode while the grid current increases. The bus voltage regulation point also changes from 360V to 390V, indicating that the system now is in grid connected mode.

4.4.2   Case Study II — dynamic responses at load power changes in grid-connected mode

As shown in Figure 65, when the load step up from 1kW to 4kW, the packed-u-cell inverter switches from selling electricity to buying electricity to make up for the added load demand. On the other hand, when the load step down from 4kW to 1kW, the packed-u-cell inverter switches from buying electricity to selling electricity to balance the sudden decreased load.

4.4.3 Case Study III — transition from grid-connected mode to islanding mode; PV arrays regulate the bus volts

As shown in Figure 66, since battery is being charged with maximum current and the grid doesn't absorb the power from the DC microgrid anymore, the PV arrays have to decrease the
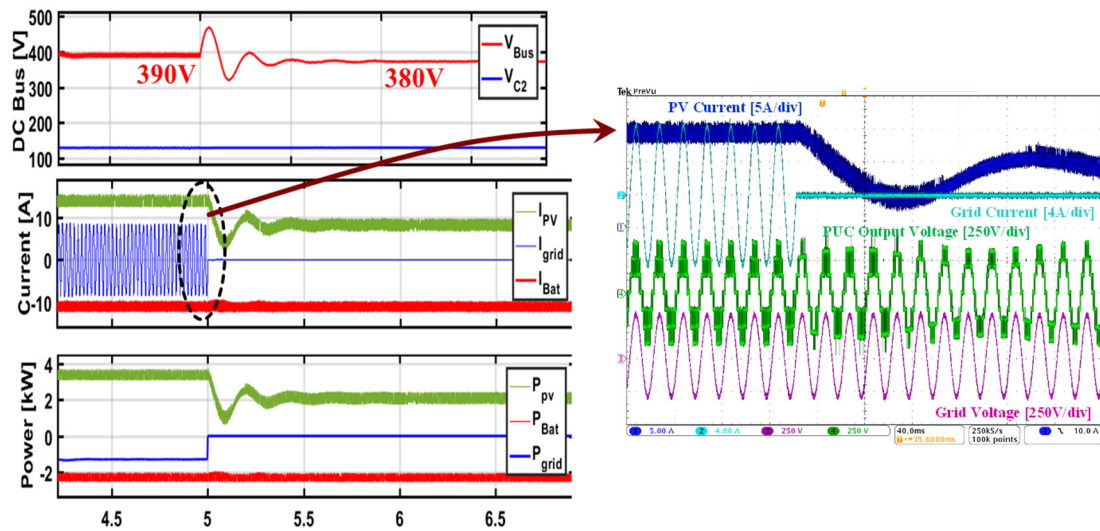
Figure 66 Case Study 3: Transition from grid-connected mode to islanding mode; PV regulates the bus volts
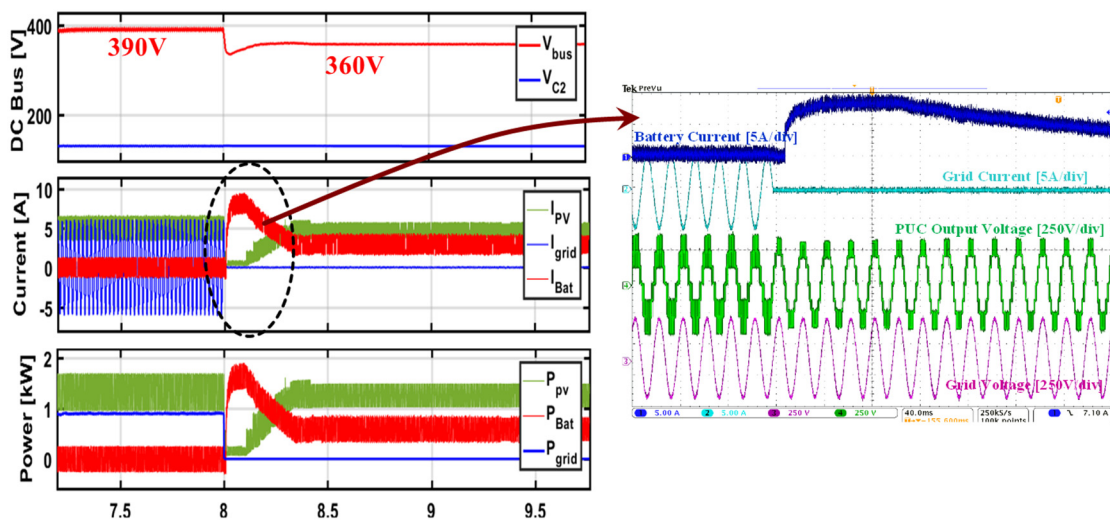
Figure 67 Case Study 4: Transition from grid-connected mode to islanding mode; battery regulates the bus voltage

power generation to prevent the bus voltage from going too high. The bus voltage regulation point changes from 390V to 380V accordingly.

4.4.4 Case Study IV — transition from grid-connected mode to islanding mode; battery storage systems regulate the bus voltage

As shown in Figure 67, when the grid no longer provides the power after 8s and considering the PV array cannot provide any more power, battery has to restore the bus voltage by providing power to the grid. The bus voltage regulation point also changes from 390V to 360V accordingly.
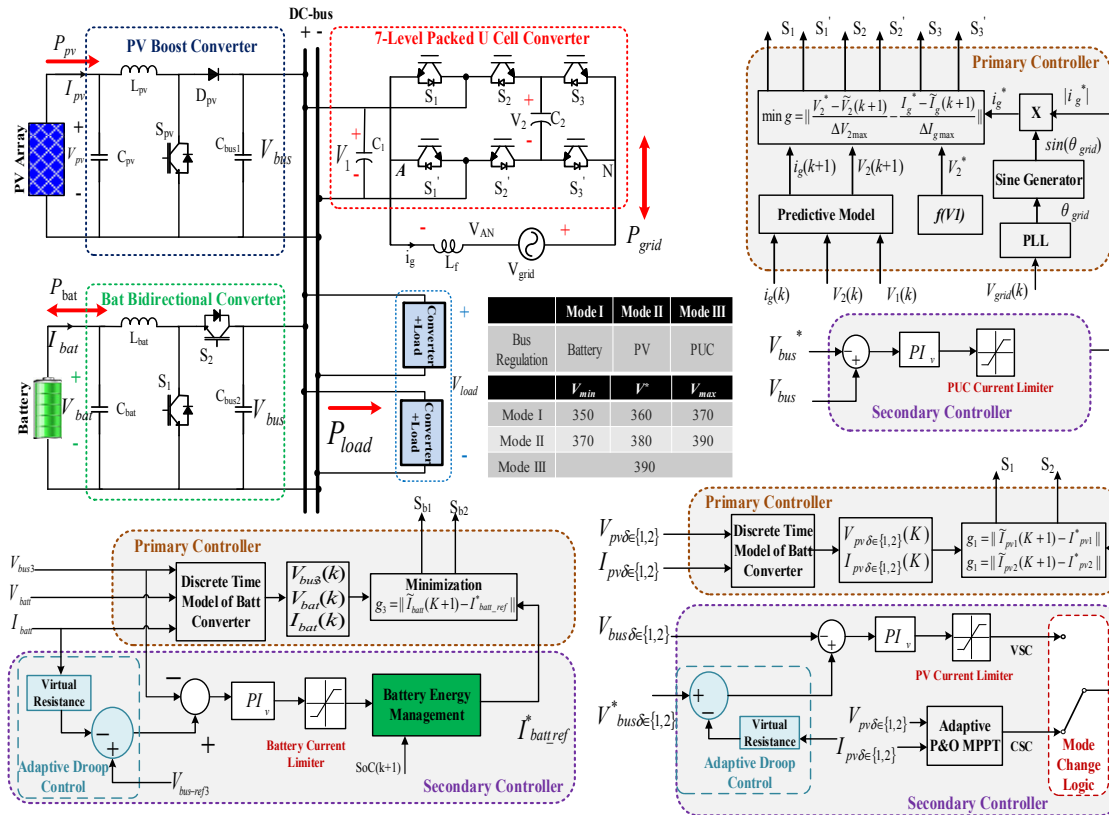
Figure 68 Complete overview of the control blocks of DC microgrid with grid-connected

The complete overview of the control blocks of DC microgrid with grid-connected is shown as the Figure 68 below.

4.5 MPC for grid-connected battery systems using PUC multilevel inverter

Utility scale grid-connected energy storage systems, used in uninterruptible power supply (UPS) applications, supply power to critical loads during emergencies. The use of DC micro-girds with energy storage allows for the distributed generation of many renewable energy sources such as solar and wind [114]. Additionally, storage helps maintain the stability of the DC bus against intermittent power flow caused by sporadic renewable energy sources generation [115]. Among many energy storage candidates such as flywheels, super capacitors and thermal storages, batteries are competitive for their availability, reliability, and high energy density [116].

Multilevel Inverters (MLI) are an attractive alternative to the traditional inverters for interfacing the battery storage system with the grid due to their high quality output voltage, lower switching losses, less voltage stress on power switches, and higher efficiency [112, 113, 117, 118]. Among the well-known MLI topologies are the Flying Capacitors Inverter (FCI) and the Cascaded H-Bridge (CHB) inverters. For a 7-level output voltage generation, FCI uses six capacitors, twelve switching devices and one DC source. Similarly, CHB uses three capacitors, twelve switching devices and three DC sources. In this paper, a Packed U Cells (PUC) MLI is used interface the battery charger system with the grid. In contrast with traditional MLIs, the PUC topology can generate the same number of voltage levels with only two capacitors, six switching devices and one DC source, leading to lower installations costs [113]. The use of only one DC source is a great advantage as it significantly reduces the amount of transformers or converters used in the system.

MPC is considered an intuitive control strategy, that is easy to understand, and easy to implement. Additionally, MPC allows the inclusion of constraints with different natures, dealing with different system non-linearites. Grouping all the aforementioned features, the MPC technique is considered as an alternative method to PI controller [119-121]. It provides fast dynamic response

while enabling the consideration of other control goals (harmonic distortion, switching frequency, etc.).

In this section, the system under study is a two-quadrant non-isolated buck-boost converter feeding a 3-cell PUC inverter for interfacing the storage batteries with the grid. Such converter
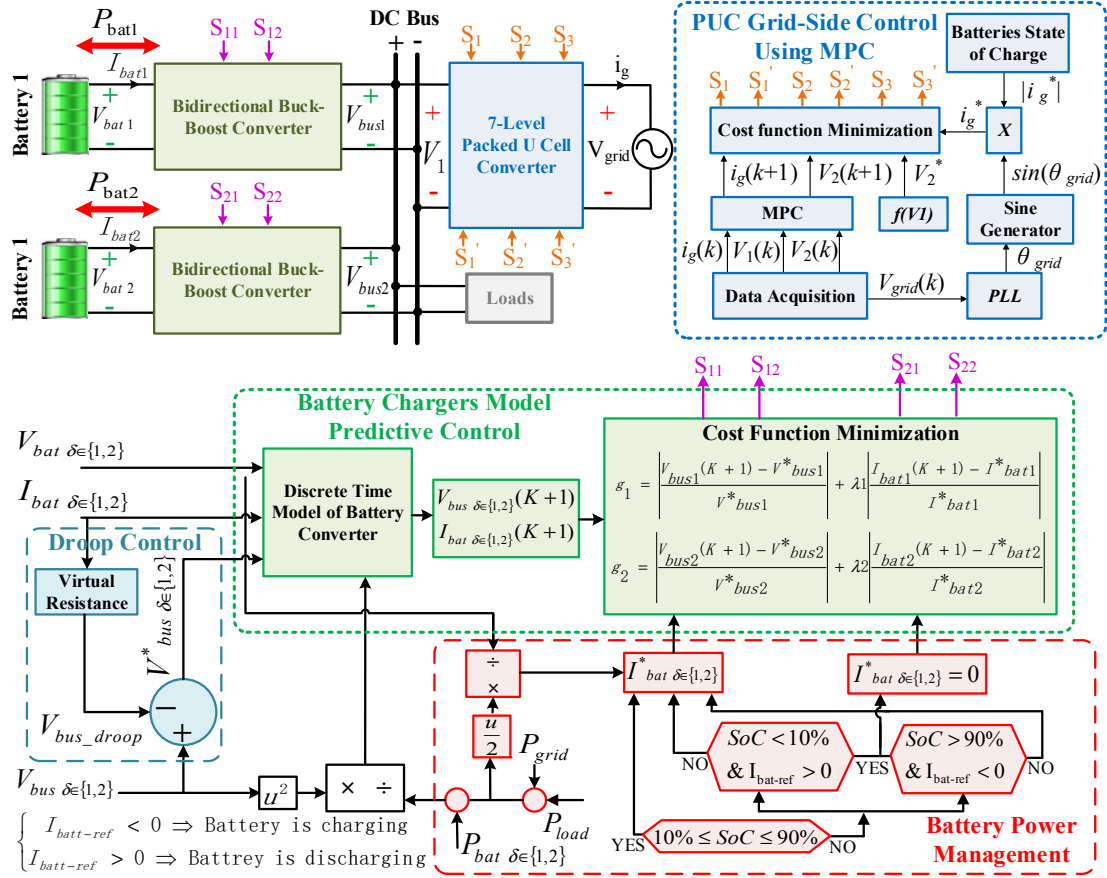
Figure 69 Control Blocks of the battery charge systems with PUC inverter.

provides a simple configuration and unified charging and discharging control [122]. The proposed grid-connected battery storage system, illustrated in Figure 69, consists of two parallel-connected battery chargers and a Packed U cell seven level inverter. The main contribution of this work is the implementation of a multi-objective MPC to control the power flow of the battery charger by minimizing the battery current and the bus voltage ripples. Considering multiple battery converters

88

connected to the DC bus, current sharing problems are tackled by combining droop control with MPC. In addition, MPC is used on the grid connected bidirectional 7-level PUC to control the capacitors' voltages and the grid current. This section is organized as follows: Section 4.5.1 introduces the theoretical background of Packed U Cells (PUC) inverter. Section 4.5.2 describes the MPC applied to the system combined with droop control. The simulation, implementation results, and discussion of three different case studies are explained in Section 4.5.3. Finally, Section 4.6 concludes the section 4.

4.5.1 System configuration

In the system in study Figure 69, the DC battery system is connected to the main grid via a 7-level packed u cell inverter (PUC). Here, to simplify the discussion, only two battery converters represent the energy storage system.

4.5.2 Control strategies on multiple batteries

The two-quadrant synchronous buck topology is chosen as the battery charger for its simple control and high efficiency. When working in the boost mode, the battery energy discharges to the DC bus; while in buck mode, the battery charges from the DC bus. The two switches in the converter should work in complimentary mode. As a result, the discrete model of the converter using Euler forward method given by (5) and (6) is used to implement MPC in this topology to predict the behavior of system at the next sampling time (K+1) [18-20].

$$i_{bat}(k+1) = \frac{T_s}{L_{bat}}\left[v_{bat}(k) - (1-\sigma)v_{bus}(k)\right] + \frac{i_{bat}}{L_{bat}}$$

(5)

$$v_{bus}(k+1) = \frac{T_s}{C_{bus}}\left[(1-\sigma)i_{bat}(k) - \frac{v_{bus}(k)}{R_o(k)}\right] + \frac{v_{bus}(k)}{C_{bus}}$$

(6)

Where $\sigma \in \{0,1\}$ represents the switching state, Ts is the sampling time. The battery charger parameters are shown in Table 11. To predict the next sampling value of Vbus, a simple and effective load resistive observer model is proposed [21], where P_{grid} (k), P_{bat} (k), and P_{load} (k) are the average power of grid, battery and resistive load bank on DC bus. The resistive load observer model is given by:

$$R_o(k) = \frac{v_{bus}^2(k)}{P_{grid}(k) + P_{load}(k) - P_{bat}(k)} \tag{7}$$

The inputs to the predictive controller are the battery current and voltage, DC bus voltage as well as the reference current that is calculated by the battery power management and constrained by state of charge (SoC) availability in Figure 47. SoC can be determined using various techniques [22]; however, coulomb counting method is used in this work.

The proposed technique predicts the tracking error of the next sampling for both possible switching states per converter (switch ON and OFF) by calculating the cost functions g1 and g2 in (12) and (13). The switching state that minimizes these cost functions are applied to their corresponding converters. The complete procedure of the controller is summarized in Figure 69. In the cost function, normalization of voltage and current is proposed to use the MPC in multi-objective constraints optimization problem.

$$g_1 = \left| \frac{V_{bus1}(K+1) - V^*_{bus1}}{V^*_{bus1}} \right| + \lambda 1 \left| \frac{I_{bat1}(K+1) - I^*_{bat1}}{I^*_{bat1}} \right| \tag{8}$$

$$g_2 = \left| \frac{V_{bus2}(K+1) - V^*_{bus2}}{V^*_{bus2}} \right| + \lambda 2 \left| \frac{I_{bat2}(K+1) - I^*_{bat2}}{I^*_{bat2}} \right| \tag{9}$$

where λ is a weighting factor, which can be adjusted according to the desired performance.

In the proposed system, there are two battery chargers connected to the DC bus. In most cases, the specifications such as nominal voltage and amp-hour of the two batteries may vary. To allow for a more accurate and consistent system, different battery ratings are used in simulating this system as in Table 11. Different battery parameters may cause current sharing issues between the two charger converters, due to their shared connection at the DC bus. Droop control combined with MPC is proposed for better management of current differences. A virtual resistance is selected for each charger and multiplied by feedback battery current to generate the voltage droop [32, 123], and then subtracted by the DC bus voltage to generate the output voltage reference of the corresponding charger.

4.5.3 Results and discussion

Digital simulations are carried out using Matlab/Simulink to show the performance and effectiveness of the proposed MPC in controlling the presented prototype of the utility-scale grid-

Table 11 System Parameters of Battery Charger System with PUC Inverter

Parameter	Value
Virtual Resistance for Battery 1	4 Ω
Virtual Resistance for Battery 2	8 Ω
Grid RMS voltage	120 V
DC bus voltage	150 V
Battery 1 Rated Voltage	60 V
Battery 2 Rated Voltage	100 V
Battery Power Capability	6.5 kwh
Battery Rated Power	750 W
SoC Estimation Technique	Coulomb Counting
Grid Rated Power	600 W
Load Rated Power	150 W
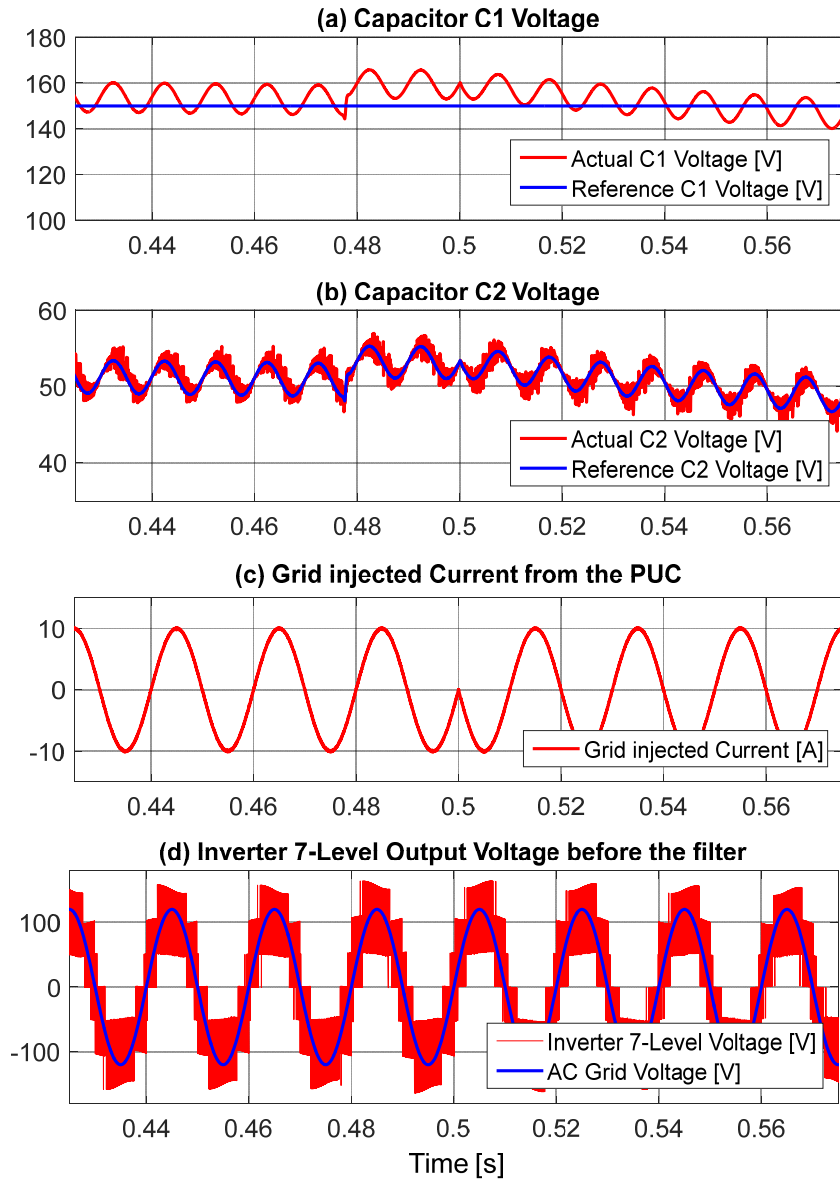
Figure 70 Packed U Cell waveforms. (a) Capacitor C1 Voltage; (b) Capacitor C2 Voltage; (c) Grid injected Current from PUC; (d) Inverter 7-level output voltage before filtering.

connected system. The power ratings and other key system parameters of the prototype are also in

Table 11. Three case studies are analyzed to evaluate the system performance of bidirectional

power flow and battery power management.

1. Case Study I—transition from discharging mode to charging mode
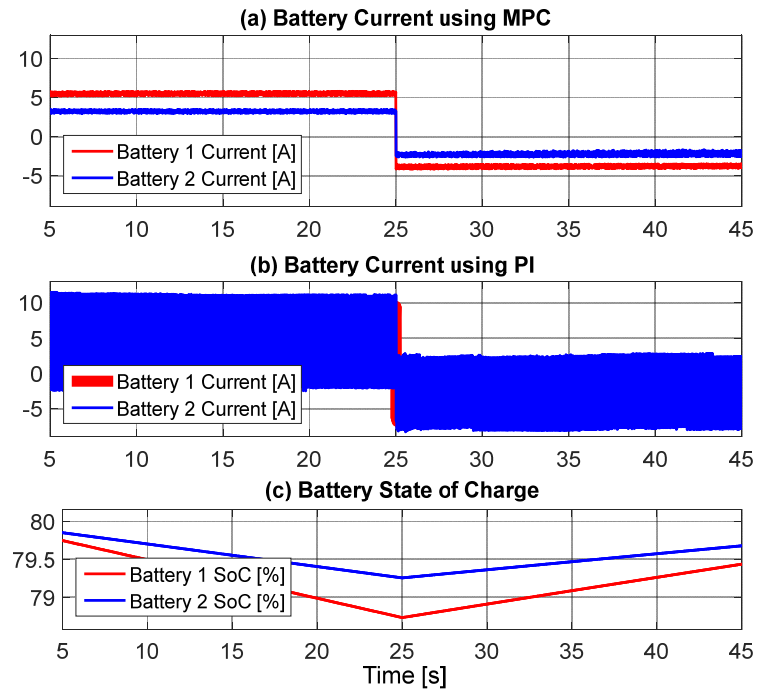
Figure 71 Battery currents comparison using PI and MPC. (a) Battery current using MPC; (b) Battery current using PI controller; (c) Battery state of charge.
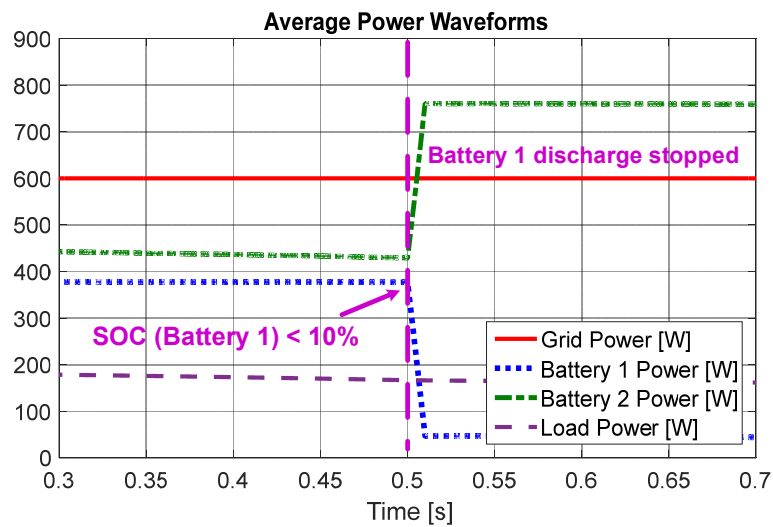
Figure 72 Power waveforms in case II

In this case, the initial SoCs of both batteries are within 10% to 90%, and they both provide power to the DC bus. To present the system capability of bidirectional power flow, grid current steps from 10A to -10A at time 0.5s. In response to this, the batteries will transit from discharging mode to charging mode, which is common in UPS systems. As shown in Figure 70, the PUC tracks the bus voltage at 150V with the capacitor C_2 voltage regulated to be one third of bus voltage during the transient period. The output voltage maintains 7-level waveform. Grid current total harmonic distortion is about 2% which is below the IEEE 519 standard [124]. The bus voltage deviates from the reference DC bus value 150 V within 10% because of droop control, which is acceptable for real world load applications. In Figure 71, the simulation time is intentionally set large to demonstrate stability over longer time ranges. Compared to the traditional PI control, the biggest benefits of MPC here is greatly reduced battery currents ripple shown. Because the MPC combines voltage and current control in the same priority, avoiding unnecessary large current variations introduced by PI inner current loop [13].

2. Case Study II—cut off one battery charger in case of overdischaring

The case II shown in Figure 72, DC bus current sharing before 0.5s demonstrate regular performance when powers are close sharing the same DC bus voltage. As battery 1 SoC drops below 10% at 0.5s, it enters into low power discharging mode to avoid over-discharging. The battery 1 power and current decrease gradually to less than 1 A, while battery 2 current increases to 7.5 A to compensate the power difference, providing power to the grid and load alone.

3. Case Study III—cut off one battery charger in case of overcharing

In this case, the battery 1 SoC reaches the threshold 90% at 0.5s in Figure 73. In case of overcharging, battery 1 power changes to a very low value and enters into trickling charging mode. As a result, the battery 2 power steps from -190W to -400W, where negative sign indicates battery

94
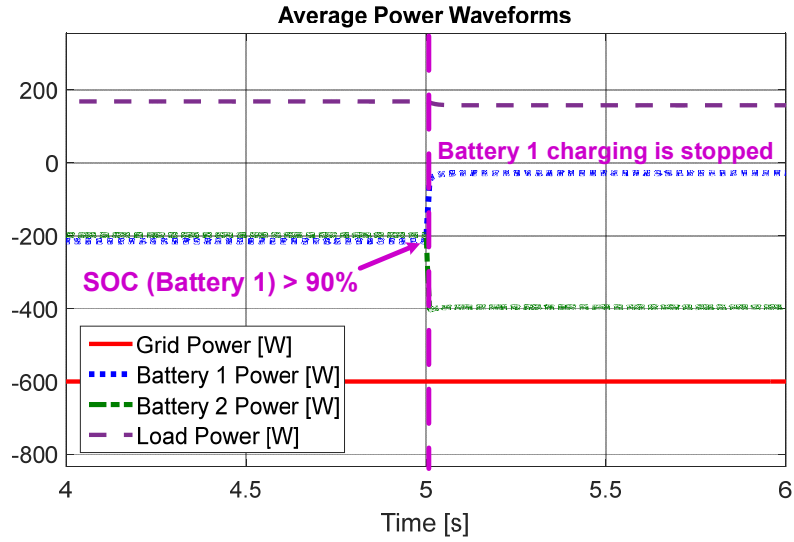
Figure 73 Power waveforms in case III.
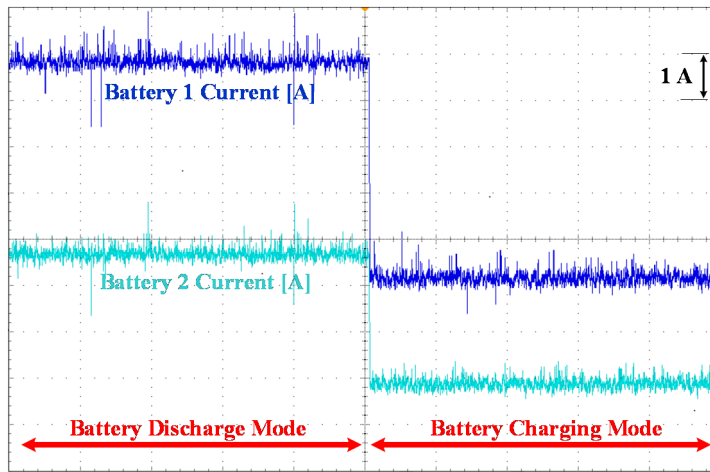
Figure 74 dSPACE Implementation of Battery Current using MPC

charging. The converter uses the battery to regulate the bus voltage to 150 V since the DC resistive load power stays at 150W.

Finally, case study I was reproduced using dSPACE 1007 to verify simulation results. Both battery currents are shown in Figure 74, which shows the transition from battery discharge mode to battery charging mode. Output of PUC is also demonstrated using dSpace 1007 in Figure 61,

95

which verifies the presence of the 7-level of the output voltage before filtering and levels are labeled according to their corresponding switching state according to Table 12.

Table 12 Switching table of the 3-Cell PUC Inverter

State	V_{AN}	s_1	s_2	s_3
1	0	0	0	0
2	$-V_2$	0	0	1
3	V_2-V_1	0	1	0
4	$-V_1$	0	1	1
5	V_1	1	0	0
6	V_1-V_2	1	0	1
7	V_2	1	1	0
8	0	1	1	1

4.6 Summary

First, continue with the section 3, a novel autonomous and distributed control strategies are proposed for the DC microgrid in grid-connected mode with distributed renewable energy units and storage system in detailed modeling, achieving regulated DC bus and accurate power sharing under several of conditions. The Model predictive control as the primary aims to improve the system dynamic responses and to enable the play and plug feature of distributed renewable energy sources and battery storage systems. An improved droop control based on DC bus signaling to realize the autonomous operation of the Dc-microgrid in grid-connected mode with the effective seamless transfer between modes of change of the whole system.

Later in this chapter, a model predictive control technique has been effectively applied for a power conditioning system composed of two battery chargers and one packed U cells inverter. In addition, the current sharing problem between parallel chargers is addressed properly with droop control. The proposed control technique is validated by simulation and dSPACE implementation results to be able to realize unity power factor, low total harmonics distortion at grid side, and reliable control of bi-directional power flow of the whole system, while balancing/tracking the two PUC capacitor voltages at its desired values. When compared to traditional PI control, the proposed method gains benefit in less battery current ripple, which can potentially increase the battery life in UPS or electrical vehicle.

5. ACTIVE POWER DECOUPLING METHOD BASED ON DUAL BUCK CIRCUIT[4]

5.1 Introduction

Single-phase rectifiers and inverters, which have wide applications in residential and industrial power conditioning systems, is a key component in a DC microgrid. However, the inherent double line frequency ripple power in single-phase system could be adverse to both DC and ac side, thus could adversely affect the whole DC microgrid system [125-128]. For grid-connected photovoltaic (PV) application, it could affect the maximum power point tracking (MPPT) efficiency of PV. For grid-connected energy storage systems, the low-frequency ripple power will result in overheating and other deleterious effects on the batteries, including shortening the operation lifetime [111]. A bulky electrolytic capacitor is typically connected at DC side to store the ripple power [129-131]. But the electrolytic capacitor has the disadvantages of large size, low reliability and short life span especially at high temperatures [132, 133].

To address this problem, active decoupling methods are considered to transfer the ripple power to smaller storage components through added active circuit, which permits large fluctuation of voltage or current (usually ac), therefore both the auxiliary circuit components and the DC-link capacitor can be small in size and weight [134-140]. Since the voltage of storage capacitor may vary in a much wider range than the one in passive power decoupling method without affecting the proper operation of the system, the capacitance required can be significantly reduced.

---

4 © 2018 IEEE. Reprinted, with permission, from S. Xiao, R S. Balog, "Dual Buck Based Power Decoupling Circuit for Single Phase Inverter/Rectifier", Applied Power Electronics Conference and Exposition (APEC), San Antonio, TX, USA, 2018 IEEE. © 2016 IEEE. Reprinted, with permission, from Xiao Li, S. Xiao, Haiyu Zhang, R S. Balog, Baoming Ge "Dual Buck Based Power Decoupling Circuit for Single Phase Inverter/Rectifier", Energy Conversion Congress and Exposition (ECCE), Milwaukee, USA, 2016 IEEE.
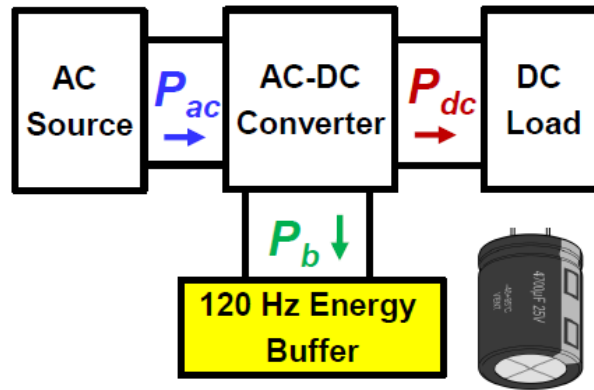
Figure 75 The Characteristic single phase rectifier or inverter

In many existing active power decoupling (APD) circuits [5-10], at least one phase leg with two switches is needed, which required dead-time control to prevent shoot through problems between the switches in one leg. In order to achieve a simple and compact design with a high reliability, an APD circuit based on the dual buck circuit is considered. Instead of one single yet bulky DC capacitor, two identical much smaller capacitors are connected in series across the DC bus. In this way, the DC-link capacitors can balance the dc bus ripple power. The voltages of the two capacitors are controlled so that the DC component magnitude are equal to the half of DC bus voltage and the ac component frequency are the same with the fundamental line frequency. Moreover, the ac components of the two capacitors are phase complementary such that the voltage ripple cancels out and the sum of voltages is constant and is equal to the DC-link voltage. The capacitors may be alternatively discharged to zero in case that high ripple power compensation is required. These two small capacitors exchange the ripple power with the main power circuit by charging and discharging, and the charging/discharging current is filtered by the inductors.

Characteristic structure of the single phase rectifier or inverter under study is shown in Figure 75. The additional active power decoupling circuit may be placed in series or in parallel
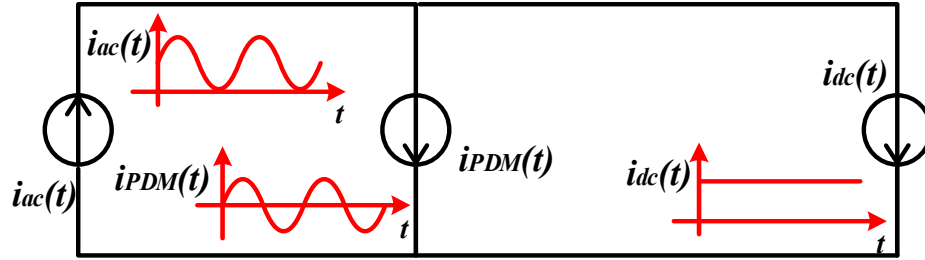
(a). Equivalent circuit of parallel power decoupling method.
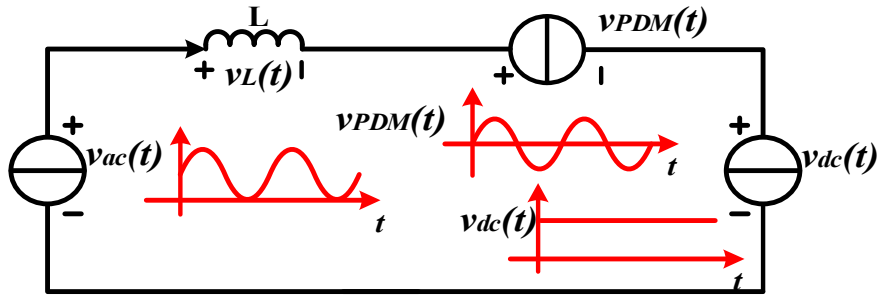
(b). Equivalent circuit of series power decoupling method.

Figure 76 Equivalent circuit of APD circuit

with the main power circuit. Their corresponding equivalent circuits are shown in Figure 76 [131].

Parallel connection has advantages over the series one because of its easiness in terms of switch

modulation and control on power decoupling circuit [141].

It is known that cross conduction between switches can result in shoot through issues, which

is the common failure mode of the circuit. Adding dead time control could prevent its occurrence, but

it may not work well in some cases, such as fault conditions. Moreover, the output waveforms may be

distorted because of the dead time effect, and the transferred equivalent power of pulse-width

modulation (PWM) could be reduced. Thus, it would be preferable to find a better solution to overcome

this challenge with the purpose of increasing the system reliability.

In order to achieve a simple and compact design with a high reliability, an active power

decoupling circuit to eliminate the double line frequency ripple power in DC microgrid with single

phase inverter/rectifier is proposed in this section [130, 131]. The split DC-link capacitors are directly utilized as energy storage components rather than a voltage stiffening component [131]. The split DC-link capacitors may not merely provide the transient DC power to support ac/DC or DC/ac conversion, but can also absorb the system ripple power. The energy stored in the split capacitors can be fully charged and discharged with a high energy utilization. Thus, a smaller total capacitance value is needed. The added power switches does not need dead time during switching, which maximizes the energy transferred to storage components. It completely eliminates the shoot through concerns, thus leading to greatly enhanced system reliability. Moreover, the body diode of MOSFET never conducts due to the unidirectional current characteristics of each phase leg. The freewheeling diodes used can be independently selected to minimize the switch losses.

In addition, a control strategy based on model predictive control (MPC) is proposed for this power decoupling circuit. MPC is a powerful class of controllers using the discrete model of a system to predict the future system behavior and choose the optimal control actuation [84, 111, 142, 143]. As such, the technique has numerous advantages over classical control methods including the simple structure for inclusion of operational constraints and multi-objectives in the MPC cost function [142]. Benefiting from the good transient performance of the MPC method, the proposed controller achieves good transient performance in tracking system load transition. Since the instantaneous ripple power is directly buffered into the power decoupling module, its energy storage capability to buffer the ripple power is fully performed. In summary, the new control method has the following benefits:

1) Fast dynamic response to the load transient compared with conventional method based on d-q transformation;

2) Maximum utilization of potential capacity to minimize the capacitance;

101
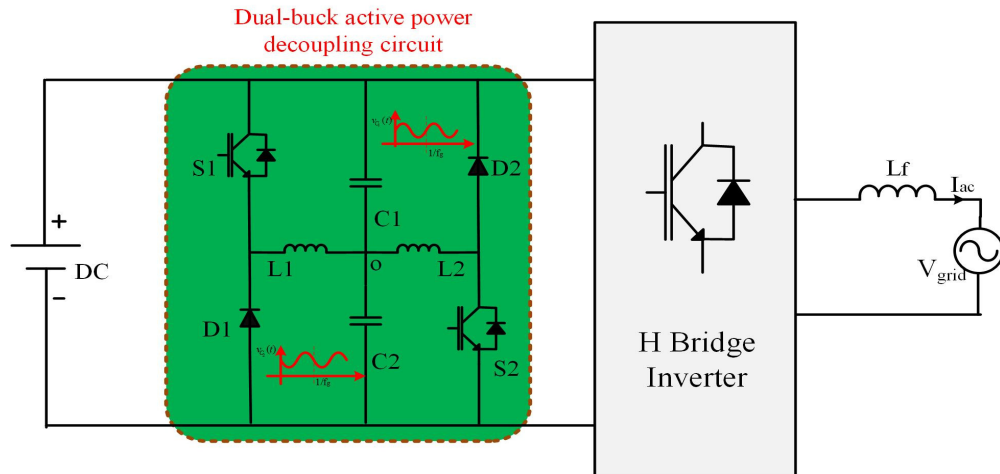
Figure 77 System configuration of APD in study

3) Simple implementation and controller design;

4) Inductor current is controlled instead of capacitor voltage, reducing the order of the control

system, enabling fast response.

The rest of this section is organized as follows. Section II describes the system

configuration, space model of the system, and prediction model of the system. Section III

illustrates the proposed model predictive control based method for dual-mode inverter in DC

microgrid. The operation modes and transition process of the system are discussed in detail.

Section IV presents the proposed phase detection and adjustment algorithm, which is followed by

the stability analysis of system in section V. Finally, a prototype is fabricated in the laboratory to

testify the proposed method. In section VI, the simulation and experimental results are provided to

verify the performance and effectiveness of the proposed control strategy.

5.2 Operation principles of the proposed dual buck based power decoupling circuit

The schematic of the proposed circuit is shown in Figure 77. The topology is, in principle,

two separate buck converters, which is made up of a left bridge leg (S1,D1,L1) and a right bridge

leg(S2,D2,L2), terminated with a split DC link, which is operated as the energy storage device or the buffer for the ripple power. Each bridge works on complimentary half cycle of the ac fundamental period, two identical capacitors are connected in series in the DC link. In this way, the DC-link capacitors may function to absorb the system ripple power. The voltages across two capacitors are controlled to have a DC component with a value equal to half of DC link voltage and an ac component with the fundamental line frequency. The ac component of the two capacitors has complementary phase relationship such that the voltage ripple cancels out and the sum of voltages is the constant DC link voltage. The capacitors can be alternatively discharged to zero in case that high ripple power compensation is required. Two capacitors exchange ripple power with main circuit by charging and discharging action. The charging/discharging current is smoothed by the inductors.

Due to the unidirectional inductor currents in both legs, each phase leg will only work in a half cycle. When current through inductor L_1 is positive, the left phase leg works. In this mode, S_2 is always OFF, and S_1 is driven by a PWM signal with the diode D_1 freewheeling the inductor current to the capacitor C_1 and C_2. Capacitor C_1 discharge its energy while capacitor C_2 works in charging mode. When current through inductor L_2 is positive, the right phase leg works. In this mode, S_1 is always OFF, and S_2 is driven by a PWM signal with the diode D_2 freewheeling the inductor current to the capacitor C_1 and C_2. Capacitor C_2 discharge its energy while capacitor C_1 works in charging mode.

As buck converter, each phase leg can operate in either continuous conduction mode (CCM) or discontinuous mode operation (DCM). To simplify the analysis of the operational principle, it is assumed that all inductors and capacitors are idea, $C_1=C_2$, $L_1=L_2$. Furthermore, power switches and diodes are thought to be ideal devices ignoring switching loss and conduction
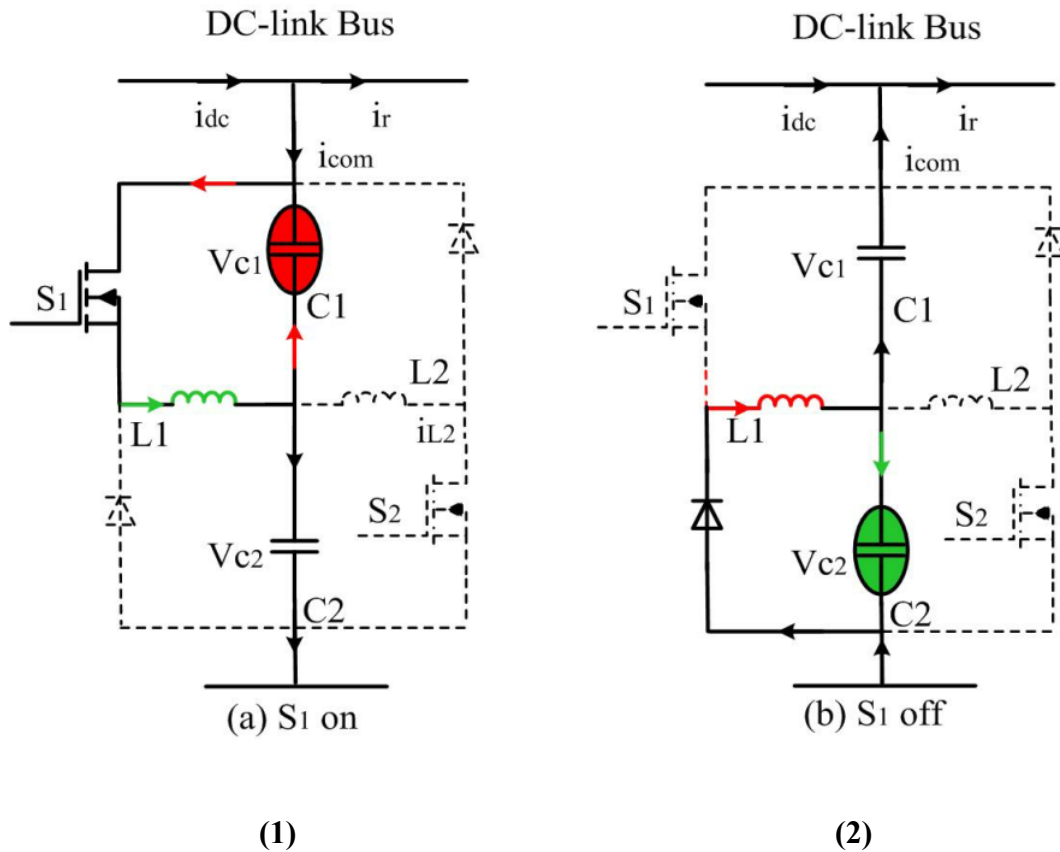
Figure 78 Operating modes of the power decoupling circuit (1) and (2).

voltage drops in the analysis. The operating procedures of the right bridge leg are the same as those of the left bridge leg.

There are four operating modes for the proposed decoupling circuit. Each phase leg has two operating modes during every switching period, and only works in half cycle, which is determined by the capacitor current. The operating condition and typical waveforms are illustrated in Figure 78 and Figure 79. The following analysis is based on the CCM operating condition, while the operating principle and analysis are also applicable to DCM.

(1)   When S1 is ON, S2 is OFF. The circuit operation is shown as Figure 78 (1), the inductor current increases linearly

Figure 79 Operating modes of the power decoupling circuit (3) and (4)

$$L_1 \frac{di_{L1}}{dt} = V_{dc} - V_{C2} = V_{C1} \tag{1}$$

In this case, C1 works in discharging condition and it sends energy to L1. While current through C2 is determined by condition of main circuit and the ripple power value. The voltage stress of the freewheeling diode D1 is the input voltage.

(2)   When S1 is OFF, S2 is OFF and the current through inductor L1 is nonzero. The current iL1 will continue to run through the freewheeling diode D1. The circuit operation is shown as Figure 78 (2), the inductor current decreases linearly

105

$$L_1 \frac{di_{L1}}{dt} = -V_{C2}$$

(2)

In this case, the current through C1 is equal to icom. While current through C2 is equal to the sum of icom and iL1. The voltage stress of the switch S1 is the input voltage.
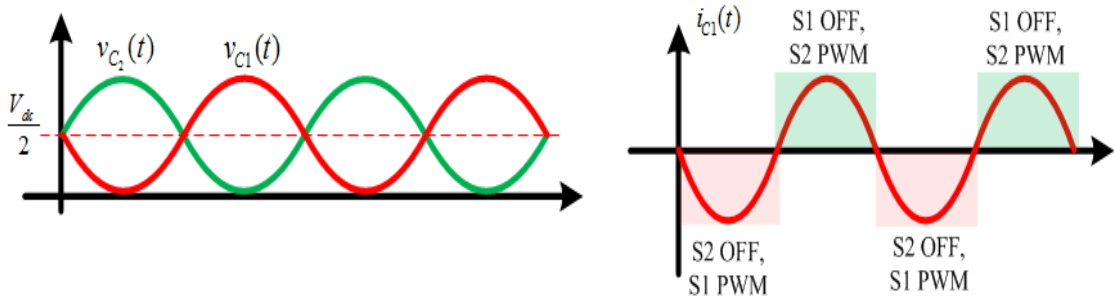
Figure 80 Operating waveform and conditions

When the capacitor current changes direction, another phase leg begins to operate and then the circuit operate in the other two modes. When the right phase leg operates, the switch in left phase leg will keep off.

(3)   When S2 is ON, S1 is OFF. The circuit operation is shown as Figure 79 (3), the inductor current increases linearly

$$L_2 \frac{di_{L2}}{dt} = V_{dc} - V_{C1} = V_{C2}$$

(3)

In this case, C1 works in discharging condition and sends energy to L2. While current through C1 is determined by condition of main circuit and the ripple power value. The voltage stress of the freewheeling diode D2 is the input voltage.

(4)   When S2 is OFF, S1 is OFF and the current through inductor L2 is nonzero. The current iL2 will continue to run through the freewheeling diode D1. The circuit operation is shown as Figure 79 (4), the inductor current decreases linearly

106

$$L_2 \frac{di_{L2}}{dt} = -V_{C1}$$

(4)

In this case, the current through C2 is equal to icom. While current through C1 is equal to the sum of icom and iL2. The voltage stress of the switch S2 is the input voltage.

This circuit has the following advantages: High reliability since no shoot-through concern and no need of deadtime consideration; Less storage components since DC link capacitors are used to buffer DC power and decouple ac power simultaneously; Simple and reliable control due to its independent power decoupling module with main circuit.

5.3 Prototype design

To simplify the analysis, assume the dual-buck converter works at continuous conduction mode (CCM). Then, the average small-signal model of the voltage balancer under CCM is derived to help select the right components and system parameters. The duty cycles of S1 and S2 are defined as d1(d1 = D1 + d1) and d2(d2 = D2 + d2), respectively, where D1, D2, d1, and d2 are stable duty ratios and the perturbations of S1 and S2.

5.3.1   Average small-signal model

The following shows the average small-signal model derivation when switch S1 operates in PWM mode and S2 keeps off.

When S1 is on

$$\begin{cases} v_{L1} = L_1 \frac{di_{L1}}{dt} = v_{in} - v_{C2} \\ i_{C2} = C_2 \frac{dv_{C2}}{dt} = i_{L1} + C_1 \frac{d(v_{in} - v_{C2})}{dt} \end{cases}$$

(5)

When S1 is off

$$\begin{cases} v_{L1} = L_1 \dfrac{di_{L1}}{dt} = v_{C2} \\ i_{C2} = C_2 \dfrac{dv_{C2}}{dt} = i_{L1} + C_1 \dfrac{d(v_{in} - v_{C2})}{dt} \end{cases} \tag{6}$$

The average model can be derived ($C_1 = C_2$) as

$$\begin{cases} L_1 \dfrac{d\tilde{i}_{L1}}{dt} = D_1 \tilde{v}_{in} + \tilde{d}_1 v_{in} - \tilde{v}_{C2} \\ 2C \dfrac{d\tilde{v}_{C2}}{dt} = \tilde{i}_{L1} + C \dfrac{d\tilde{v}_{in}}{dt} \end{cases} \tag{7}$$

The transfer function of the output voltage versus the duty cycle is

$$G(s) = \left. \frac{\tilde{v}_{C2}(s)}{\tilde{d}_1(s)} \right|_{\tilde{v}_{in}(s)=0} = \frac{V_{in}}{2LCs^2 + \dfrac{I_{ac}}{V_{ac}} Ls} \tag{8}$$

The following shows the average small-signal model derivation when switch S2 operates in PWM mode and S1 keeps off.

When S2 is on

$$\begin{cases} v_{L2} = L_2 \dfrac{di_{L2}}{dt} = v_{C2} \\ i_{C1} = C_1 \dfrac{dv_{C1}}{dt} = i_{L2} + C_2 \dfrac{d(v_{in} - v_{C1})}{dt} \end{cases} \tag{9}$$

When S2 is off

$$\begin{cases} v_{L2} = L_2 \dfrac{di_{L2}}{dt} = v_{in} - v_{C2} \\ i_{C1} = C_1 \dfrac{dv_{C1}}{dt} = i_{L2} + C_2 \dfrac{d(v_{in} - v_{C1})}{dt} \end{cases} \tag{10}$$

The average model can be derived ($C_1 = C_2$) as

108

$$\begin{cases} L_1 \dfrac{d\tilde{i}_{L1}}{dt} = D_1 \tilde{v}_{in} + \tilde{d}_1 v_{in} - \tilde{v}_{C2} \\ 2C \dfrac{d\tilde{v}_{C2}}{dt} = \tilde{i}_{L1} + C \dfrac{d\tilde{v}_{in}}{dt} \end{cases} \tag{11}$$

The transfer function of the output voltage versus the duty cycle is

$$G(s) = \left. \frac{\tilde{v}_{C2}(s)}{\tilde{d}_2(s)} \right|_{\tilde{v}_{in}(s)=0} = \frac{-V_{in}}{2LCs^2 + \dfrac{I_{ac}}{V_{ac}} Ls} \tag{12}$$

5.3.2 Components selection and system parameters

The main function of C_1 and C_2 is to store the ripple power. Large voltage ripple is allowed. Their capacitance value is mainly determined by storing capacity. They have to be large enough to store and transfer the ripple power completely. The minimum capacitance value needed considering the fully charged and discharged case can be represented as

$$C_1 = C_2 = \frac{P_{ac,\max}}{\omega V_{dc}^2} \tag{13}$$

The main function of inductor L_1 and L_2 is to smooth the current ripple in each phase leg. Large inductor may lead to more energy stored in it, which would decrease the energy storing capability of the power decoupling module. The critical value to make the circuit operate in CCM is listed as follows.

$$L_{cri} = Tv_{C2}\left(1 - \frac{v_{C2}}{\sqrt{\dfrac{V_{ac} I_{ac}}{2C\omega}}}\right) / 2i_L \tag{14}$$

Based on the analysis made above, a prototype shown in Figure 81 was designed to experimentally verify the performance of proposed power decoupling system and its operating
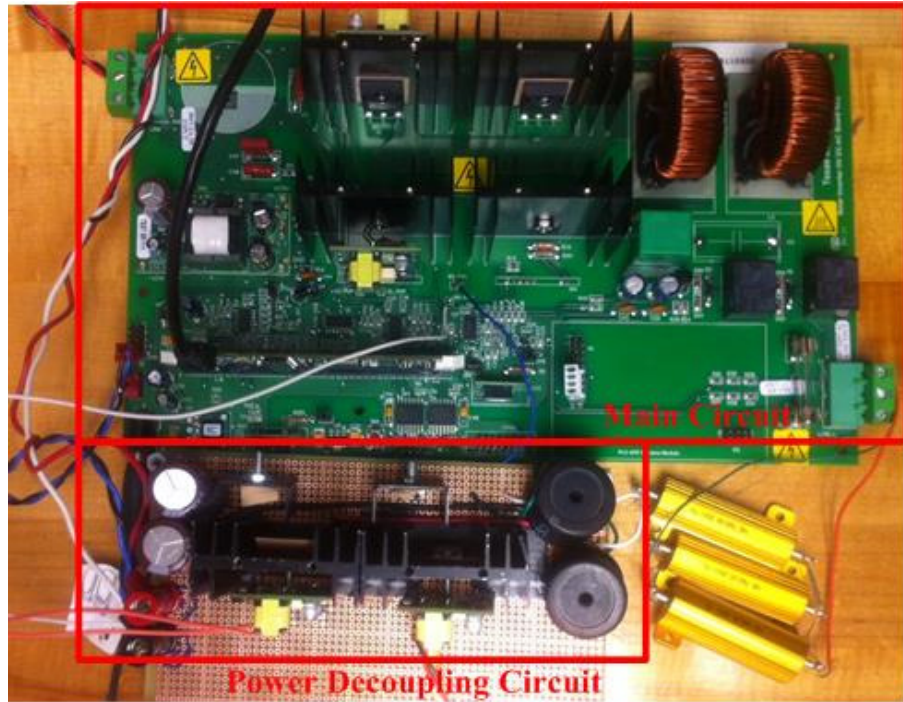
Figure 81 Experimental setup of Dual Buck APD

Table 13 System Parameters of Dual Buck APD Circuit

Parameter	Value
System power rating, P_m	1 kW
DC-link voltage, V_{dc}	300 V
DC-link capacitance, C	110 μF
AC output frequency, f_0	60 Hz
APD's inductance, L_1	1 mH
Filter inductance, L_f	3mH
AC voltage,$v_{ac\ (RMS)}$	110 V
Sampling Time, T_s	1 us

principle. The system parameters are shown in Table 13. The control algorithm was implemented based on TI Piccolo F28035 DSP, in which 3 different timer based tasks are scheduled to deal with the non-urgent tasks. Besides, 3 interrupt service routines are used on the background to deal with the urgent things, such as the close loop controllers, the capture event and protection. Three channels of ADC are used to sample three variables: output voltage main circuit (V_{ac}), load current of main circuit (I_{ac}) and voltage of decoupling capacitor C2(V_c). There are mainly four parts in the main routine: a) sample variables; b) rms value of the reference voltage (Vref) determination and mode selection; and c) loop compensation d) update the gate signal.

5.4 Ripple compensation design with traditional PI controller

5.4.1   Controller design

Assuming the voltage and current at AC side can be represented as

$$\begin{cases} v_{ac}(t) = V_{ac} \sin \omega t \\ i_{ac}(t) = I_{ac} \sin(\omega t + \theta) \end{cases}$$

(15)

Then the instantaneous power is

$$p_{ac}(t) = \frac{1}{2} V_{ac} I_{ac} \cos \theta - \left[\frac{1}{2} V_{ac} I_{ac} \cos(2\omega t - \theta) + \frac{\omega L I_{ac}^2}{2} \sin(2\omega t + 2\theta) \right]$$

(16)

In order to store the double-line frequency ripple power in two storage capacitors while holding the DC link voltage, the voltage of them are controlled to be sinusoidal with fundamental frequency and an offset DC value that equals to half of the DC-link voltage $V_{dc}/2$. Their instantaneous value together with their individual currents can be represented as

$$\begin{cases} v_{C2}(t) = \frac{V_{dc}}{2} + V_c \sin(\omega t + \theta_c) \\ v_{C1}(t) = \frac{V_{dc}}{2} - V_c \sin(\omega t + \theta_c) \end{cases}$$

(17)

111
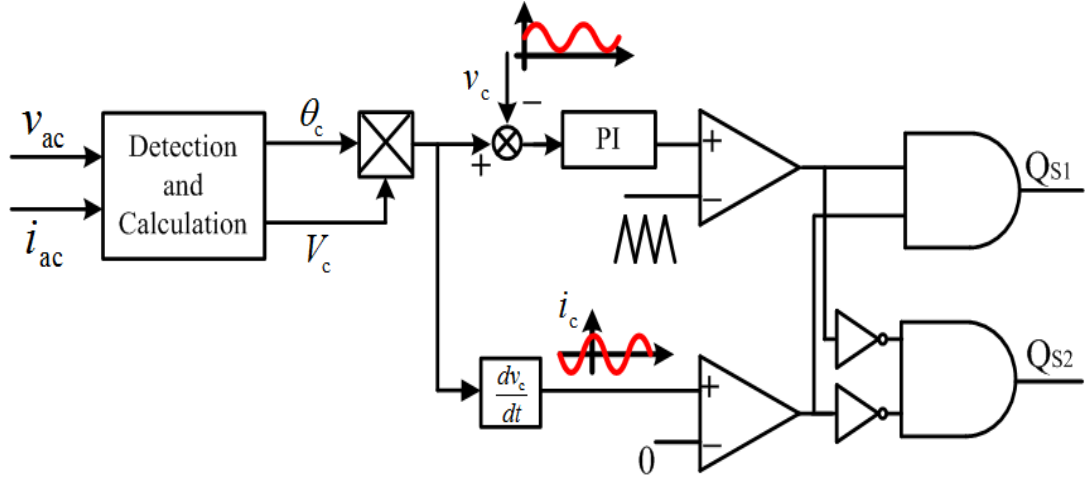
Figure 82 Control strategy of power decoupling circuit.

In this case, two identical capacitors are connected in series, $C_1=C_2=C$. The instantaneous power pc (t) provided by these two capacitors is

$$p_c(t) = v_{C1}i_{C1} + v_{C2}i_{C2} = C\omega V_c^2 \sin(2wt + 2\theta_c)$$

(18)

According to (6) and (8), and assuming the stored energy in the inductor is negligible, the following equations are derived:

$$V_C = \sqrt{\frac{V_{ac}I_{ac}}{2C\omega}} \; , \; \theta_c = \theta - \frac{\pi}{4}$$

(19)

The equation above shows the condition to completely buffer ripple power through power decoupling circuit. Based on that, a control strategy is proposed to regulate the decoupling performance with feedback loop. The proposed control strategy is presented in Figure 82 and Figure 83. A voltage loop is formed to regulate the capacitor voltage and ensure its value tracks the derived reference value which is determined by the voltage and current condition in ac side of main circuit. The output signal of the voltage regulator is directly sent to modulate the switches, and its differential value determine the conduction cycle of phase legs.

112
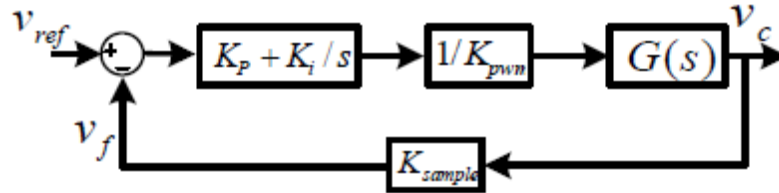
Figure 83 Block diagram of the controller.

The closed loop transfer function of the control system, $\Gamma(s)$ can be obtained based on block

diagram as

$$\Gamma(s) = \frac{(K_p + K_i / s)G(s)}{K_{pwm} + K_{sample}(K_p + K_i / s)G(s)}$$

(20)

5.4.2 Simulation and experimental results

Table 14 Electrical specifications in simulation

	Without power decoupling circuit	With power decoupling circuit
V_{dc}=30V M=0.3, Rload=2Ω	C_{dc} = 470 uF V_{ripple} = 16%	$C_1 = C_2 = 220$ uF V_{ripple} = 4.7%
V_{dc}=300V M(modulation index of inverter)=0.6, R_{load}=10Ω	Cdc = 470 uF V_{ripple} = 9.3%	C1 = C2 = 90 uF Vripple = 3.3%
	Cdc = 1500 uF V_{ripple} = 3%	C1=C2 = 220 uF Vripple = 1.1%

The proposed power decoupling circuit is evaluated based on single phase inverter

prototype. Table 14 lists the system specifications in different cases. In order to show the

effectiveness of the proposed power decoupling system, the comparative simulation and experimental results are given between single phase inverter systems with and without the proposed power decoupling circuit.
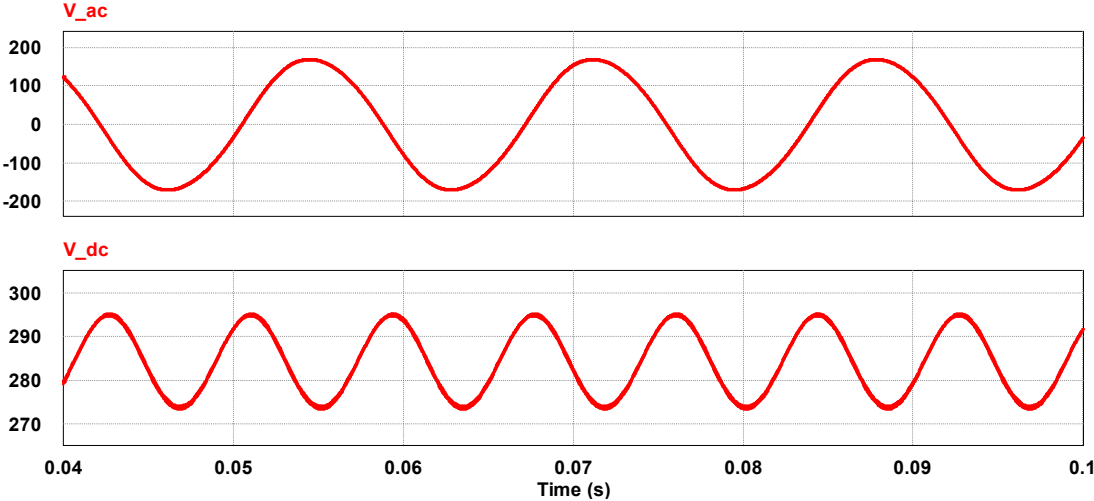
Figure 84 Simulation results of system without proposed APD circuit but with C_{dc}=470 uF
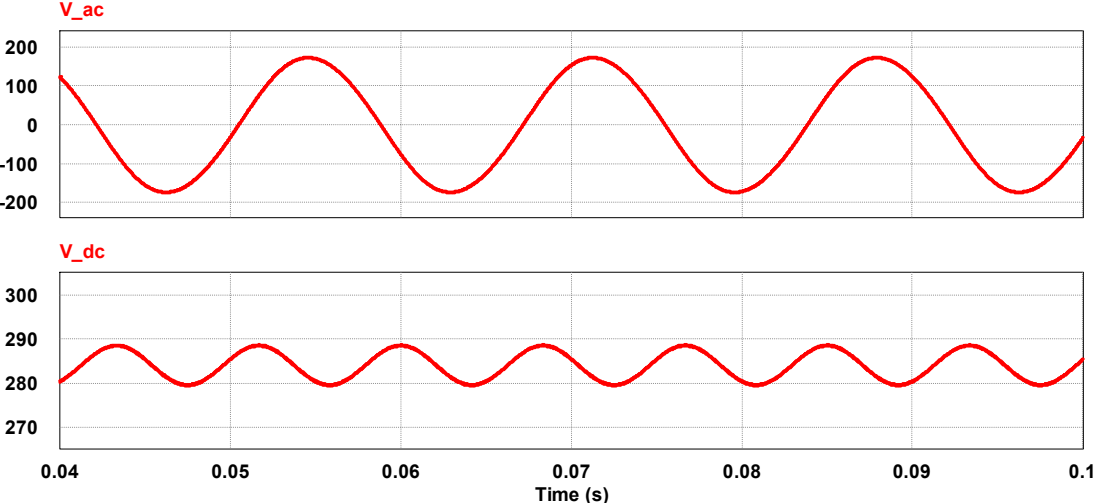
Figure 85 Simulation results of system without proposed APD circuit but with C_{dc}=1500 uF

Figure 84-Figure 87 show the comparative steady state simulation results of single phase inverter system with and without proposed power decoupling circuit when the DC link voltage is

114
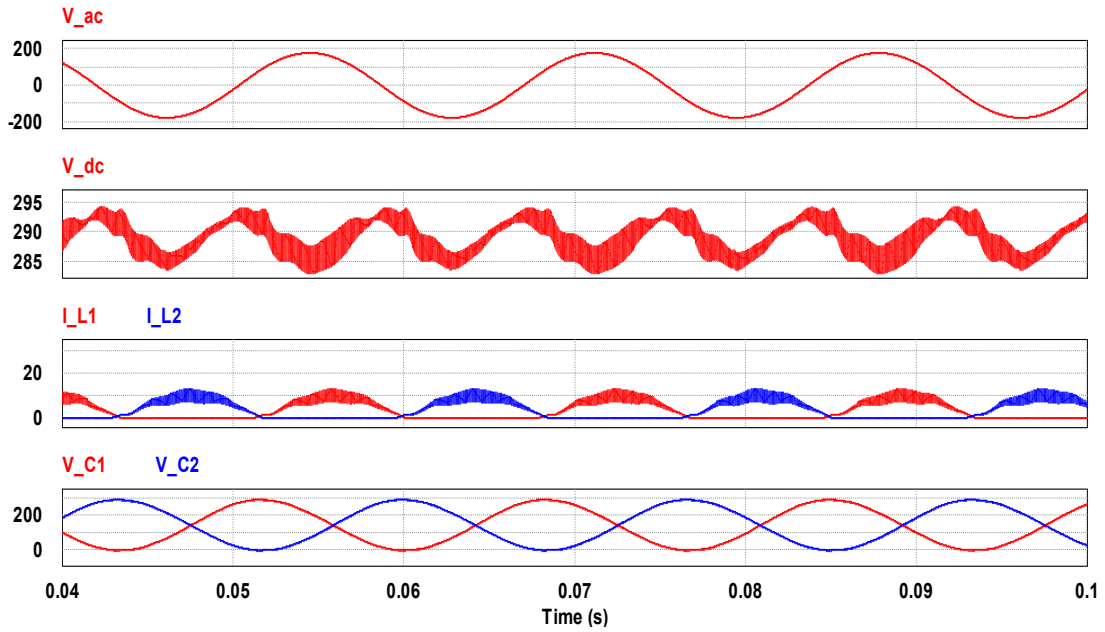
Figure 86 Simulation results with proposed APD circuit with two small DC caps $C_1 = C_2 = 90$ uF
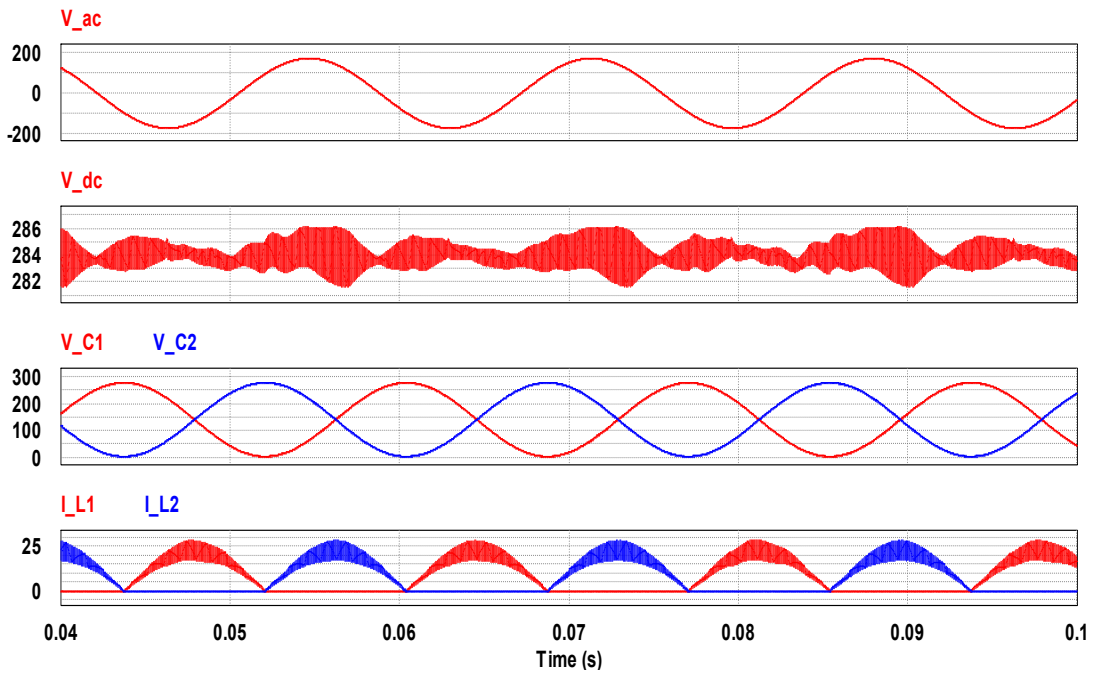
Figure 87 Simulation results with proposed APD circuit with two small DC caps $C_1 = C_2 = 220$ uF

300V. As shown in Figure 75, normally there is a big capacitor connected in DC-link, there still remains a big voltage ripple and current ripple at DC side. With an active power decoupling circuit with smaller capacitors, the DC link voltage ripple could be reduced largely. When the DC link voltage is 300 V, with a much smaller DC link capacitor, the DC link voltage ripple could be regulated well with the proposed power decoupling circuit as shown in Figure 86 and Figure 87. The steady-state simulation results of DC link voltage and component waveforms are shown in details. Thanks to the smooth DC-link voltage, the output voltage of ac load can be regulated well with sinusoidal waveform and smaller THD value. The two film capacitors can provide the required double-line frequency ripple power, and the DC-link voltage has much smaller voltage variation. It can be seen that the proposed power decoupling circuit has a significant reduction in 2ω ripple at DC link even with smaller capacitor.
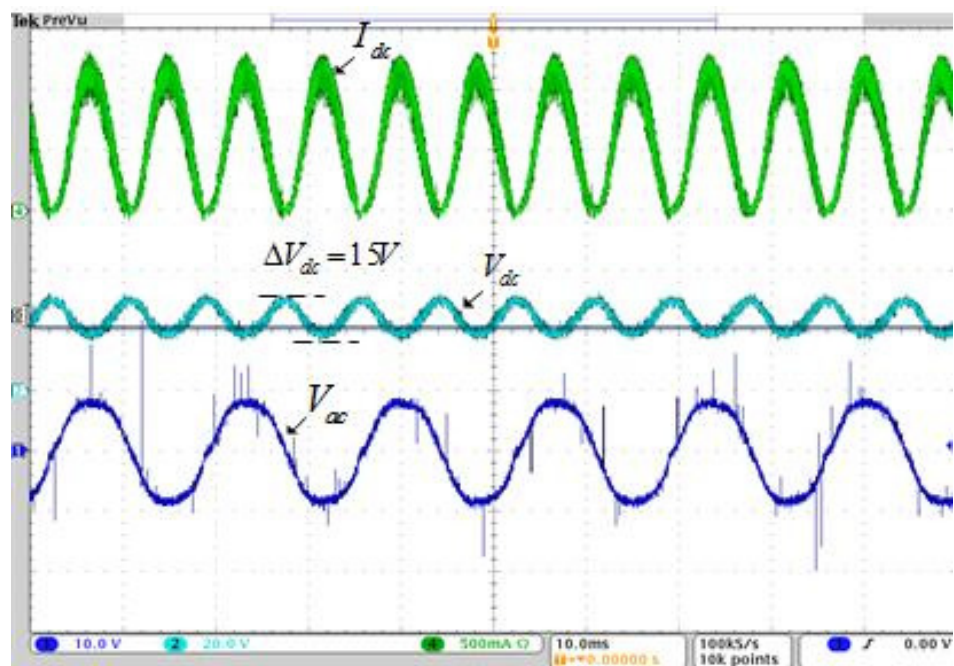
Figure 88 Steady state performance without power decoupling circuit

116
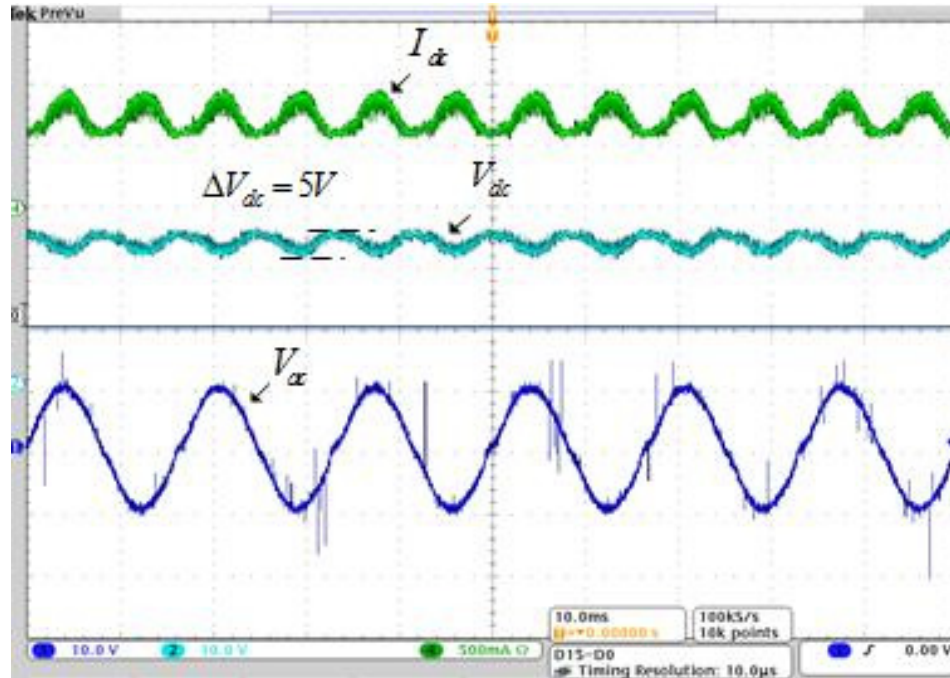
Figure 89 Experimental results of steady state performance of main circuit
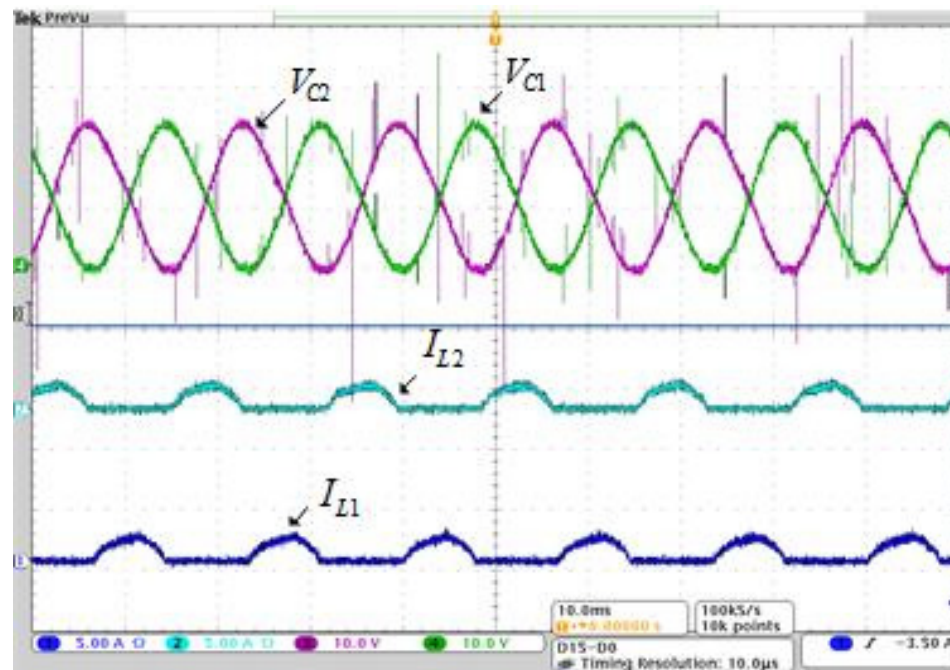
Figure 90 Experimental results of steady state performance of power decoupling circuit

Figure 88 shows the system experimental performance without proposed power decoupling module. The DC-link capacitor used in this case is 470 uF. Figure 89 shows experimental results after power decoupling module is added. It can be seen that the proposed topology and control method can eliminate double line frequency ripple power and diminish the voltage ripple at DC link greatly even with smaller capacitor. The voltage of DC link capacitors and current through smoothing inductors are shown in Figure 90. As shown in results, the voltage in two capacitors have complementary ac component, which ensures the small fluctuation on DC link voltage. Each phase leg in power decoupling module operates in half cycle. The experimental results coincide well with simulation results.

5.5 Ripple compensation design with model predictive controller

5.5.1 Controller design

To simplify the analysis, assume the dual-buck converter works at continuous conduction mode (CCM) and assume the voltage and current at AC side are in the form as

$$\begin{cases} v_{ac}(t) = V_{ac}\sin\omega t \\ i_{ac}(t) = I_{ac}\sin(\omega t + \theta) \end{cases} \tag{20}$$

Then the instantaneous power can be calculated as

$$p_{ac}(t) = \frac{1}{2}V_{ac}I_{ac}\cos\theta - \left[\frac{1}{2}V_{ac}I_{ac}\cos(2\omega t - \theta) + \frac{\omega L_f I_{ac}^2}{2}\sin(2\omega t + 2\theta)\right] \tag{21}$$

As indicated above, the C1/C2 voltages and currents should be controlled as equation (7):

$$\begin{cases} v_{C2}(t) = \dfrac{V_{dc}}{2} + V_c\sin(\omega t + \theta_c) \\ v_{C1}(t) = \dfrac{V_{dc}}{2} - V_c\sin(\omega t + \theta_c) \end{cases}$$

$$\begin{cases} i_{C2}(t) = C\omega V_c \cos(\omega t + \theta_c) \\ i_{C1}(t) = -C\omega V_c \cos(\omega t + \theta_c) \end{cases} \tag{22}$$

Here, the two decoupling capacitors are assumed to be equal to each other i.e. $C_1 = C_2 = C$. Since the working principle of the two buck converters are identical, only the left bridge leg is discussed in the rest paper. Taking the inductor reactive power into consideration, the instantaneous C1 ripple power $P_{c1}(t)$ is

$$p_{c1}(t) = \frac{v_{ac} i_{ac}}{2} - L_1 \frac{di_{ac}}{dt} i_{ac} \tag{23}$$
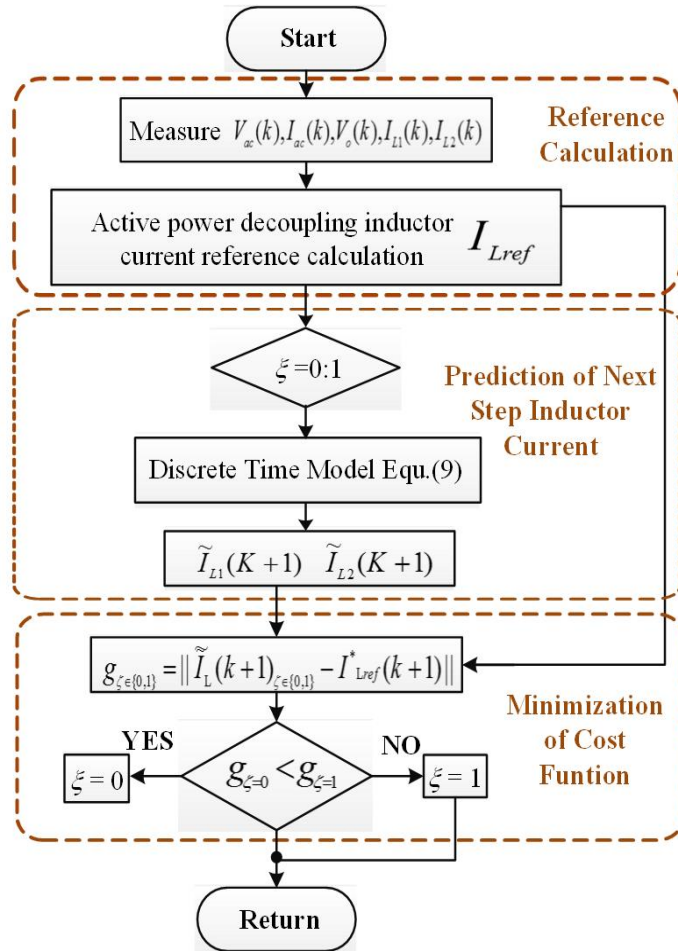
Figure 91 Flow Chart of the MPC Implementation

119

In each half cycle, the average energy stored in the inductor is zero and from equations (6) to (8), the following equations are derived which are used to generate the current reference i_{Lref} for the inductors in the APD circuit:

$$I_{ref} = 2 * I_{C1} = \sqrt{\frac{P_{ac\_2w}}{2(\frac{1}{C\omega} - wL)}}$$

$$\begin{cases} \theta_c = \theta - \frac{\pi}{4} \\ P_{ac\_2w} = \sqrt{(V_{ac}I_{ac})^2 + 2wLV_{ac}I^3_{ac}\sin(\theta)} \end{cases} \tag{24}$$
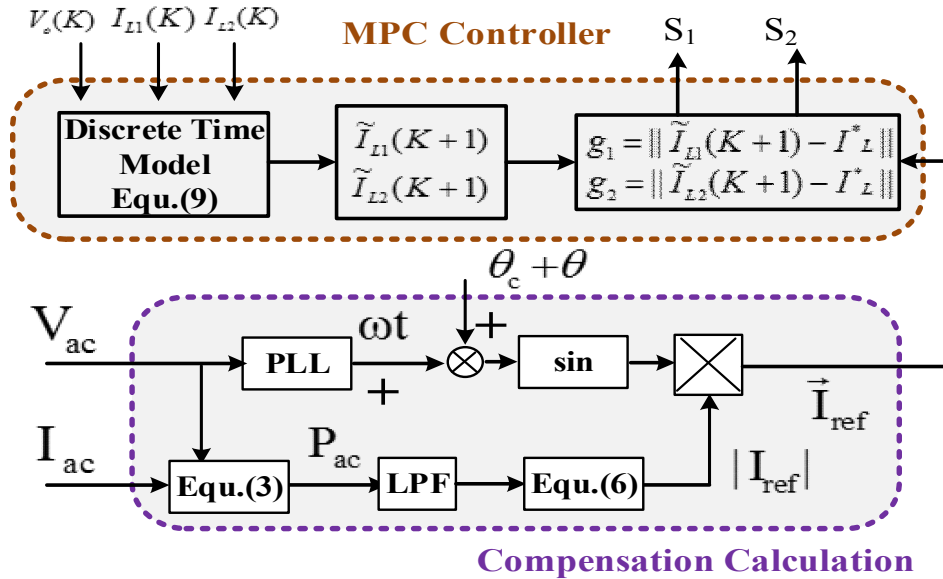
Figure 92 System control strategies

The voltage of inductor L1 is

$$v_{L1} = L_1 \frac{di_{c1}}{dt} i_{c1} = v_{s1} - v_o \tag{25}$$

Converting (1) into a discrete time model by the Euler forward method, the inductor current can be predicted by

120

$$i_{L1}(k+1) = i_{L1}(k) + \frac{T_s}{L_1}(v_{s1} - v_o) \tag{26}$$

Thus the behavior of the system can be predicted at the next sampling time (K+1) and the predicted model of the inductor when switch is ON and OFF is given as

$$\begin{cases} i_{L1}(k+1) = i_{L1}(k) + \dfrac{T_s}{L_1}(V_{dc}(k) - v_o(k)) & \zeta = 1 \\[2mm] i_{L1}(k+1) = i_{L1}(k) + \dfrac{T_s}{L_1}(0 - v_o(k)) & \zeta = 0 \end{cases} \tag{27}$$

Where T_s is the sampling period; $i_{L1}(k)$ is the inductor L1 current at the kth time instant; $i_{L1}(k+1)$ is the predicted current at the $(k+1)$th time instant; $V_{dc}(k)$ and $vo(k)$ are the voltages of DC bus and neutral point respectively.

The proposed technique predicts the tracking error of the next sampling for both possible

Table 15 Comparison of Vdc_ripple without/with the proposed APD

V_{dc}=300V **M=0.6** **R$_{load}$=10Ω**	**C_{dc} = 470 uF**	**$\Delta V_{dc}/V_{dc}$ = 9.3%**
	C_{dc} = 1500 uF	**$\Delta V_{dc}/V_{dc}$ = 3%**
	C_1 = C_2 = 180 uF	**$\Delta V_{dc}/V_{dc}$ = 3.3%**
	C_1 = C_2 = 320 uF	**$\Delta V_{dc}/V_{dc}$ = 1.1%**

switching states per converter (switch ON and OFF) by calculating the cost functions (g0 and g1) as the equation (10):

$$g_{\zeta \in \{0,1\}} = \| \tilde{I}_L(k+1)_{\zeta \in \{0,1\}} - I^*_{Lref}(k+1) \| \tag{28}$$
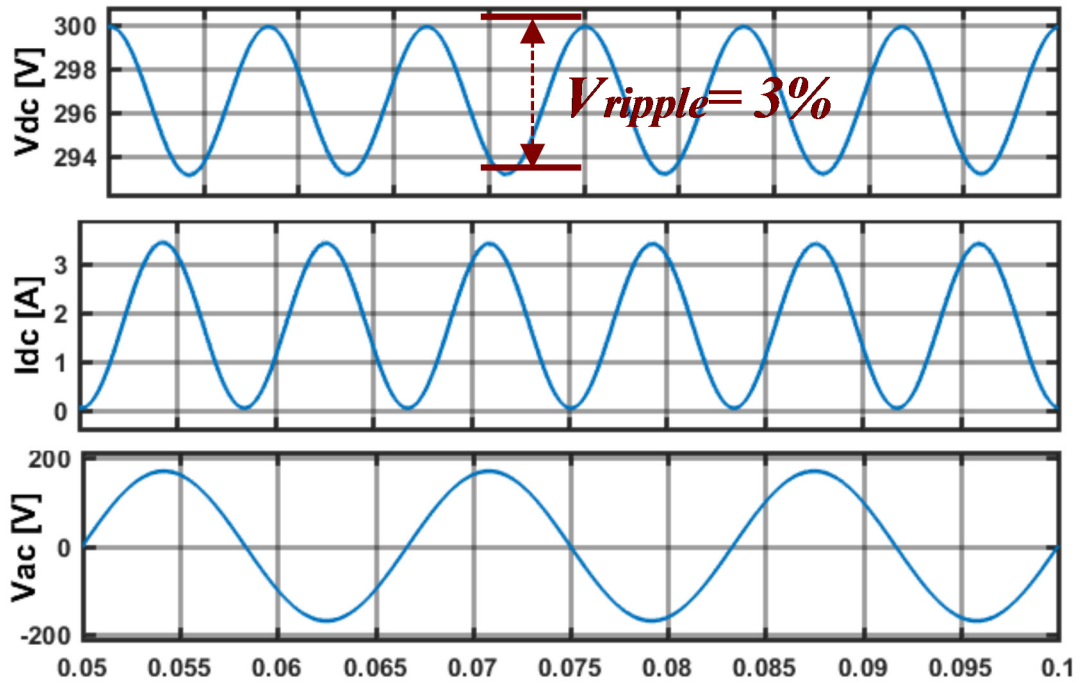
Figure 93 Case 1: Steady state Vdc, Idc and Vac waveforms without APD
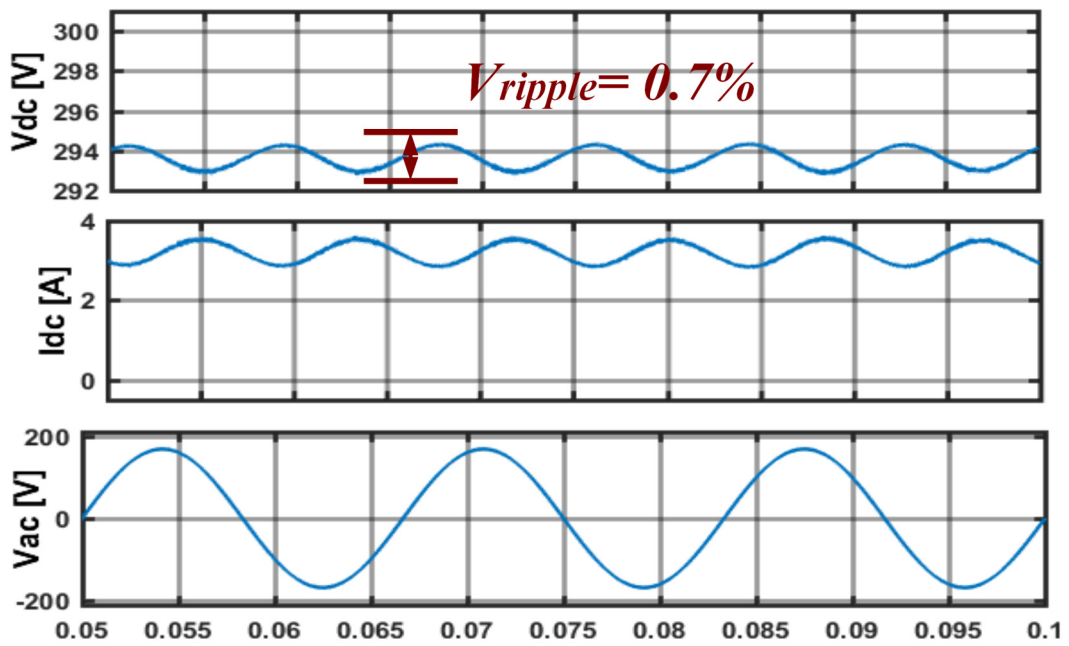
Figure 94 Case 1: Steady state Vdc, Idc and Vac waveforms with APD
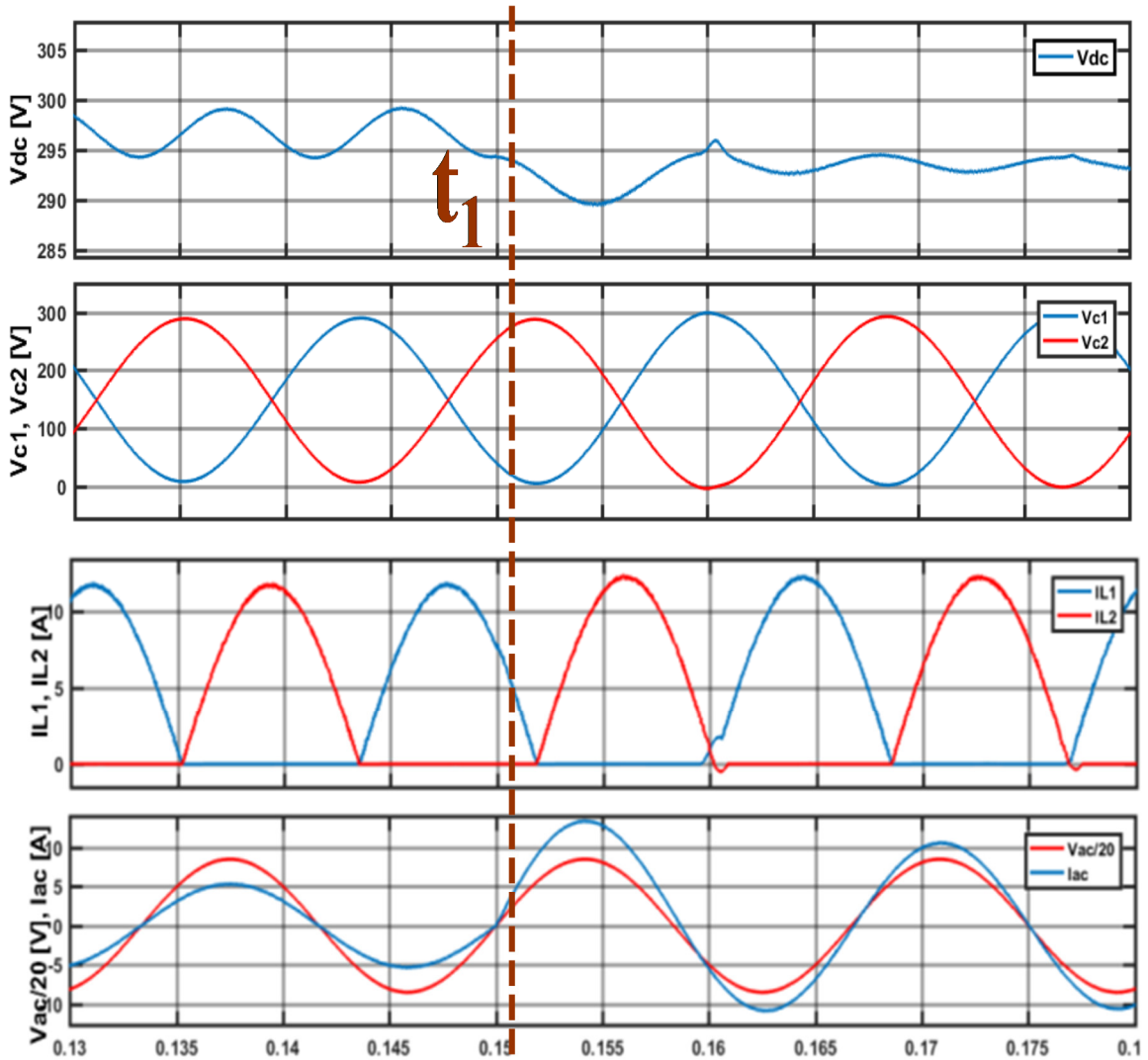
Figure 95 Case 2: Dynamic responses during ac transient

The switching state that minimizes these cost function equation (10) will be applied to their corresponding converters as shown in Figure 77. The control of the proposed active power decoupling circuit is independent with the control of the H bridge inverter, which is also controlled by the MPC but is not the focus of this paper. Figure 91 shows the detailed flowchart of the proposed MPC algorithm for the dual-buck APD circuit.

5.5.2 Simulation and experimental results

A 1kW prototype shown in Figure 76 was used to experimentally verify the performance of proposed power decoupling system and its operating principle. Table 15 lists the system specifications of the circuit under different cases. The DC-link capacitor used is only 110 uF, which is orders of magnitude smaller than the bulky capacitor without the active power decoupling circuit. The results of two case studies are discussed here to show the effectiveness of the proposed power decoupling system.

1. Case Study I— Steady state performance with and without the proposed APD circuit

The steady state ac side active power is set to be 900W. When the proposed active power decoupling system is disabled, the ripple component in the DC bus voltage (3%) and current are noticeable as shown in Figure 93. In Figure 94, those two waveforms have much smaller 2w ripple components under the same scale. The ripple magnitudes are reduced to 16.7% of those without the implementation of the proposed APD method, which clearly demonstrates the effectiveness of the proposed control system in diminishing the ripple power.

2. Case Study II— Dynamic performance during ac transient

Figure 95 shows the power dynamic response of the system when the active power steps from 450W to 900W at T_1 (0.15s). The ac voltage magnitude is scaled down by 20 to compare with the ac current on the same axis. In experimental result in Figure 96, the capacitor voltages V_{C1}, V_{C2} are controlled to ranging from 0 to V_{dc} (200V), exploiting the full energy buffer capacity of the two small DC split capacitors. Moreover, the inductor current i_{L1}, i_{L2} tracks the i_{Lref} accurately in each half cycle even during ac load transient, thanks to the fast dynamic characteristic of the MPC. Therefore, the DC bus voltage always remains relatively clean even under load transient. It can be seen that the proposed topology and control method can eliminate double line
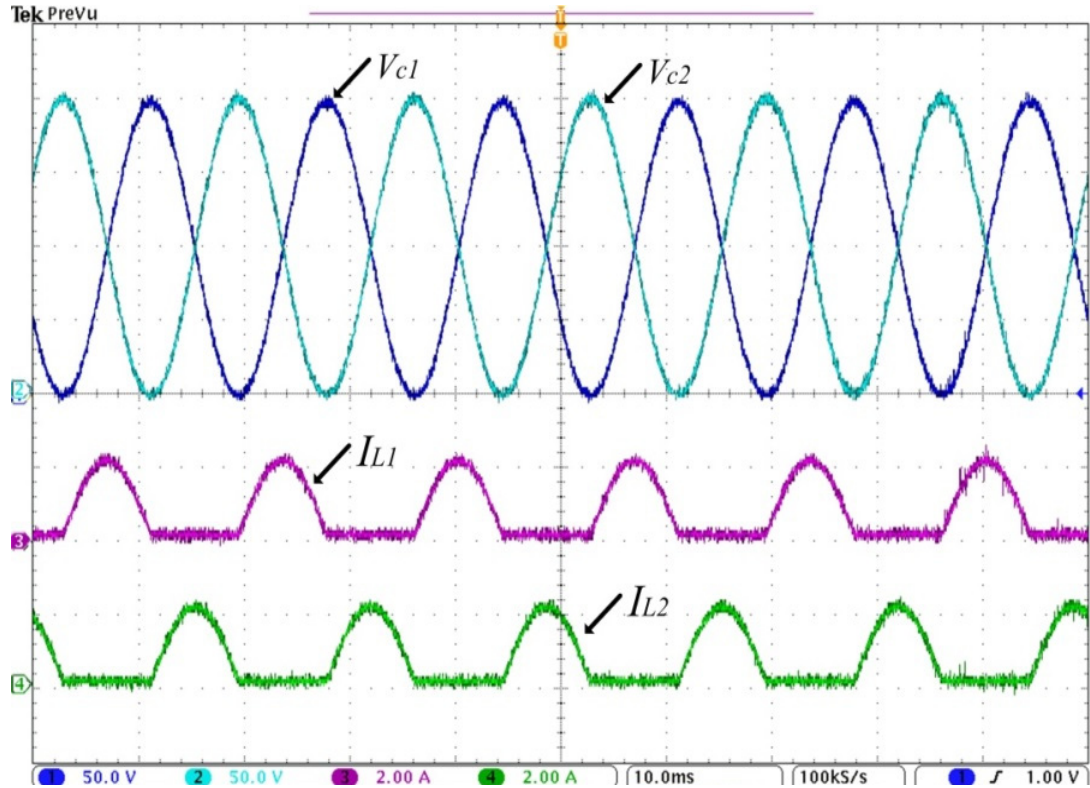
Figure 96 Experimental results of steady state performance of power decoupling circuit.

frequency ripple power and diminish the voltage ripple at DC link greatly even with smaller capacitor. The voltage in two capacitors have complementary ac component, which ensures the small fluctuation on DC link voltage. Each phase leg in power decoupling module operates in half cycle. The experimental results coincide well with simulation results.

5.6 Summary

In this section, a power decoupling circuit with dual buck converters and two different control strategies are proposed. The ripple power is stored in split DC link capacitors with high energy utilization. The proposed power decoupling circuit does not need any external storage component except DC-link component. It does not have shoot-through problem, thus it could enhance the overall system reliability. There is no need of dead time, thus more energy can be

transferred without introducing dead-time distortion into the current waveforms. Detailed description on circuit's working fundamental and its design process on circuit components and controller is presented. The proposed power decoupling circuit could heavily reduce the storage capacitance needed, which is validated through simulation and hardware results. In addition, with the model predictive control, the design process is greatly simplified without sacrificing the control effectiveness even with better dynamic system performance.

6. CONCLUSIONS AND FUTURE WORKS

6.1 Conclusions

This dissertation presents an advanced hierarchy autonomous control strategies for a DC microgrid consisted of distributed renewable energy sources, energy storage system, and grid-connected inverters. Verified by many possible scenarios, the proposed control strategies achieved reliable and economic operation of the DC microgrid, enabling the concept a more wide scale adoption. At the same time, new maximum power point tracking and double line frequency power decoupling techniques have been investigated to improve the system performances. The main contributions of this dissertation from the author's point of view can be summarized as below:

1. An adaptive maximum power tracking technique to mitigate the oscillation around maximum power point (MPP). This control method is proved independent with the environmental conditions and has much smaller oscillations around the MPP compared to existing ones. Therefore, it helps increase the energy harvest efficiency of the DC microgrid with less continuous DC power ripple.

2. Proposed the DC microgrid with distributed renewable energy units, storage system and multilevel inverter in detailed modeling, achieving regulated DC bus control and accurate power sharing under several of conditions.

3. Model predictive control is adopted as the primary loop controller of the proposed hierarchy autonomous control strategies to improve the system dynamic responses and to enable the play and plug feature of the distributed renewable energy sources and battery storage systems. Compared with traditional PI controllers, MPC speeds up the control loop since it predicts error before the switching signal is applied to the converter. It is also free of tuning through

the minimization of a flexible user-defined cost function. Thus, the proposed primary loop enables the system to be expandable by adding additional energy generation units without affecting the existing ones.

4. An improved distributed droop control based on DC bus signaling is proposed as the secondary loop of the proposed hierarchy autonomous control strategies. To reduce the dependence on the high bandwidth communication line, the DC bus voltage is utilized as the trigger signal to the change of operation modes. With the sacrifice of some small bus voltage variations, a fully autonomous control can be realized. The proposed distributed droop control of different unit converters also eliminates the potential conflicts when more than two converters compete for the VSC mode.

5. The DC microgrid normally operate with the grid connected. However, it must be disconnected from the utility when fault happens at grid side. The proposed control ensures an effective seamless transfer between modes of change, i.e. the switch between the grid-connected modes to the islanded mode when the DC microgrid operate alone without the grid connected.

6. The model predictive control for the grid-connected battery systems with PUC inverter is proposed. A packed U cells (PUC) seven-level inverter has been selected as the interface between the battery charger and the grid for its low cost and fewer numbers of components. Additionally, PUC has higher energy conversion quality when compared to traditional H-bridge. The proposed MPC technique may realize unity power factor, low grid current total harmonics distortion at grid side, and reliable control of bi-directional power flow in the batteries-PUC system.

7. DC bus low frequency power ripple reduction with the proposed dual buck active power decoupling circuit controlled by two different control algorithms. The topology is free of shoot-

through and deadtime concern and the control is independent with that of the main power stage circuit, which makes the design simpler and more reliable. While, both methods present satisfied decoupling performances on the system, the proposed MPC is simpler to be implemented.

6.2 Future works

Although many aspects have been explored in this dissertation for advanced control of DC microgrids, there are still a lot of possibilities for further technology improvement. Some issues of high interest for future investigations are listed below:

- As mentioned in the first section, thought the DC microgrid has advantages for its inherent DC coupling to renewable energy sources, the ac microgrid can still find many applications where ac loads are dominant. Moreover, both the DC and ac microgrids share some common features, such as the bus voltage regulation, the energy storage management and the seamless transfer between grid-connected and islanded modes. In light of these, it would be practical to modify the proposed control strategies of a DC microgrid by only adding phase/frequency detection/synchronization control, and then applied it to the control of an ac microgrid.

- The proposed control strategies are only validated by real-time simulation on the laboratory DC microgrid, which is less than 10kW. Future work may consider trying to implement the control into MW-scale distributed real world microgrids, where new challenges not being encountered in the laboratory such as the obstacles from the government and utility grid, will emerge. Moreover, applying the proposed control methods on the future microgrids based on new power devices (e.g. wide-bandgap devices) is still open, and might be an interesting study.

- Besides, the proposed hierarchy control extensively employs the model predictive control to the power electronics interfaced converters and inverters, due to its preferred advantages

129

compared to PI control. However, limited research can be found on the modelling and stability analysis of model predictive controlled system. In addition, power electronic-interfaced units dominated in the DC microgrid also introduce low inertia side effect that may lead to severe system instability. As a result, a great deal of research work is necessary on the theory analysis of improving the reliability of the DC microgrid.

- Furthermore, the dissertation is only focused on the control of a single DC microgrid. The optimization and coordinated control of the DC microgrid clusters opens new doors for future study. For example, the grid codes need to be upgraded to accommodate the distinguished characteristics of DC microgrid. Additionally, the investigation on the feasibility of new grid protection scheme will be another interesting research direction.

REFERENCES

[1]   (2017). *Renewables 2017 Global Status Report*. Available: http://www.ren21.net/status-of-renewables/global-status-report/

[2]   (2013). *World   Energy   Outlook   2013*.   Available: https://www.iea.org/publications/freepublications/publication/WEO2013.pdf

[3]   (2017). *Renewables Global Futures Report*. Available: http://www.ren21.net/future-of-renewables/global-futures-report/

[4]   R. S. Balog, "Autonomous Local Control In Distributed DC Power Systems," Ph.D., University of Illinois at Urbana-Champaign, 2006.

[5]   M. S. Shur and R. Zukauskas, "Solid-State Lighting: Toward Superior Illumination," *Proceedings of the IEEE,* vol. 93, no. 10, pp. 1691-1703, 2005.

[6]   J. R. Wells, B. M. Nee, M. Amrhein, P. T. Krein, and P. L. Chapman, "Low-cost single-phase powered induction machine drive for residential applications," in *Applied Power Electronics Conference and Exposition, 2004. APEC '04. Nineteenth Annual IEEE*, 2004, vol. 3, pp. 1579-1583 Vol.3.

[7]   M. E. Baran and N. R. Mahajan, "DC distribution for industrial systems: opportunities and challenges," *IEEE Transactions on Industry Applications,* vol. 39, no. 6, pp. 1596-1601, 2003.

[8]   X. Chen, M. Shi, H. Sun, Y. Li, and H. He, "Distributed Cooperative Control and Stability Analysis of Multiple DC Electric Springs in DC Microgrid," *IEEE Transactions on Industrial Electronics,* vol. PP, no. 99, pp. 1-1, 2017.

[9]   J. M. Guerrero, J. C. Vasquez, J. Matas, M. Castilla, and L. G. d. Vicuna, "Control Strategy for Flexible Microgrid Based on Parallel Line-Interactive UPS Systems," *IEEE Transactions on Industrial Electronics,* vol. 56, no. 3, pp. 726-736, 2009.

[10]   P. H. Huang, P. C. Liu, W. Xiao, and M. S. E. Moursi, "A Novel Droop-Based Average Voltage Sharing Control Strategy for DC Microgrids," *IEEE Transactions on Smart Grid,* vol. 6, no. 3, pp. 1096-1106, 2015.

[11]   A. T. Ghareeb, A. A. Mohamed, and O. A. Mohammed, "DC microgrids and distribution systems: An overview," in *2013 IEEE Power & Energy Society General Meeting*, 2013, pp. 1-5.

[12]   D. E. Olivares *et al.*, "Trends in Microgrid Control," *IEEE Transactions on Smart Grid,* vol. 5, no. 4, pp. 1905-1919, 2014.

[13]   K. Sun, L. Zhang, Y. Xing, and J. M. Guerrero, "A Distributed Control Strategy Based on DC Bus Signaling for Modular Photovoltaic Generation Systems With Battery Energy Storage," *IEEE Transactions on Power Electronics,* vol. 26, no. 10, pp. 3032-3045, 2011.

[14]   N. Pogaku, M. Prodanovic, and T. C. Green, "Modeling, Analysis and Testing of Autonomous Operation of an Inverter-Based Microgrid," *IEEE Transactions on Power Electronics,* vol. 22, no. 2, pp. 613-625, 2007.

[15]   X. Yu, X. She, X. Zhou, and A. Q. Huang, "Power Management for DC Microgrid Enabled by Solid-State Transformer," *IEEE Transactions on Smart Grid,* vol. 5, no. 2, pp. 954-965, 2014.

[16]   X. Yu, X. She, X. Ni, and A. Q. Huang, "System Integration and Hierarchical Power Management Strategy for a Solid-State Transformer Interfaced Microgrid System," *IEEE Transactions on Power Electronics,* vol. 29, no. 8, pp. 4414-4425, 2014.

[17]   "Market Data: Microgrids, Campus/Institutional, Commercial & Industrial, Community, Community Resilience, Military, Utility Distribution, and Remote Microgrid Deployments: Global Capacity and Revenue Forecasts," *Navigant Research, Report 1Q 2016.*

[18]   "Microgrid Deployment Tracker 2Q17, Commercial and Industrial, Community, Utility Distribution, Institutional/Campus, Remote, and DC Microgrids: Projects by Region, Segment, and Top 10 Countries and Companies," *Navigant Research, Report 2Q 2017.*

[19]   "C&I Microgrids, Grid-Tied and Remote Microgrid Forecasts, Technology and Policy Market Drivers, and Key Players," *Navigant Research, Report 2Q 2017.*

[20]   "Utility Distribution Microgrids, Utility Technology Disruption Report," *Navigant Research, Report 2Q 2016.*

[21]   A. Kwasinski, W. Weaver, and R. S. Balog, *Microgrids and Other Local Area Power and Energy Systems*. Cambridge University Press, 2016.

[22]   *Think Microgrid – A Policy Discussion Guide*. Available: https://microgridknowledge.com/think-microgrid/

[23]   *CHP Technical Assistance Partnerships of U.S. Department of Energy*. Available: http://www.southwestchptap.org/profiles

[24]   *The Microgrids Group at Berkeley Lab*. Available: https://building-microgrid.lbl.gov/sendai-microgrid

[25]   P. Piagi and R. H. Lasseter, "Autonomous control of microgrids," in *2006 IEEE Power Engineering Society General Meeting*, 2006, pp. 1-8.

[26] A. Kwasinski and P. T. Krein, "Stabilization of constant power loads in Dc-Dc converters using passivity-based control," in *INTELEC 07 - 29th International Telecommunications Energy Conference*, 2007, pp. 867-874.

[27] A. Kwasinski and P. T. Krein, "Passivity-Based Control of Buck Converters with Constant-Power Loads," in *2007 IEEE Power Electronics Specialists Conference*, 2007, pp. 259-265.

[28] D. J. Hammerstrom, "AC Versus DC Distribution SystemsDid We Get it Right?," in *2007 IEEE Power Engineering Society General Meeting*, 2007, pp. 1-5.

[29] R. L. Nailen, "Battery protection-where do we stand?," *IEEE Transactions on Industry Applications,* vol. 27, no. 4, pp. 658-667, 1991.

[30] B. K. Johnson and R. Lasseter, "An industrial power distribution system featuring UPS properties," in *Power Electronics Specialists Conference, 1993. PESC '93 Record., 24th Annual IEEE*, 1993, pp. 759-765.

[31] W. A. Tabisz, M. M. Jovanovic, and F. C. Lee, "Present and future of distributed power systems," in *Applied Power Electronics Conference and Exposition, 1992. APEC '92. Conference Proceedings 1992., Seventh Annual*, 1992, pp. 11-18.

[32] X. Lu, J. M. Guerrero, K. Sun, and J. C. Vasquez, "An Improved Droop Control Method for DC Microgrids Based on Low Bandwidth Communication With DC Bus Voltage Restoration and Enhanced Current Sharing Accuracy," *IEEE Transactions on Power Electronics,* vol. 29, no. 4, pp. 1800-1812, 2014.

[33] Y. Nanfang, D. Paire, G. Fei, and A. Miraoui, "Power management strategies for microgrid-A short review," in *2013 IEEE Industry Applications Society Annual Meeting*, 2013, pp. 1-9.

[34]   F. Blaabjerg, R. Teodorescu, M. Liserre, and A. V. Timbus, "Overview of Control and Grid Synchronization for Distributed Power Generation Systems," *IEEE Transactions on Industrial Electronics,* vol. 53, no. 5, pp. 1398-1409, 2006.

[35]   I. Y. Chung, W. Liu, D. A. Cartes, E. G. Collins, and S. I. Moon, "Control Methods of Inverter-Interfaced Distributed Generators in a Microgrid System," *IEEE Transactions on Industry Applications,* vol. 46, no. 3, pp. 1078-1088, 2010.

[36]   Y. A. R. I. Mohamed and E. F. El-Saadany, "Adaptive Decentralized Droop Controller to Preserve Power Sharing Stability of Paralleled Inverters in Distributed Generation Microgrids," *IEEE Transactions on Power Electronics,* vol. 23, no. 6, pp. 2806-2816, 2008.

[37]   F. Diaz-Franco, T. Vu, T. E. Mezyani, and C. S. Edrington, "Low-voltage ride-through for PV systems using model predictive control approach," in *2016 North American Power Symposium (NAPS)*, 2016, pp. 1-6.

[38]   M. Mosa, H. Abu-Rub, and J. Rodríguez, "High performance predictive control applied to three phase grid connected Quasi-Z-Source Inverter," in *IECON 2013 - 39th Annual Conference of the IEEE Industrial Electronics Society*, 2013, pp. 5812-5817.

[39]   T. Wang, H. Kamath, and S. Willard, "Control and Optimization of Grid-Tied Photovoltaic Storage Systems Using Model Predictive Control," *IEEE Transactions on Smart Grid,* vol. 5, no. 2, pp. 1010-1017, 2014.

[40]   H. Z. Xiao Li, Mohammad, "Model Predictive Control of Voltage Source Inverter with Seamless Transition between Islanded and Gridconnected Operations."

[41]   S. Chakraborty, M. D. Weiss, and M. G. Simoes, "Distributed Intelligent Energy Management System for a Single-Phase High-Frequency AC Microgrid," *IEEE Transactions on Industrial Electronics,* vol. 54, no. 1, pp. 97-109, 2007.

[42]   D. Grider *et al.*, "10 kV/120 A SiC DMOSFET half H-bridge power modules for 1 MVA solid state power substation," in *2011 IEEE Electric Ship Technologies Symposium*, 2011, pp. 131-134.

[43]   X. She, R. Burgos, G. Wang, F. Wang, and A. Q. Huang, "Review of solid state transformer in the distribution system: From components to field application," in *2012 IEEE Energy Conversion Congress and Exposition (ECCE)*, 2012, pp. 4077-4084.

[44]   R. Zamora and A. K. Srivastava, "Controls for microgrids with storage: Review, challenges, and research needs," *Renewable and Sustainable Energy Reviews,* vol. 14, no. 7, pp. 2009-2018, 2010/09/01/ 2010.

[45]   J. M. Guerrero, L. Hang, and J. Uceda, "Control of Distributed Uninterruptible Power Supply Systems," *IEEE Transactions on Industrial Electronics,* vol. 55, no. 8, pp. 2845-2859, 2008.

[46]   M. N. Marwali, J. Jin-Woo, and A. Keyhani, "Control of distributed generation systems - Part II: Load sharing control," *IEEE Transactions on Power Electronics,* vol. 19, no. 6, pp. 1551-1561, 2004.

[47]   M. N. Marwali and A. Keyhani, "Control of distributed generation systems-Part I: Voltages and currents control," *IEEE Transactions on Power Electronics,* vol. 19, no. 6, pp. 1541-1550, 2004.

[48]   P. Miquel and F. Gourvil, "Distributed power architecture in the context of the cost effective data center," in *24th Annual International Telecommunications Energy Conference*, 2002, pp. 427-431.

[49]   A. Ghazanfari, M. Hamzeh, H. Mokhtari, and H. Karimi, "Active Power Management of Multihybrid Fuel Cell/Supercapacitor Power Conversion System in a Medium Voltage Microgrid," *IEEE Transactions on Smart Grid,* vol. 3, no. 4, pp. 1903-1910, 2012.

[50]   J. A. P. Lopes, C. L. Moreira, and A. G. Madureira, "Defining control strategies for analysing microgrids islanded operation," in *2005 IEEE Russia Power Tech*, 2005, pp. 1-7.

[51]   A. Bidram and A. Davoudi, "Hierarchical Structure of Microgrids Control System," *IEEE Transactions on Smart Grid,* vol. 3, no. 4, pp. 1963-1976, 2012.

[52]   M. Prodanovic and T. C. Green, "High-Quality Power Generation Through Distributed Control of a Power Park Microgrid," *IEEE Transactions on Industrial Electronics,* vol. 53, no. 5, pp. 1471-1482, 2006.

[53]   S. Anand, B. G. Fernandes, and J. Guerrero, "Distributed Control to Ensure Proportional Load Sharing and Improve Voltage Regulation in Low-Voltage DC Microgrids," *IEEE Transactions on Power Electronics,* vol. 28, no. 4, pp. 1900-1913, 2013.

[54]   T. Dragicevic, J. M. Guerrero, J. C. Vasquez, and D. Skrlec, "Supervisory Control of an Adaptive-Droop Regulated DC Microgrid With Battery Management Capability," *IEEE Transactions on Power Electronics,* vol. 29, no. 2, pp. 695-706, 2014.

[55]   V. Nasirian, A. Davoudi, F. L. Lewis, and J. M. Guerrero, "Distributed Adaptive Droop Control for DC Distribution Systems," *IEEE Transactions on Energy Conversion,* vol. 29, no. 4, pp. 944-956, 2014.

[56] P. Wang, X. Lu, X. Yang, W. Wang, and D. Xu, "An Improved Distributed Secondary Control Method for DC Microgrids With Enhanced Dynamic Current Sharing Performance," *IEEE Transactions on Power Electronics,* vol. 31, no. 9, pp. 6658-6673, 2016.

[57] K. Rouzbehi, A. Miranian, J. I. Candela, A. Luna, and P. Rodriguez, "A Generalized Voltage Droop Strategy for Control of Multiterminal DC Grids," *IEEE Transactions on Industry Applications,* vol. 51, no. 1, pp. 607-618, 2015.

[58] F. Katiraei, M. R. Iravani, and P. W. Lehn, "Micro-grid autonomous operation during and subsequent to islanding process," *IEEE Transactions on Power Delivery,* vol. 20, no. 1, pp. 248-257, 2005.

[59] H. Liu *et al.*, "An Enhanced Dual Droop Control Scheme for Resilient Active Power Sharing Among Paralleled Two-Stage Converters," *IEEE Transactions on Power Electronics,* vol. 32, no. 8, pp. 6091-6104, 2017.

[60] M. B. Shadmand, R. S. Balog, and H. Abu-Rub, "Model Predictive Control of PV Sources in a Smart DC Distribution System: Maximum Power Point Tracking and Droop Control," *IEEE Transactions on Energy Conversion,* vol. 29, no. 4, pp. 913-921, 2014.

[61] H. Karimi, H. Nikkhajoei, and R. Iravani, "Control of an Electronically-Coupled Distributed Resource Unit Subsequent to an Islanding Event," *IEEE Transactions on Power Delivery,* vol. 23, no. 1, pp. 493-501, 2008.

[62] K. D. Brabandere, B. Bolsens, J. V. d. Keybus, A. Woyte, J. Driesen, and R. Belmans, "A Voltage and Frequency Droop Control Method for Parallel Inverters," *IEEE Transactions on Power Electronics,* vol. 22, no. 4, pp. 1107-1115, 2007.

[63]   C. T. Lee, C. C. Chu, and P. T. Cheng, "A New Droop Control Method for the Autonomous Operation of Distributed Energy Resource Interface Converters," *IEEE Transactions on Power Electronics,* vol. 28, no. 4, pp. 1980-1993, 2013.

[64]   H. Karimi, A. Yazdani, and R. Iravani, "Negative-Sequence Current Injection for Fast Islanding Detection of a Distributed Resource Unit," *IEEE Transactions on Power Electronics,* vol. 23, no. 1, pp. 298-307, 2008.

[65]   J. M. Guerrero, J. Matas, L. G. d. Vicuna, M. Castilla, and J. Miret, "Decentralized Control for Parallel Operation of Distributed Generation Inverters Using Resistive Output Impedance," *IEEE Transactions on Industrial Electronics,* vol. 54, no. 2, pp. 994-1004, 2007.

[66]   M. B. Delghavi and A. Yazdani, "An Adaptive Feedforward Compensation for Stability Enhancement in Droop-Controlled Inverter-Based Microgrids," *IEEE Transactions on Power Delivery,* vol. 26, no. 3, pp. 1764-1773, 2011.

[67]   R. Majumder, B. Chaudhuri, A. Ghosh, R. Majumder, G. Ledwich, and F. Zare, "Improvement of Stability and Load Sharing in an Autonomous Microgrid Using Supplementary Droop Control Loop," *IEEE Transactions on Power Systems,* vol. 25, no. 2, pp. 796-808, 2010.

[68]   R. Majumder, G. Ledwich, A. Ghosh, S. Chakrabarti, and F. Zare, "Droop Control of Converter-Interfaced Microsources in Rural Distributed Generation," *IEEE Transactions on Power Delivery,* vol. 25, no. 4, pp. 2768-2778, 2010.

[69]   E. Barklund, N. Pogaku, M. Prodanovic, C. Hernandez-Aramburo, and T. C. Green, "Energy Management in Autonomous Microgrid Using Stability-Constrained Droop

Control of Inverters," *IEEE Transactions on Power Electronics,* vol. 23, no. 5, pp. 2346-2352, 2008.

[70] S. V. Iyer, M. N. Belur, and M. C. Chandorkar, "A Generalized Computational Method to Determine Stability of a Multi-inverter Microgrid," *IEEE Transactions on Power Electronics,* vol. 25, no. 9, pp. 2420-2432, 2010.

[71] T. L. Vandoorn, B. Meersman, L. Degroote, B. Renders, and L. Vandevelde, "A Control Strategy for Islanded Microgrids With DC-Link Voltage Control," *IEEE Transactions on Power Delivery,* vol. 26, no. 2, pp. 703-713, 2011.

[72] J. M. Guerrero, V. Luis Garcia de, J. Matas, M. Castilla, and J. Miret, "Output impedance design of parallel-connected UPS inverters with wireless load-sharing control," *IEEE Transactions on Industrial Electronics,* vol. 52, no. 4, pp. 1126-1135, 2005.

[73] J. M. Guerrero, L. G. d. Vicuna, J. Matas, M. Castilla, and J. Miret, "A wireless controller to enhance dynamic performance of parallel inverters in distributed generation systems," *IEEE Transactions on Power Electronics,* vol. 19, no. 5, pp. 1205-1213, 2004.

[74] T. Logenthiran, D. Srinivasan, A. M. Khambadkone, and H. N. Aung, "Multi-Agent System (MAS) for short-term generation scheduling of a microgrid," in *2010 IEEE International Conference on Sustainable Energy Technologies (ICSET)*, 2010, pp. 1-6.

[75] A. Chaouachi, R. M. Kamel, R. Andoulsi, and K. Nagasaka, "Multiobjective Intelligent Energy Management for a Microgrid," *IEEE Transactions on Industrial Electronics,* vol. 60, no. 4, pp. 1688-1699, 2013.

[76] V. Salehi, A. Mohamed, and O. A. Mohammed, "Implementation of real-time optimal power flow management system on hybrid AC/DC smart microgrid," in *2012 IEEE Industry Applications Society Annual Meeting*, 2012, pp. 1-8.

[77] C. Chen, S. Duan, T. Cai, B. Liu, and G. Hu, "Smart energy management system for optimal microgrid economic operation," *IET Renewable Power Generation,* vol. 5, no. 3, pp. 258-267, 2011.

[78] B. Khorramdel and M. Raoofat, "Optimal stochastic reactive power scheduling in a microgrid considering voltage droop scheme of DGs and uncertainty of wind farms," *Energy,* vol. 45, no. 1, pp. 994-1006, 2012/09/01/ 2012.

[79] "World Energy Investment Outlook | Special Report " *International Energy Agency,* 2014.

[80] S. Xiao and R. S. Balog, "An improved adaptive perturb & observe maximum power point tracking technique," in *2018 IEEE Texas Power and Energy Conference (TPEC)*, 2018, pp. 1-6.

[81] T. Esram and P. L. Chapman, "Comparison of Photovoltaic Array Maximum Power Point Tracking Techniques," *IEEE Transactions on Energy Conversion,* vol. 22, no. 2, pp. 439-449, 2007.

[82] O. Wasynczuk, "Dynamic Behavior of a Class of Photovoltaic Power Systems," *IEEE Power Engineering Review,* vol. PER-3, no. 9, pp. 36-37, Sept 1983.

[83] R. Zhao, S. Y. Yu, S. Xiao, and K. Xu, "An enhanced control design scheme for multiple-input converters based on time-sharing switching," in *2017 IEEE Applied Power Electronics Conference and Exposition (APEC)*, 2017, pp. 3522-3529.

[84] S. Xiao, M. B. Shadmand, and R. S. Balog, "Model predictive control of multi-string PV systems with battery back-up in a community dc microgrid," in *2017 IEEE Applied Power Electronics Conference and Exposition (APEC)*, 2017, pp. 1284-1290.

[85]   S. Jain and V. Agarwal, "Comparison of the performance of maximum power point tracking schemes applied to single-stage grid-connected photovoltaic systems," *IET Electric Power Applications,* vol. 1, no. 5, pp. 753-762, Sept 2007.

[86]   A. K. Abdelsalam, A. M. Massoud, S. Ahmed, and P. N. Enjeti, "High-Performance Adaptive Perturb and Observe MPPT Technique for Photovoltaic-Based Microgrids," *IEEE Transactions on Power Electronics,* vol. 26, no. 4, pp. 1010-1021, 2011.

[87]   W. Xiao and W. G. Dunford, "A modified adaptive hill climbing MPPT method for photovoltaic power systems," *2004 IEEE 35th Annual Power Electronics Specialists Conference (IEEE Cat. No.04CH37551),* vol. 3, pp. 1957-1963, 2004.

[88]   A. Pandey, N. Dasgupta, and A. K. Mukerjee, "High-Performance Algorithms for Drift Avoidance and Fast Tracking in Solar MPPT System," *IEEE Transactions on Energy Conversion,* vol. 23, no. 2, pp. 681-689, 2008.

[89]   H. Patel and V. Agarwal, "MPPT Scheme for a PV-Fed Single-Phase Single-Stage Grid-Connected Inverter Operating in CCM With Only One Current Sensor," *IEEE Transactions on Energy Conversion,* vol. 24, no. 1, pp. 256-263, 2009.

[90]   L. Zhang, A. Al-Amoudi, and B. Yunfei, "Real-time maximum power point tracking for grid-connected photovoltaic systems," in *2000 Eighth International Conference on Power Electronics and Variable Speed Drives (IEE Conf. Publ. No. 475)*, 2000, pp. 124-129.

[91]   N. Femia, G. Petrone, G. Spagnuolo, and M. Vitelli, "Optimization of perturb and observe maximum power point tracking method," *IEEE Transactions on Power Electronics,* vol. 20, no. 4, pp. 963-973, 2005.

[92]   S. Jain and V. Agarwal, "A new algorithm for rapid tracking of approximate maximum power point in photovoltaic systems," *IEEE Power Electronics Letters,* vol. 2, no. 1, pp. 16-19, 2004.

[93]   N. S. D. Souza, L. A. C. Lopes, and L. XueJun, "An Intelligent Maximum Power Point Tracker Using Peak Current Control," in *2005 IEEE 36th Power Electronics Specialists Conference*, 2005, p. 172.

[94]   M. Metry, M. B. Shadmand, R. S. Balog, and H. A. Rub, "A variable step-size MPPT for sensorless current model predictive control for photovoltaic systems," in *2016 IEEE Energy Conversion Congress and Exposition (ECCE)*, 2016, pp. 1-8.

[95]   J. Lu and R. Niu, "False information injection attack on dynamic state estimation in multi-sensor systems," in *17th International Conference on Information Fusion (FUSION)*, 2014, pp. 1-8.

[96]   E. Koutroulis, K. Kalaitzakis, and N. C. Voulgaris, "Development of a microcontroller-based, photovoltaic maximum power point tracking control system," *IEEE Transactions on Power Electronics,* vol. 16, no. 1, pp. 46-54, 2001.

[97]   A. Al-Amoudi and L. Zhang, "Optimal control of a grid-connected PV system for maximum power point tracking and unity power factor," in *1998 Seventh International Conference on Power Electronics and Variable Speed Drives (IEE Conf. Publ. No. 456)*, 1998, pp. 80-85.

[98]   S. Xiao and R. S. Balog, "An improved hierarchy and autonomous control for DC microgrid based on both model predictive and distributed droop control," in *2018 IEEE Applied Power Electronics Conference and Exposition (APEC)*, 2018, pp. 3319-3325.

[99]   J. Holtz and S. Stadtfeld, "A predictive controller for the stator current vector of AC machines fed from a switched voltage source," in *International Power Electronics Conference (IPEC)*, 1983, pp. 1665–1675.

[100] J. Rodriguez and P. Cortes, *Predictive control of power converters and electrical drives*. John Wiley & Sons, 2012.

[101] J. Rodriguez *et al.*, "State of the Art of Finite Control Set Model Predictive Control in Power Electronics," *IEEE Transactions on Industrial Informatics,* vol. 9, no. 2, pp. 1003-1016, 2013.

[102] P. Cortes, A. Wilson, S. Kouro, J. Rodriguez, and H. Abu-Rub, "Model Predictive Control of Multilevel Cascaded H-Bridge Inverters," *IEEE Transactions on Industrial Electronics,* vol. 57, no. 8, pp. 2691-2699, 2010.

[103] M. B. Shadmand, M. Mosa, R. S. Balog, and H. A. Rub, "An Improved MPPT Technique of High Gain DC-DC Converter by Model Predictive Control for Photovoltaic Applications," in *IEEE Applied Power Electronics Conference & Exposition (APEC)*, 2014, pp. 2993 - 2999.

[104] M. Mosa, H. Abu-Rub, and J. Rodriguez, "High performance predictive control applied to three phase grid connected Quasi-Z-Source Inverter," in *IEEE Industrial Electronics Society Annual Conference (IECON)*, 2013, pp. 5812-5817.

[105] M. Mosa, O. Ellabban, A. Kouzou, H. Abu-Rub, and J. Rodriguez, "Model Predictive Control applied for Quasi-Z-source inverter," in *IEEE Applied Power Electronics Conference and Exposition (APEC)*, 2013, pp. 165-169.

[106] M. Shadmand, R. S. Balog, and H. Abu Rub, "Maximum Power Point Tracking using Model Predictive Control of a flyback converter for photovoltaic applications," in *IEEE Power and Energy Conference at Illinois (PECI)*, 2014, pp. 1-5.

[107] P. Cortes *et al.*, "Guidelines for weighting factors design in Model Predictive Control of power converters and drives," in *IEEE International Conference on Industrial Technology (ICIT)*, 2009, pp. 1-7.

[108] M. B. Shadmand, M. Mosa, R. S. Balog, and H. A. Rub, "An improved MPPT technique for high gain DC-DC converter using model predictive control for photovoltaic applications," in *2014 IEEE Applied Power Electronics Conference and Exposition - APEC 2014*, 2014, pp. 2993-2999.

[109] M. Mosa, H. A. Rub, M. E. Ahmed, and J. Rodriguez, "Modified MPPT with using model predictive control for multilevel boost converter," in *IECON 2012 - 38th Annual Conference on IEEE Industrial Electronics Society*, 2012, pp. 5080-5085.

[110] M. Coleman, C. K. Lee, C. Zhu, and W. G. Hurley, "State-of-Charge Determination From EMF Voltage Estimation: Using Impedance, Terminal Voltage, and Current for Lead-Acid and Lithium-Ion Batteries," *IEEE Transactions on Industrial Electronics,* vol. 54, no. 5, pp. 2550-2557, 2007.

[111] S. Xiao, M. Metry, M. Trabelsi, R. S. Balog, and H. Abu-Rub, "A Model Predictive Control Technique for Utility-Scale Grid Connected Battery Systems Using Packed U Cells Multilevel Inverter," presented at the IEEE Ind. Electron. Conf. (IECON), Florence, Italy, 24-27 Oct 2016, 2016.

[112] M. Trabelsi, S. Bayhan, M. Metry, H. Abu Rub, L. Ben-Brahim, and R. S. Balog, "An Effective Model Predictive Control for Grid Connected Packed U Cells Multilevel Inverter," presented at the Power and Energy Conference at Illinois (PECI), Illinois, 2016.

[113] Y. Ounejjar, K. Al-Haddad, and L.-A. Gregoire, "Packed U Cells Multilevel Converter Topology: Theoretical Study and Experimental Validation," *IEEE Transaction on Industrial Electronics,* vol. 58, no. 4, pp. 1294-1306, 2011.

[114] M. Shadmand and R. Balog, "Multi-Objective Optimization and Design of Photovoltaic-Wind Hybrid System for Community Smart DC Microgrid," *IEEE Transactions on Smart Grid,* vol. 5, no. 5, pp. 2635-2643, 2014.

[115] J. M. Guerrero, P. C. Loh, T. L. Lee, and M. Chandorkar, "Advanced Control Architectures for Intelligent Microgrids Part II: Power Quality, Energy Storage, and AC/DC Microgrids," *IEEE Transactions on Industrial Electronics,* vol. 60, no. 4, pp. 1263-1270, 2013.

[116] I. Hadjipaschalis, A. Poullikkas, and V. Efthimiou, "Overview of current and future energy storage technologies for electric power applications," *Renewable and Sustainable Energy Reviews,* vol. 13, no. 6–7, pp. 1513-1522, 2009.

[117] M. Metry, S. Bayhan, R. S. Balog, and H. Abu Rub, "Model Predictive Control for PV Maximum Power Point Tracking of Single-Phase subMultilevel Inverter," presented at the Power and Energy Conference at Illinois (PECI), Illinois, 2016.

[118] J. Rodríguez, S. Bernet, B. Wu, J. O. Pontt, and S. Kouro, "Multilevel Voltage-Source-Converter Topologies for Industrial Medium-Voltage Drives," *IEEE Transaction Industrial Electronics,* vol. 54, no. 6, pp. 2930-2945, 2007.

[119] J. Lee, "Model Predictive Control: Review of the Three Decades of Development," *International Journal of Control Automation and Systems,* vol. 9, no. 3, pp. 415-424, 2011.

[120]   M. A. Perez, S. Bernet, J. Rodriguez, S. Kouro, and R. Lizana, "Circuit Topologies, Modeling, Control Schemes, and Applications of Modular Multilevel Converters," *IEEE Transactions on Power Electronics,* vol. 30, no. 1, pp. 4-17, 2015/01 2015.

[121]   H. Abu-Rub, M. Malinowski, and K. Al-Haddad, *Power Electronics for Renewable Energy Systems, Transportation and Industrial Applications*, 1 ed. Wiley-Blackwell, 2014.

[122]   R. W. Erickson and D. Maksimovic, *Fundamentals of power electronics*. Kluwer Academic Pub, 2001.

[123]   T. Dragi, J. M. Guerrero, J. C. Vasquez, and D. Skrlec, "Supervisory Control of an Adaptive-Droop Regulated DC Microgrid With Battery Management Capability," *IEEE Transactions on Power Electronics,* vol. 29, no. 2, pp. 695-706, 2014.

[124]   I. W. Group, "IEEE Recommended Practice and Requirements for Harmonic Control in Electric Power Systems," *IEEE Std 519-2014 (Revision of IEEE Std 519-1992),* pp. 1-29, 2014.

[125]   X. Liu and H. Li, "An Electrolytic-Capacitor-Free Single-Phase High-Power Fuel Cell Converter With Direct Double-Frequency Ripple Current Control," *IEEE Transactions on Industry Applications,* vol. 51, no. 1, pp. 297-308, 2015.

[126]   M. Yilmaz and P. T. Krein, "Review of Battery Charger Topologies, Charging Power Levels, and Infrastructure for Plug-In Electric and Hybrid Vehicles," *IEEE Transactions on Power Electronics,* vol. 28, no. 5, pp. 2151-2169, 2013.

[127]   S. Harb, M. Kedia, H. Zhang, and R. S. Balog, "Microinverter and string inverter grid-connected photovoltaic system: A comprehensive study," in *2013 IEEE 39th Photovoltaic Specialists Conference (PVSC)*, 2013, pp. 2885-2890.

[128] H. Zhang, X. Li, B. Ge, and R. S. Balog, "Capacitance, dc Voltage Utilizaton, and Current Stress: Comparison of Double-Line Frequency Ripple Power Decoupling for Single-Phase Systems," *IEEE Industrial Electronics Magazine,* vol. 11, no. 3, pp. 37-49, 2017.

[129] X. Li and R. S. Balog, "PLL-less robust active and reactive power controller for single phase grid-connected inverter with LCL filter," in *2015 IEEE Applied Power Electronics Conference and Exposition (APEC)*, 2015, pp. 2154-2159.

[130] S. Xiao, X. Li, H. Zhang, and R. S. Balog, "Active power decoupling method based on dual buck circuit with model predictive control," in *2018 IEEE Applied Power Electronics Conference and Exposition (APEC)*, 2018, pp. 3089-3094.

[131] X. Li, S. Xiao, H. Zhang, R. S. Balog, and B. Ge, "Dual buck based power decoupling circuit for single phase inverter/rectifier," in *2016 IEEE Energy Conversion Congress and Exposition (ECCE)*, 2016, pp. 1-6.

[132] M. Su, P. Pan, X. Long, Y. Sun, and J. Yang, "An Active Power-Decoupling Method for Single-Phase AC-DC Converters," *IEEE Transactions on Industrial Informatics,* vol. 10, no. 1, pp. 461-468, 2014.

[133] P. T. Krein, R. S. Balog, and M. Mirjafari, "Minimum Energy and Capacitance Requirements for Single-Phase Inverters and Rectifiers Using a Ripple Port," *IEEE Transactions on Power Electronics,* vol. 27, no. 11, pp. 4690-4698, 2012.

[134] H. Han, Y. Liu, Y. Sun, M. Su, and W. Xiong, "Single-phase current source converter with power decoupling capability using a series-connected active buffer," *IET Power Electronics,* vol. 8, no. 5, pp. 700-707, 2015.

[135] S. Harb and R. S. Balog, "Reliability of Candidate Photovoltaic Module-Integrated-Inverter (PV-MII) Topologies: A Usage Model Approach," *IEEE Transactions on Power Electronics,* vol. 28, no. 6, pp. 3019-3027, 2013.

[136] Y. Tang, F. Blaabjerg, P. C. Loh, C. Jin, and P. Wang, "Decoupling of Fluctuating Power in Single-Phase Systems Through a Symmetrical Half-Bridge Circuit," *IEEE Transactions on Power Electronics,* vol. 30, no. 4, pp. 1855-1865, 2015.

[137] G. R. Zhu, S. C. Tan, Y. Chen, and C. K. Tse, "Mitigation of Low-Frequency Current Ripple in Fuel-Cell Inverter Systems Through Waveform Control," *IEEE Transactions on Power Electronics,* vol. 28, no. 2, pp. 779-792, 2013.

[138] P. F. Ksiazek and M. Ordonez, "Swinging Bus Technique for Ripple Current Elimination in Fuel Cell Power Conversion," *IEEE Transactions on Power Electronics,* vol. 29, no. 1, pp. 170-178, 2014.

[139] R. Wang *et al.*, "A High Power Density Single-Phase PWM Rectifier With Active Ripple Energy Storage," *IEEE Transactions on Power Electronics,* vol. 26, no. 5, pp. 1430-1443, 2011.

[140] B. Ge *et al.*, "An Active Filter Method to Eliminate DC-Side Low-Frequency Power for a Single-Phase Quasi-Z-Source Inverter," *IEEE Transactions on Industrial Electronics,* vol. 63, no. 8, pp. 4838-4848, 2016.

[141] Y. Sun, Y. Liu, M. Su, W. Xiong, and J. Yang, "Review of Active Power Decoupling Topologies in Single-Phase Systems," *IEEE Transactions on Power Electronics,* vol. 31, no. 7, pp. 4778-4794, 2016.

[142]   C. Bordons and C. Montero, "Basic Principles of MPC for Power Converters: Bridging the Gap Between Theory and Practice," *IEEE Industrial Electronics Magazine,* vol. 9, no. 3, pp. 31-43, 2015.

[143]   J. Lu and R. Niu, "A state estimation and malicious attack game in multi-sensor dynamic systems," in *2015 18th International Conference on Information Fusion (Fusion)*, 2015, pp. 932-936.